UNIVERSITÀ DEGLI STUDI DI PADOVA

UNIVERSITA' DEGLI STUDI DI PADOVA

Dipartimento di Ingegneria Industriale DII

Corso di Laurea Magistrale in Ingegneria Meccanica

Tesi di Laurea Magistrale

Additive Manufacturing, the characterization of additively manufactured tensile and compression specimens

Relatori:

Prof. Stefania Bruschi

Prof. Marion Merklein

Correlatore:

M. Sc. Thomas Papke

Laureando:

Gianmarco Muraro 1182858

Anno Accademico 2019/2020

Desidero ringraziare la Professoressa Bruschi e il Professore Bariani per avermi dato la possibilità di svolgere la tesi alla Friedrich-Alexander Universität, un'esperienza che mi ha arricchito sia sul piano professionale sia umano.
Un pensiero particolare alla Professoressa Marion Merklein e al M. Sc. Thomas Papke per avermi seguito nei sei mesi di ricerca.
Ringrazio di cuore la mia famiglia per avermi sempre sostenuto e consentito di portare a termine gli studi universitari.

Ai miei fratelli e a mio nonno

List of variables, symbols and abbreviations used

Symbol	Unit	Description
AM	-	Additive Manufacturing
BD	-	Building direction
PBF	-	Powder Bed Fusion
L-PBF	-	Laser Powder Bed Fusion
316L (1.4404)	-	Austenitic stainless steel of alloy 316L
SLM		Selective Laser Melting
DMLS		Direct Metal Laser Sintering
V	-	Vertical build orientation
H	-	Horizontal build orientation
45°	-	45° build orientation
Conv	-	Conventional
RT	-	Room temperature
CAD	-	Computer-Aided Design
σ	MPa	Stress
ε	$\frac{mm}{mm}$	Strain
E	MPa	Young's modulus
$\sigma_{0.2}$ (compression test)	MPa	Offset Yield Strength 0.2%
$\sigma_{0.05}$ (compression test)	MPa	Offset Yield Strength 0.05%
σ max (compression test)	MPa	Maximum Yield Strength
σ, 55% h reduction (compression test)	MPa	Yield Strength with a 55% height reduction
ε_{el} (compression test)	%	Elastic strain amount with a 55% height reduction (with scattering)
ε_{pl} (compression test)	%	Plastic strain amount with a 55% height reduction (unless scattering)
$R_{p0.2}$ (tensile test)	MPa	Offset Yield Stress 0.2%
Rm or UTS (tensile test)	MPa	Maximum stress
A (tensile test)	%	Uniform elongation
Z (tensile test)	%	Area reduction
E_v	J/mm^3	Energy density
P_{eff}	W	Effective laser power
h	mm	Hatch distance
d	mm	Layer thickness
v	mm/s	Scan speed
t	mm	Specimen thickness
w	J	Deformation energy
PBF-EB	-	Electron Beam Powder Bed Fusion
DED-Powder	-	Powder Direct Energy Deposition
DED-Wire	-	Wire Direct Energy Deposition
MJ	-	Material Jetting
EXT	-	Extrusion Process
BJ	-	Binder Jetting
n	-	Number of repetitions

Contents

Abstract

Laser Powder Bed Fusion process (Selective Laser Melting), is an Additive Manufacturing technology, often employed as an alternative to conventional manufacturing due to the work-piece's complexity. The main advantages for the adoption of this technology are represented by unlimited drawing freedom and reduction in material waste.
Austenitic stainless steel of alloy 316L has been chosen due to its good weldability together with its corrosion and chemical resistance.
The aim of the present work is to analyze the mechanical properties of the selected material in order to evaluate its formability. Knowledge about the metal formability allows to have a hybrid manufacturing approach between AM and later forming, under control. This complementary approach reduces the time and material waste associated with a traditional process chain. The Laser Powder Bed Fusion process allows to obtain printed features that are close in terms of precision to those obtained through later forming, thanks to the flow curves knowledge found in this research work.
The mechanical properties have been investigated by carrying out compression and tensile tests of additively manufactured specimens both at high temperature and room temperature.
For the compression tests, cylinder specimens are manufactured by Lasertec 30 SLM DGM Mori machine. The compression tests are conducted at high temperature with Gleeble 3500 machine and at room temperature with Walter+Bai 300 machine, in order to evaluate the temperature influence and the building direction influence:

- temperature influence for equal build orientation;
- build orientation influence for equal prove temperature.

For the high temperature tests, the heating phase is managed through the commercial software QuikSim2.
For the tensile tests, specimens with the typical tensile form are manufactured by the same machine. The tensile tests are conducted to evaluate the building orientation influence at room temperature with Walter+Bai 300 machine.
The obtained results have allowed to find the deformation energy of the several additive building directions with compression and tensile load cases. The tensile results are limited due to the absence of proves at high temperatures.
An introduction of the present work is done in Chapter 1. An overview about Powder Bed Fusion and the material is reported in Chapter 2, by considering the state of art before the thesis results. The aims and methodology are showed using a concept map in Chapter 3. In Chapter 4 the material and the machines used are presented. The Chapter 5, the results chapter, shows first the compression and then the tensile results through diagrams and histograms, with a constant comparison to the conventional and the state of art results. Finally, Chapter 6 compares the entire results and provides a general outlook, underlining the necessary future steps.

Riassunto esteso

Il processo di Laser Powder Bed Fusion (Selective Laser Melting), è una tecnologia di produzione additiva che si pone come alternativa alle lavorazioni convenzionali soprattutto nel caso di componenti dalla forma molto complessa. L'illimitata libertà di disegno e il risparmio di materiale sono le ragioni principali che spingono verso il passaggio a questa tecnologia.
Il materiale scelto è l'acciaio austenitico inossidabile della lega 316L, grazie alla buona saldabilità, alla resistenza chimica e alla corrosione.
Lo scopo del presente lavoro è l'analisi delle proprietà meccaniche del materiale selezionato a diverse temperature in modo da poterne valutare la formabilità. La conoscenza della formabilità permette un approccio ibrido tra produzione additiva e successive lavorazioni per deformazione plastica. Tale approccio complementare riduce il tempo e gli scarti di materiale, tipici della catena di processo tradizionale. Il processo additivo Laser Powder Bed Fusion permette di produrre una geometria vicino al target di forma, ottimizzata poi con operazioni tradizionali di formatura, grazie alla conoscenza delle curve di flusso del materiale additivo, derivante dai dati sperimentali ottenuti nel presente lavoro.

Lo studio delle proprietà meccaniche è condotto attraverso prove di compressione e trazione ad alta temperatura e a temperatura ambiente di provini prodotti in maniera additiva.
Per quanto concerne i test di compressione, provini cilindrici sono stampanti dalla macchina Lasertec 30 SLM DGM Mori. I test di compressione sono condotti ad alte temperature mediante il sistema termo-meccanico Geeble 3500 e a temperatura ambiente tramite il sistema Walter+Bai 300, per valutare:

- l'influenza della temperatura a parità di direzione di costruzione;
- l'influenza della direzione di costruzione a parità di temperatura di prova.

Per i test ad alta temperatura, la fase di riscaldamento è gestita attraverso il software commerciale QuickSim2.
Per quanto riguarda invece i test di trazione, i provini sono prodotti dalla stessa macchina additiva. I tests di trazione sono condotti per valutare l'influenza della direzione di costruzione a temperatura ambiente sempre mediante l'uso del sistema Walter+Bai 300.
I risultati ottenuti hanno permesso di delineare l'energia di deformazione delle diverse direzioni di costruzione additiva. I risultati della prova di trazione sono limitati a causa dell'assenza di prove ad alta temperatura.
Un'introduzione del presente lavoro è fornita nel Capitolo 1. Una panoramica riguardante il processo di Powder Bed Fusion e il materiale è riportata nel Capitolo 2, considerando lo stato dell'arte antecedente ai risultati di questa tesi. Gli obbiettivi e la metodologia sono mostrati attraverso una mappa concettuale nel Capitolo 3. Nel Capitolo 4 sono presenti il materiale e le macchine usate. Il Capitolo 5 riporta i risultati attraverso diagrammi e istogrammi, con un confronto costante al materiale convenzionale e ai risultati presenti nello stato dell'arte. Infine, il capitolo 6 sintetizza i risultati e fornisce una visione generale, sottolineando i futuri steps necessari.

1 Introduction

Additive Manufacturing processes constitute a new industrial concept, based on the minimization of waste material. Less material means lower costs, more specifically, it means material quantity only in the loading directions through a topology optimization [1]. Through Additive Manufacturing technologies the most complex shapes are possible due to its intrinsic mechanics: layers upon layers each workpiece is realized.
The actual power of AM is the cooperation with conventional processes. The hybrid AM-forming approach is beneficial for less material waste and a short process chain since geometries can be manufactured close to the target geometry by AM.
This approach can overcome the traditional multi-stage forming process where operations with machining removal up to more than 90% are necessary to produce the final geometry [2].
Moreover, the only actual post-processing operation that allows to produce a ready to use component is the machining.
Combining AM and forming, two possible manufacturing routes can be put into practice.
The first route is a basic formed geometry followed by AM, that allows the simple creation of variants, complex and near-net-shape components, parts repairing and local properties, as shown in Figure 1.1.

Figure 1.1. *Formed geometry followed by AM* [2]

It also allows to have a more flexible process chain, less affected by the rapid changes of the market. If during a year, there are periods with a dominance of the variant 1 and others with variant 2, the process chain can change quickly.

The second type of manufacturing route presents an initial pre-form generated by AM that will be formed into its final shape by using only one single forming step, as shown in Figure 1.2. Regarding this, the second approach, one of the most typical methods is the hot forging application on the Laser Powder Bed Fusion structure. For sure, the AM-hot-forging workpiece needs a deep postprocessing, that embraces the heat-treatment but also Hot Isostatic Pressing and the surface finish processes. These post-processing operations can be done at the same time with the lastest technologies, as for example the HIQ60 System [3].

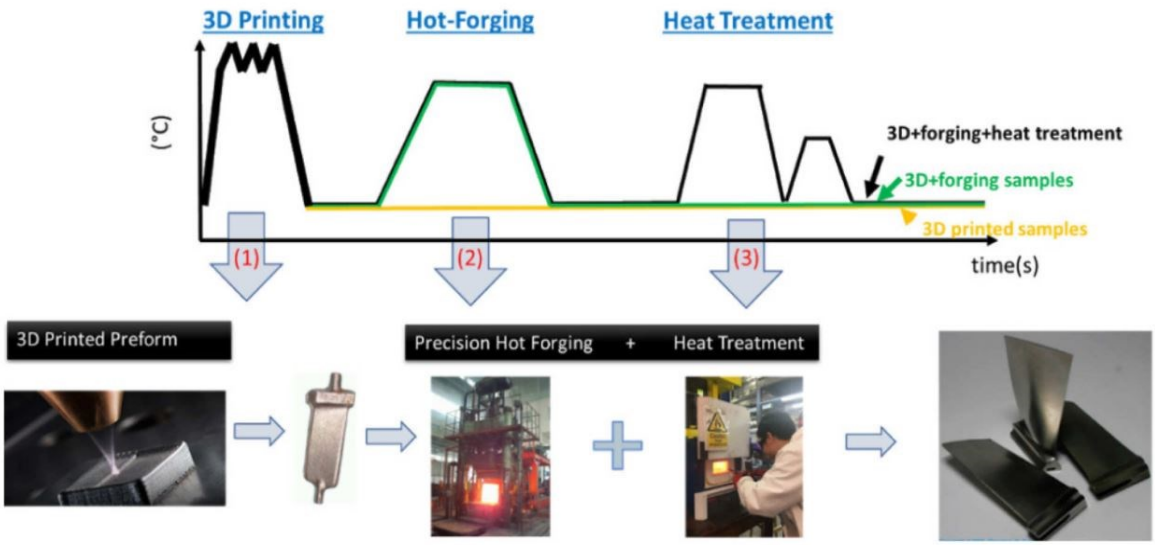

Figure 1.2. *Near-net-shape AM geometry followed by Hot-Forging* [3]

From the literature laser powder, layer thickness, hatch distance, laser current and lens position represent the strongest factors of impact. Important advances have been made in the last years with a parallel working between simulation and experimental stage to analyze the fundamental aspects of melting [4].

Powder bed fusion is the object of this research work. Powder Bed Fusion (PBF), also known as Laser Sintering (LS), Selective Laser Melting (SLM) and Direct Metal Laser Sintering (DMLS) [5], is an innovative additive manufacturing process where a part is build up in a powder bed.
The reports will focus largely on laser PBF and on 316L stainless steel (1.4404) because of good weldability and high corrosion resistance that allow their use in a wide range of applications, especially, in the automotive, medical sector and aerospace industry.

As things are today, it is not possible to know the form material after loading cycles. Since in a PBF process there are 130 independent parameters [5], to use this new technology it is necessary to know in depth the mechanical properties of the chosen material. Confidence can be found through a macro and micro-understanding of the physics of the process. Experiments are essential for a broad understanding of interactions in Additive Manufacturing processes.

Therefore, the mechanical properties can show anisotropic behavior regarding to the orientation of specimens to the building direction. Hence, it has to be investigated by methods of material characterization as compression and tensile tests. To evaluate the mechanical properties of AM material a constant comparison has to be conducted with the conventional manufactured material in the same setup conditions.
The purpose of this master thesis is the mechanical properties investigation through compression and tensile tests, taking into account building direction and temperature impact.

2 State of art

In the state of art, a correct description of process parameters, material microstructure and mechanical properties through previous research works allow to contextualize the aim of thesis.

2.1 Powder Bed Fusion

In this chapter is analysed the business of AM and the actual technological level regarding Powder Bed Fusion process.

2.1.1 Powder Bed Fusion market

Powder Bed Fusion is a manufacturing process steadily improving to directly produce net-shape or net-shape metal tools or functional products. PBF presents a drawing freedom unlimited: complex shapes with a rapid, flexible and economical way, where the traditional techniques show their limits. Stability and small weight turn this technology suitable for the medical sector, but also automotive and aerospace fields [6]. However this technology presents also challenges: high material costs, slow setup, laborious post-processing and restrictions on material compatibility [7].

If recently PBF meant part performance with small batches, as shown in Figure 2.1, now due to the last improvements in the state of the art, such as accuracy together speed, is happening the passage from a rapid-prototyping technology to a production technology [8]: this makes PBF really attractive.

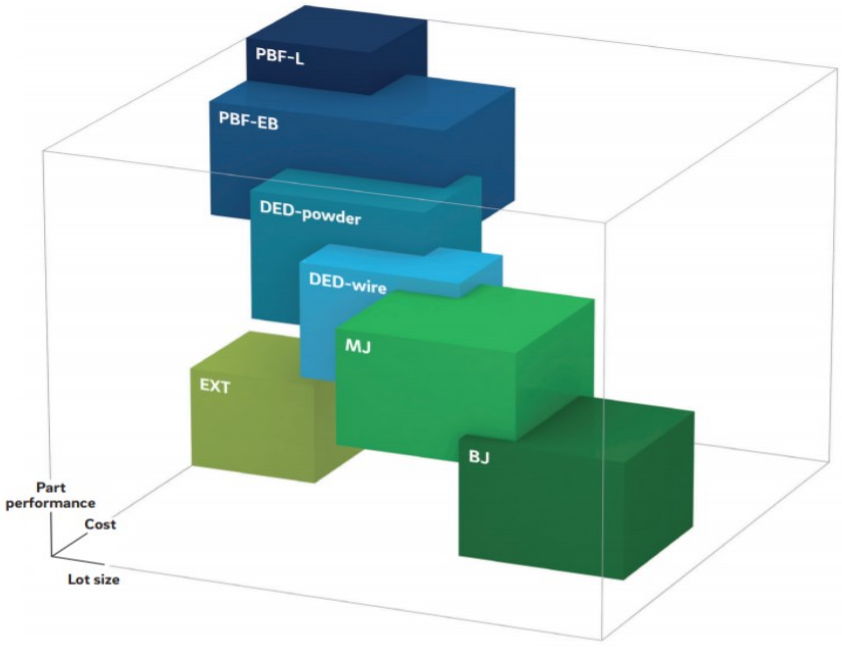

Figure 2.1. *Comparison between major AM technologies: Laser Powder Bed Fusion, Electron Beam Powder Bed Fusion, Powder Direct Energy Deposition, Wire Direct Energy Deposition, Material Jetting, Extrusion Process and Binder Jetting* [9]

Users and developers agree that this technology with the last developments can be used for much more than just prototyping. Significant improvements in accuracy, speed and materials have allowed a transition into testing, tooling, manufacturing and other realms that are outside

the prototyping definition [10].
If until few years ago this technology and AM technologies in general created great appeal unless solid economical investment, now the time is ripe for a large manufacturing.
Considering not only the key segments such as aerospace, healthcare, automotive but the total AM market size, in 2018 there was a development of $ 9,3 billion in revenue and an increase until $ 41 billion is estimated in 2027, as shown in Figure 2.2.

Figure 2.2. *Total AM market size 2014-2027(estimated)* [11]

Indeed, due to the modern techniques PBF workpieces near full density can be fabricated with mechanical properties at the same level of conventional parts, sometime higher. This technology is strongly suitable to the metals because it offers a nearly unlimited flexibility of geometry and complexity, together with the possibility to have fully dense parts generated without any further infiltrations.

2.1.2 Application field

The PBF applications embrace several fields depending on strength, ductility and biocompatibility [12]. Below are analyzed the most common PBF fields:

- automotive: For vehicles of upmarket as Formula 1 or supercar, light parts with high strength and a small buy-to-fly, that is a small coefficient (rough material weight/ part weight) [13], allow to the PBF to be superior than the conventional manufacturing. For example only two days pass from the flexible design to the real-time test for a shaft flange, as shown in Figure 2.3. The typical material is the 304L or 316L stainless steel.

Figure 2.3. *Shaft flange manufactured with PBF (external diameter = 15 mm)* [35]

- aeronautic: the weight reduction covers a fundamental role in aerospace sector. The aerospace fuel cost and the environment laws require the smallest consumptions; therefore it is necessary a weight reduction. In the aerospace sector the weight lost does not care of the costs. An example is an air duct made of titanium, as shown in Figure 2.4.

Figure 2.4. *Air duct manufactured with PBF (diameter = 20 mm)* [35]

- mechanical engineering: in the hydraulic plants the water flow optimization needs of specific trajectories that only AM can allow to obtain unless a great rough material loss. An example of application is a pump impeller made of aluminum and a stainless steel, as shown in Figure 2.5.

Figure 2.5. *Pump impeller manufactured with PBF (diameter = 17 mm)* [35]

- medical field: PBF applications with titanium implants are really common. Generally a leg prosthesis has to bear compression loads, so a full compression test characterization is necessary. Recent studies show that thanks to PBF it is possible to produce dental parts with gradient porosity, where the dense zone is designed for strength instead the porous zone is useful to enhance tissue growth in biocompatible implants [14]. An example are the brackets and palatal plates manufactured after a 3D scan, as shown in Figure 2.6.

Figure 2.6. *Dental plant manufactured with PBF (8 mm x 6 mm)* [35]

2.1.3 Process mechanic

An Additive Manufacturing process can be summarized in ten fundamental steps:

- workpiece representation with CAD software;
- CAD conversion in STL or AMF format, where the second one includes not only information about workpiece geometry but also about dimension, color and material;
- file transfer in the machine;
- machine setup;
- part manufacturing through a CNC program (this technology does not need tools);
- part removal;
- supports removal from part (post-processing);
- cleaning of part (post-processing);
- finishing process (postprocessing);
- heat treatments in order to reduce residual stresses (post-processing).

Focusing on Powder Bed Fusion, in agreement with ISO/ASTM standard definition, this process is defined as an: *"additive manufacturing process in which thermal energy selectively fuses regions of a powder bed "* [15]. It is the most mature and widely used metal additive manufacturing process, which prints metal using a laser or electron beam to melt lines in powder in order to produce parts where the conventional manufacturing shows limits [7].
Focusing on laser PBF, a typical machine is schematically shown in Figure 2.7. The mainly machine parts are:

- a fiber laser;
- a couple of lenses;
- a leveling roller or spreader;
- a 2D scanning mirror;
- a build platform;
- three pistons,
- powder tank;
- powder overflow.

As soon as the CAD profile is evaluated by the CNC program, the precise coordinates are defined, and the process can start. A limited lowering of the central build platform allows the placement of a correct powder amount from the leveling roller: the workpiece platform gets off, the powder platforms on both sides rise in order to preserve the requested powder amount. Meanwhile, the laser goes through the lens system and the 2D scanning mirror in order to strike a specific point on the powder bed [16], in agreement with the CNC coordinates. The laser melts the selected points and again another powder layer is applied. This cycle is repeated several times as long as the workpiece is built up completely layer by layer.

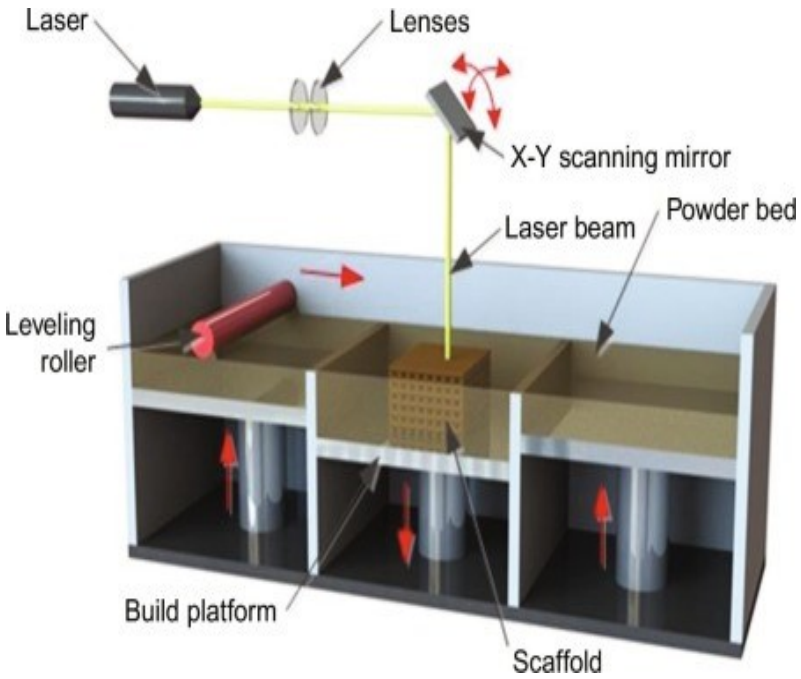

Figure 2.7. *Machine structure of Laser PBF process* [17]

Together the part, the support structure is manufactured in order to have a build plate. The support structure is also used to connect part a build plate. The support structure is represented not only from the first layers but also from higher layers, that provides stability to avoid dangerous bending. They also enable the correct heat dissipation: only a well-organized gradient temperature distribution allows the residual stresses control. The residual stress control is the correct approach in order to don't have deformations.

But sometimes this is not enough, so a post-processing thermal treatment in oven is necessary to distension of the residual stresses. First, the part has to be cleaned because it is surrounded by powder as shown in Figure 2.8. Then it can be placed in the oven, where the microstructure will be regenerated by receiving an Annealing.

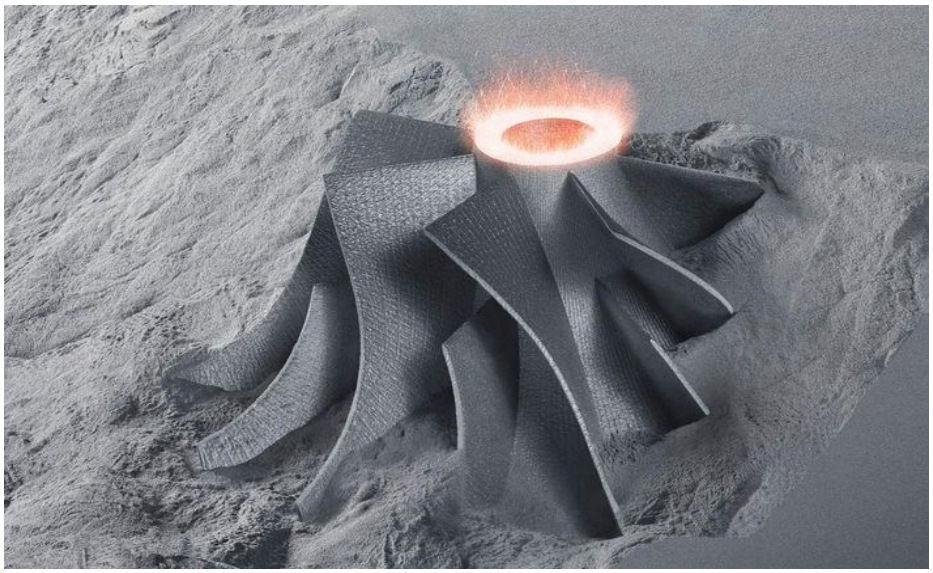

Figure 2.8. *Pump impeller manufacturing* [18]

2.1.4 Process parameters

The Powder Bed Fusion process depends on around 130 parameters that could influence, since they can be used to improve the parts property [5]. The manufacturing process goal is to produce parts with the highest possible density in combination with a low surface roughness, therefore for the used material it is necessary to optimize the most important influencing parameters [19]. The most important are the laser power, the layer thickness, scan speed, vectors lens position and the hatch distance, that is the distance between 2 scan lines. The energy density during SLM process can be calculated by using the following equation [20]:

$$Ev = \frac{Peff}{v\ d\ h} \qquad \text{Equation 1}$$

E_v = energy density [J/mm^3]
P_{eff} = effective laser power [W]
h = hatch distance [mm]
d = layer thickness [mm]
v = scan speed [mm/s] , where

$$v = \frac{\text{point distance}}{\text{exposure time}} \qquad \text{Equation 2}$$

Generally the laser power is set to high values in order to increase the speed, because an higher scan speed means an greater productivity [19].
However, also parameters such as scan speed, beam size, layer thickness, melt pool depth, scan line spacing (hatch distance), powder bed temperature, atmosphere and scanning strategy cover an important role.
These listed parameters present a mutual interaction with consequences in the microstructure and in the mechanical properties.
Powder bed temperature, laser power, scan speed, and hatch distance (scan line spacing) must be balanced to provide the best compromise between melt pool size, dimensional accuracy, surface finish, build rate, and mechanical properties [10].
Focusing on the parameters influence, low-laser-power and low-bed-temperature combinations produce better dimensional accuracy, but they mean an inferior microstructure quality because of a lower density parts and a higher tendency for layer delamination. On the other hand, high-laser-power and high-bed-temperature produce dense parts reducing residual stresses but they mean poor recyclability and a difficult part cleaning [10]. The powder bed temperature should also be kept uniform and constant to achieve repeatable results. High laser power also shows longer cracks lengths, instead low powers decrease widely the crack length [21]. Moreover, high-laser-power combined with low-bed-temperature mean tendency for nonuniform shrinkage and the residual stresses increasing, that brings to the part curling. The scanning strategies influence density, mechanical properties and residual stresses. The beam size control the length,

width, and depth of the melt pool [5]. A decreasing of laser deposition speed provokes a considerable waviness on the surface [22].
Laser power, spot size, deposition speed, and bed temperature together determine the energy input needed to fuse correctly the powder. Operating at lower laser powers requires the use of lower scan speeds in order to ensure proper particle fusion. Melt pool size is highly dependent upon settings of laser power, scan speed, spot size, and bed temperature. Hatch distance should be selected to allow a sufficient gradation of melt pool connection between adjacent lines of fused material to ensure robust mechanical properties. The powder bed density, governed by powder shape, size, distribution, and spreading mechanism, can strongly influence the part quality [10].

2.2 Austenitic Stainless AISI 316L Steel

Even if they represent only the 2% of the entire population, the stainless steels are really diffused thanks to their good resistance with corrosion. Good mechanical properties are guaranteed only if the corrosion is under control. The corrosion resistance is provided by the ≥ 12% Cr presence. On the other hand, the stainless steels present Martensite temperature under the environment temperature, therefore they cannot have hardening treatments in order to increase the mechanical characteristics. To the metal alloys can be added other elements in order to improve some specific characteristics: Carbon to give hardness, Molybdenum in order to have the pitting resistance, Sulphur to elevate the machinability and Titanium and Niobium to contrast the intracrystalline corrosion [23].
Depending on the microstructure, the stainless steels are classified as ferritic, austenitic, martensitic and duplex, where each one has a particular chemical composition (as shown in Table 2.1.

Table 2.1. *Ferritic, austenitic, martensitic and duplex steels* [24]

	C	Cr	Ni	Mo	N
AISI 304	0.06	19	9	-	-
AISI 302	0.15	18	9	-	-
AISI 316	0.06	17	12	2.5	-
AISI 304L	0.03	19	10	-	-
AISI 430	0.12	17	-	-	-
i AISI 410	0.15	12	-	-	-
23-04	0.02	23	4	-	0.10
22-05	0.02	22	5.5	3	0.14
25-07	0.02	25	7	4	0.25

The austenitic one show the best corrosion resistance, followed by the ferritic and martensitic. On the other hand, the duplex steels present the best mechanical resistance.
Concerning 316 L, it is an austenitic stainless steel alloy with attractive mechanical properties that allow it to be suitable for several engineering applications [25]. This steel has a face centred cubic crystalline structure with high toughness both at room temperature and at low temperature levels, giving a high tensile strain at a significant strain [25]. The L variant means low carbon amount (as shown in Table 2.2), this one makes the 316L suitable for large welding applications due to its immunity to grain boundary carbide precipitation. The Ni stabilizes the austenitic structure. It is has a good formability and weldability.

Table 2.2. *316L chemical composition*

Mat.	Fe	Cr	Ni	Mo	Mn	Si	P	S	C	N	O
316L 1.4404	Bal.	16.00-18.00	10.00-14.00	2.00-3.00	2.00	1.00	0.045	0.030	0.030	0.10	0.10

The thesis focuses on the build orientation and temperature influence of PBF 316L mechanical properties taking into account the conventional 316L, so a constant comparison is needed. For this reason from this point until the ending of this research work the mechanical properties of the additively manufactured specimens have to be compared with the conventional one, shown in Table 2.3.

Table 2.3. *Tensile mechanical properties at 20°C and high temperature of 316L conventionally manufactured* [26]

Mechanical data	Formula symbol and unit	Average value
Tensile strength (20°C)	R_m (MPa)	600
Offset yield strength	$R_{p0.2}$ (MPa)	290
Elongation at break	A (%)	54
Reduction in area	Z (%)	65
Young's modulus	E (GPa)	200
Vickers hardness	HV10 (-)	170
Tensile strength (100°C)	R_m (MPa)	570
Offset yield strength (100°C)	$R_{p0.2}$ (MPa)	180
Tensile strength (200°C)	R_m (MPa)	540
Offset yield strength (200°C)	$R_{p0.2}$ (MPa)	163
Tensile strength (300°C)	R_m (MPa)	510
Offset yield strength (300°C)	$R_{p0.2}$ (MPa)	145
Tensile strength (500°C)	R_m (MPa)	465
Offset yield strength (500°C)	$R_{p0.2}$ (MPa)	129

2.2.1 Microstructural aspects

The knowledge of microstructure in metal Additive Manufacturing is fundamental in order to manage location-specific mechanical properties of printed alloys. From the literature [27], it is known that directional solidification can well described through two solidification parameters:

- The temperature gradient at the solid-liquid interface (G), expressed in [K/mm]
- The growth rate of the solidifying front (R), expressed in [mm/s]

The product between these two parameters represents the material colling rate, therefore the

resulting microstructure.
The resulting microstructure in terms of length, scale, morphology and orientation depends by the systematic and quantitative correlation between process parameters (laser power, laser spot, scanning velocity, laser thickness, hatch distance) and solidification parameters (G,R). Previous research works before this thesis, considering G and R parameters, could guide to choose specific process parameters [27].
After processing, if the specimens are polished it is possible to acquire optical images in order to analyse the microstructure. The process parameters influence intimately the material microstructure. Working with low powers it is possible to have a rapid cooling with the creation of a very thin microstructure, therefore working with the vice versa (high powers and low deposition speeds) a bigger structure is obtained.
Both horizontally and vertically built specimens show that laser power, scan speed and scan spacing have a relevant effect on shear strength, hardness and density [28].
Regarding laser power, if it increases both the specimens show a higher shear strength, hardness and density. By comparison between a and b in Figure 2.9, it is possible to see how, using lower laser power, higher porosity is present.

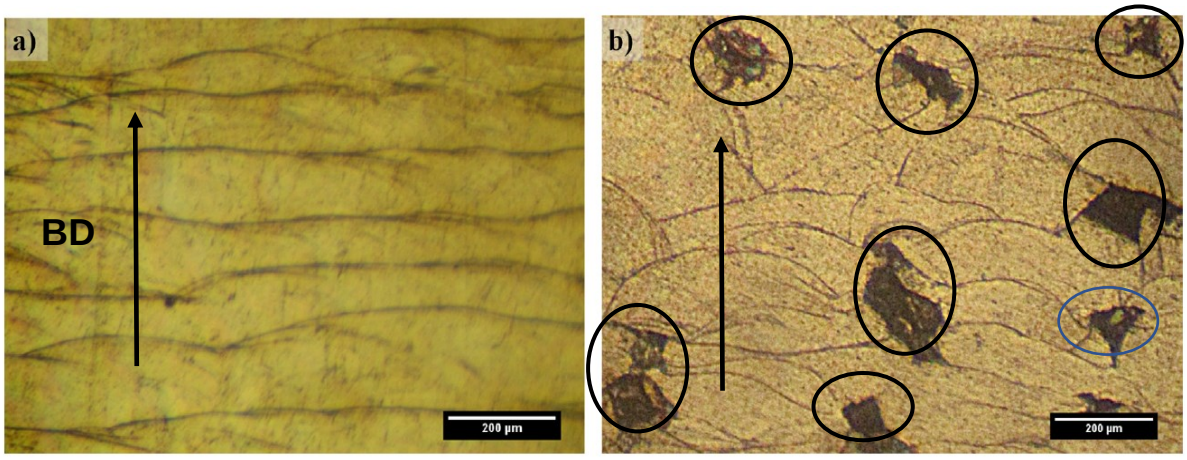

Figure 2.9. *Horizontally built specimens, in (a) with 90 W laser power, it is shown a structure totally absent of porosity, in (b) with 60 W it is possible to see consolidation defects (voids) between the adjacent lines where the lower laser power is passed* [28].

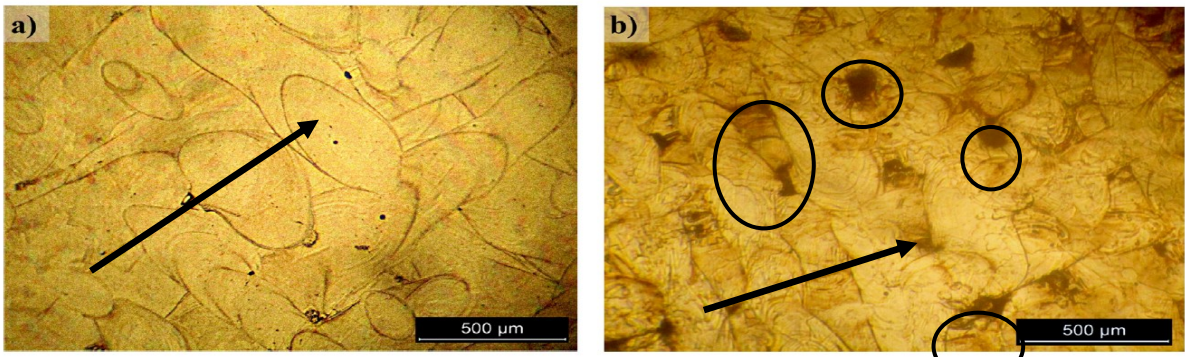

Figure 2.10. *Vertically built specimens, in (a) with 90 W laser power absent of porosity, in (b) with 60 W voids are present* [28].

Concerning scan speed, the vice versa phenomena is observed. To reduce the production time

high scan speed should be aimed, but by increasing the speed a lower energy density is delivered for second in a designated area. In the images it can registered a same trend for both the specimens directions: with an high scan speed there is the presence of voids as shown in Figure 2.10. Therefore, remembering the relationship between porosity and tensile strength, it is possible to declare an inversely relationship between scan speed and the mechanical properties.

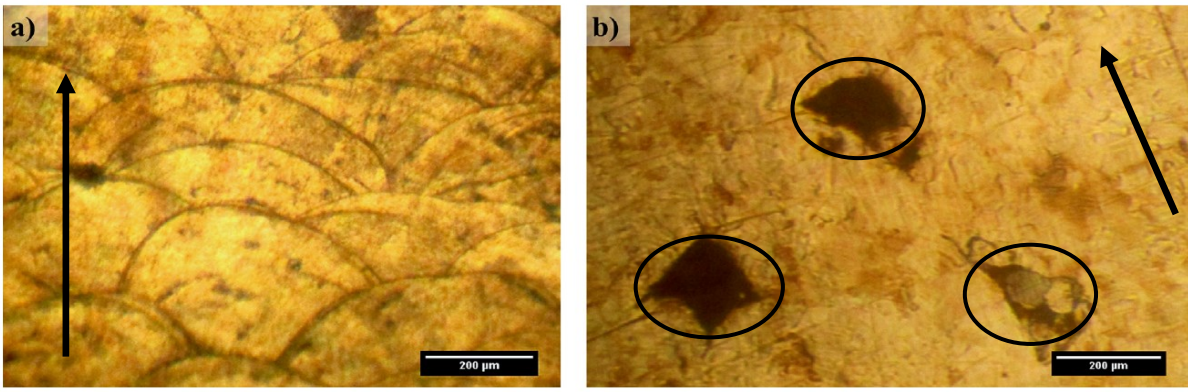

Figure 2.11. *Horizontally built specimens with scan speed of 417 mm/s (a) and 700 mm/s (b)* [28].

Moreover, an increasing of scanning speed causes a fragmentation of the scanning tracks and thus the surface is not cohesive.

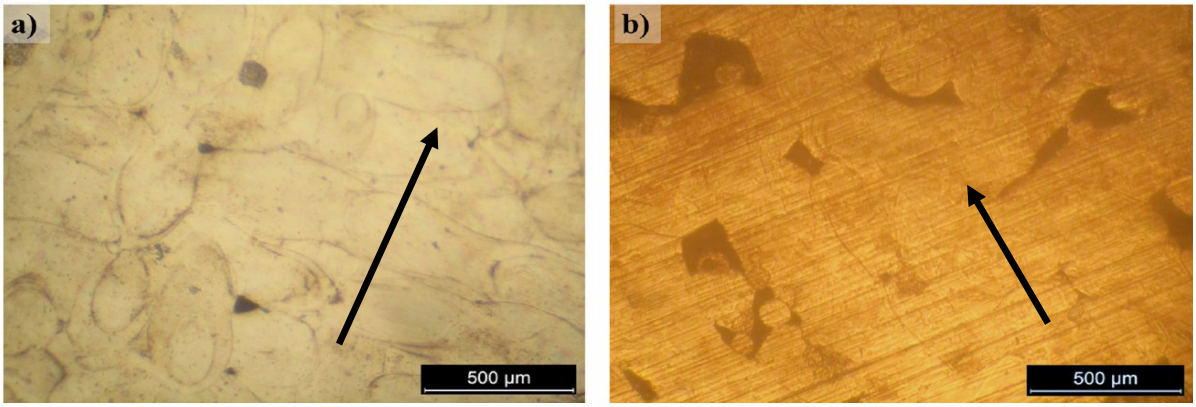

Figure 2.12. *Vertically built specimens with scan speed of 417 mm/s (a) and 700 mm/s (b)* [28].

An intimate relationship can be found between scan speed, laser power and hatch distance. About the part density, if in order to decrease the time production are necessary high speed, these one should be associated with high laser power and short scan spacing for having the same energy density. In fact, for both vertical and horizontal specimens, an high scan spacing means a poor sintering of adjacent powder regions, with a consequent imperfect bond between consecutive lines, as shown in Figure 2.13 and Figure 2.14.

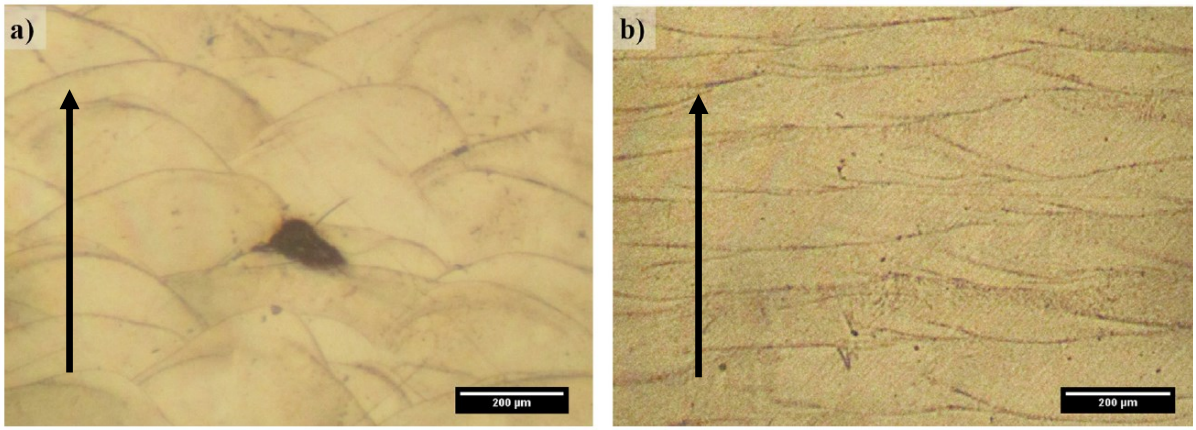

Figure 2.13. *Horizontally built specimens with scan spacing of 0.12 mm (a) and 0.08 mm (b)* [28].

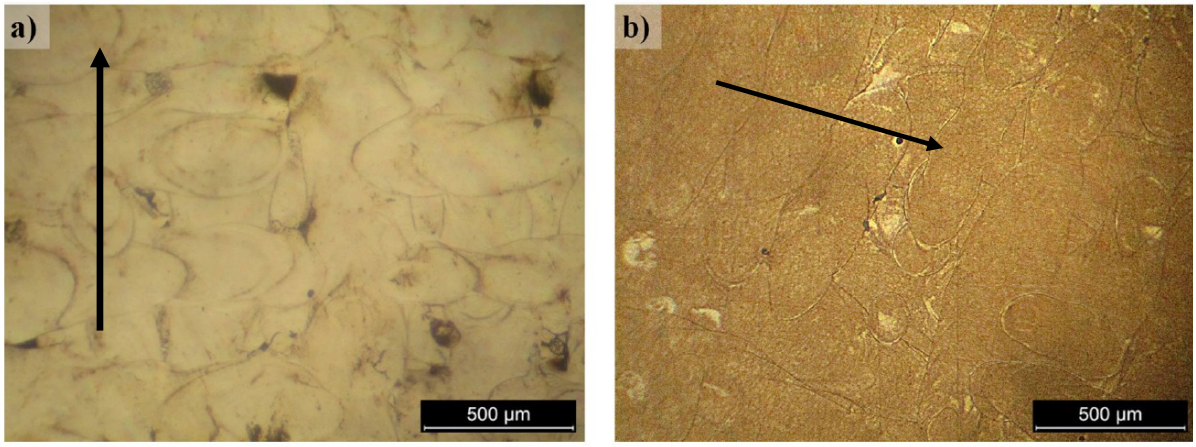

Figure 2.14. *Vertically built specimens with scan spacing of 0.12 mm (a) and 0.08 mm (b)* [28].

Moreover, to support this view, with higher spacing (or hatch distance) are obtained lower values for shear strength and hardness as a direct consequence of a low density.

2.3 Mechanical properties

This thesis project wants to contribute to the understanding of the mechanical behaviour of the materials produced using PBF manufacturing processes. Nevertheless, it can start by a recently improving knowledge about PBF state of art. This one, is a directly consequence of an improvement about the parameter management of the PBF machines. Taking into account equal parameters between conventional and PBF material using the same setup machine, is possible draw up reflections about compression and tensile test.

2.3.1 Compression test

Room temperature compression test

Focusing on the compression test, comparisons about the building direction influence can be done, analysing data set of AM cylinder specimens tested at room-temperature in agreement with EN ISO 6892-1. Considering cylindrical parts manufactured in vertical, horizontal and 45° building direction by an EOS M270 machine with the parameters in Table 2.4, is possible to

find common trends.

Table 2.4. *Adopted process parameters* [29]

Material	Laser power (W)	Laser spot size (µm)	Scanning Velocity (mm/s)	Laser thickness (µm)	Hatch distance (mm)	Energy density (J/mm$^{3)}$	Preheated build platform (°C)	Particle size (µm)	Protective gas
316L	200	100	1000	20	0.1	100	80	21-53	Argon

The process parameters are firstly related to laser, atmosphere and metal powder [30] and they affect the microstructure as well as the mechanical properties of the built part. In particular, laser power and scanning speed have a strong influence on the microhardness: this has a linear relationship with the density of parts [31].
The chosen specimens geometry presents a nominal diameter of 16 mm and a nominal height of 70 mm as shown in Figure 2.15. The used machine is an Instron 8802 testing machine with a standardized setup.

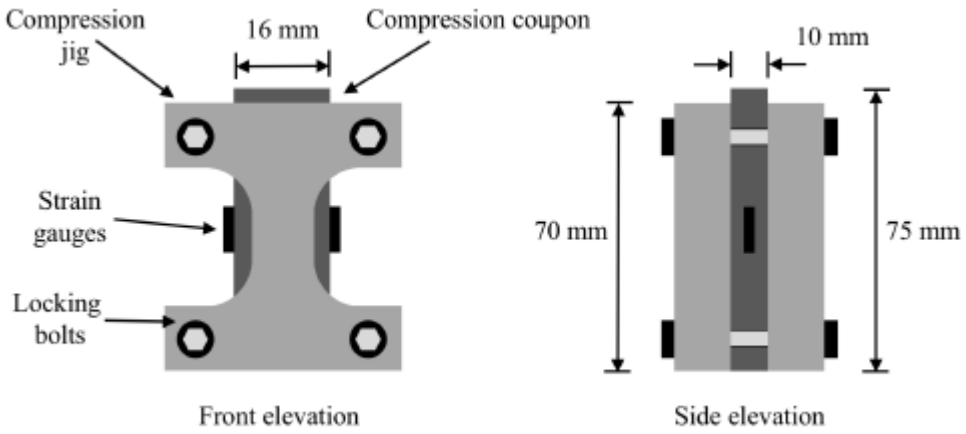

Figure 2.15. *Compression setup with Instron 8802 testing machine* [29]

Plotting the stress-strain curves for all the 316L specimens is possible to have an indication of the range of stress-strain responses. Taking into account the building direction of each specimen, the Figure 2.16 shows as for equal stress the specimens manufactured with 45° building direction present the smallest strains. This means that these specimens present a higher deformation energy, as shown in Equation 3, where w is the deformation energy per unit of volume:

$$w = \int_0^{\varepsilon} \sigma \, d\varepsilon \qquad \text{Equation 3 [32]}$$

Instead the biggest strains are shown by the parts manufactured with a vertical building direction. In other words, the stress-strain curves of the cylinders manufactured with 45° building direction stand in the middle between the other two directions.

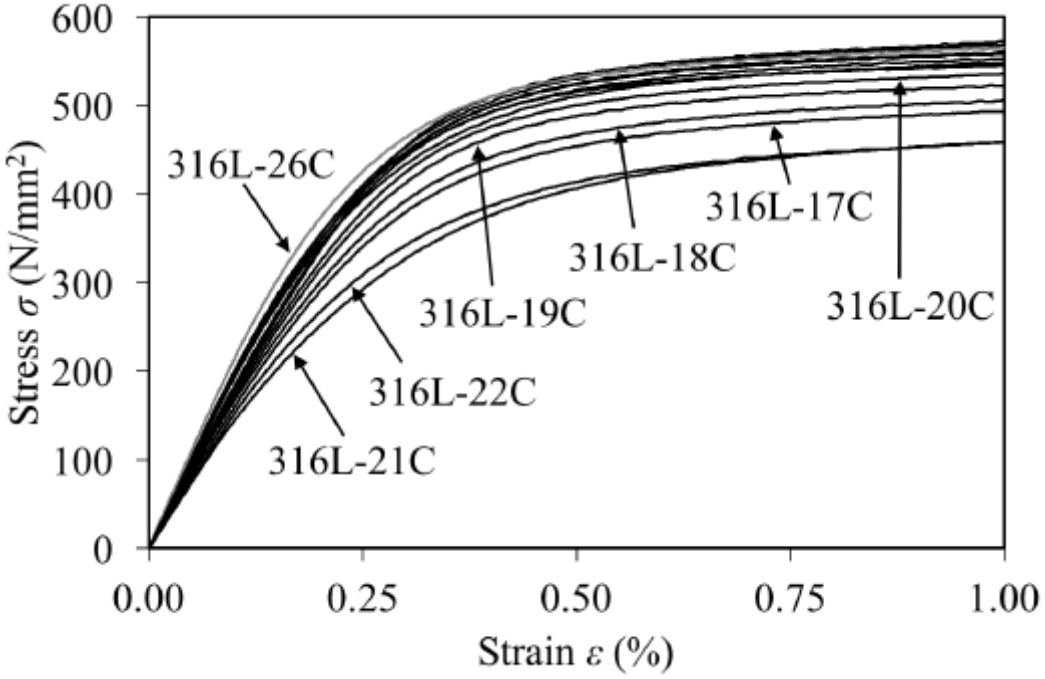

Figure 2.16. *Stress-strain curves of additive specimens in the compression test*

A correct evaluation about formability can be given only by considering also the mechanical properties. As shown in Table 2.5, by considering the mean values, the specimens manufactured with inclined direction present the best Young's modulus and the highest $\sigma_{0.2}$. Then it is possible to see as the parts with an horizontal building direction present higher E and $\sigma_{0.2}$ than the vertical one. Finally, if a comparison with the conventional manufactured 316L (with heat treatment [29]) takes place, the AM specimens show an lower average E but a really higher $\sigma_{0.2.}$

Table 2.5. *mechanical properties* [29]

Specimen	Direction	E [MPa]	$\sigma_{0.2}$ [MPa]
Average	H	174800	489 ± 32
	V	150800	403 ± 6
	45	203100	522 ± 17

Compression test at high temperature

A room temperature test gives a lot of information about the mechanical behaviour of a part build with PBF process, but only tests at higher temperature can provide a deep formability understanding. In this direction, analysing the true stress-strain curves coming from a recent high temperature compression test of 316L specimens [33], it is possible to find important trends. The room temperature curves remain an important reference. The used geometries are cylindrical specimens with nominal height of 6 mm and nominal diameter of 4 mm, coming from a box 12 x 7 x 106 mm manufactured from an EOS PBF machine in an argon atmosphere only with a vertical build direction as shown in Figure 2.17.

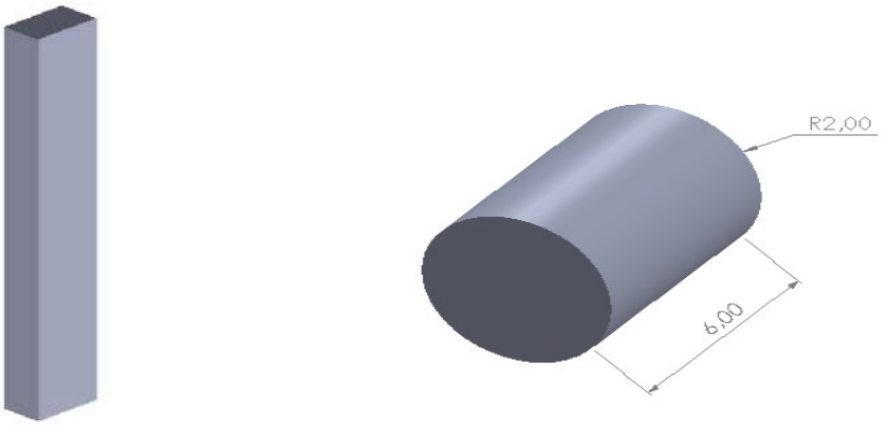

Figure 2.17. *In the left, initial 316L box (as fabricated) before the cylinder shape; in the right, specimen nominal geometry.*

The specimens are compressed with an INSTRON 8801 with a strain rate of 1 x 10^3 [s^{-1}] at 25°C, 500°C, 700°C and 900°C, as shown in Figure 2.18.

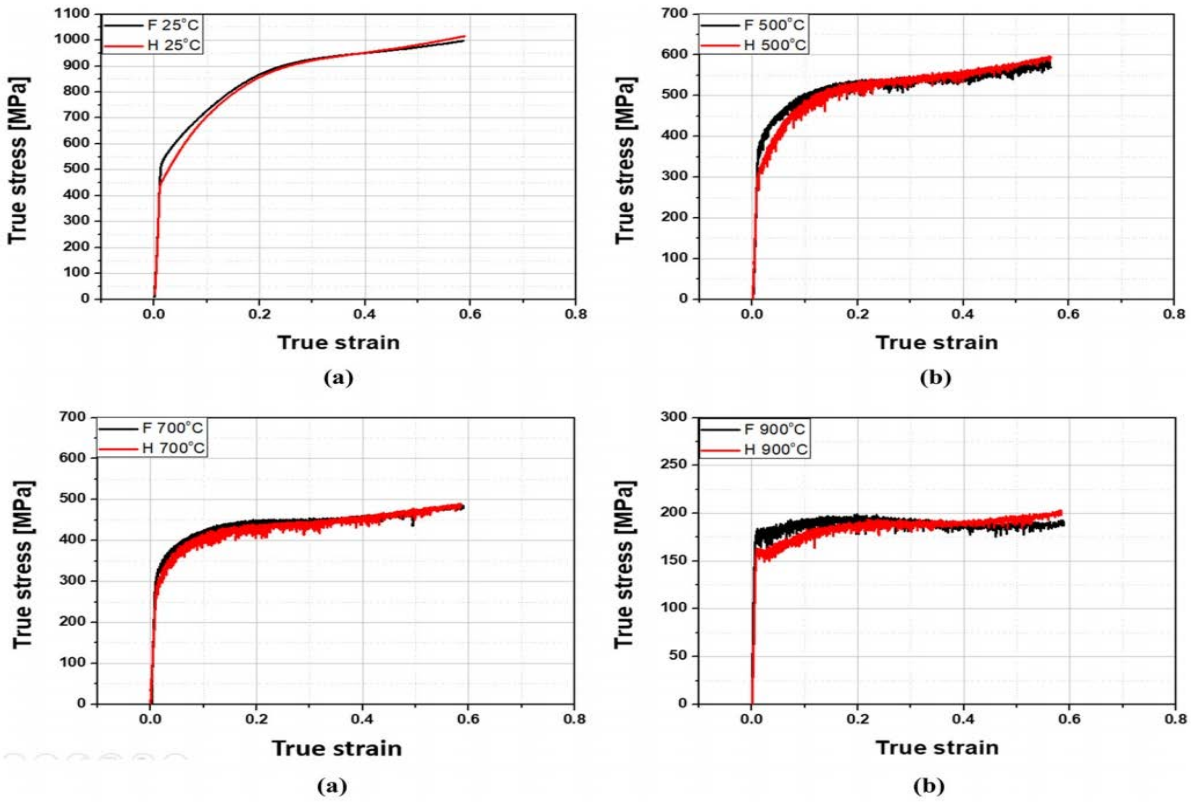

Figure 2.18. True stress-strain curves at 25°C, 500°C, 700°C and 900°C; H(with heat treatment), F(unless heat treatment)

Since the specimens are manufactured only with a vertical direction, only reasonings about the temperature influence can take place. Looking in Figure 2.19, focusing on the specimens unless heat treatment, the $\sigma_{0.2}$ at 500°C is the 1,45 % lower than $\sigma_{0.2}$ at room temperature. At 700°C the PBF 316L continues to have a tolerable resistance, but at 900°C it goes down.

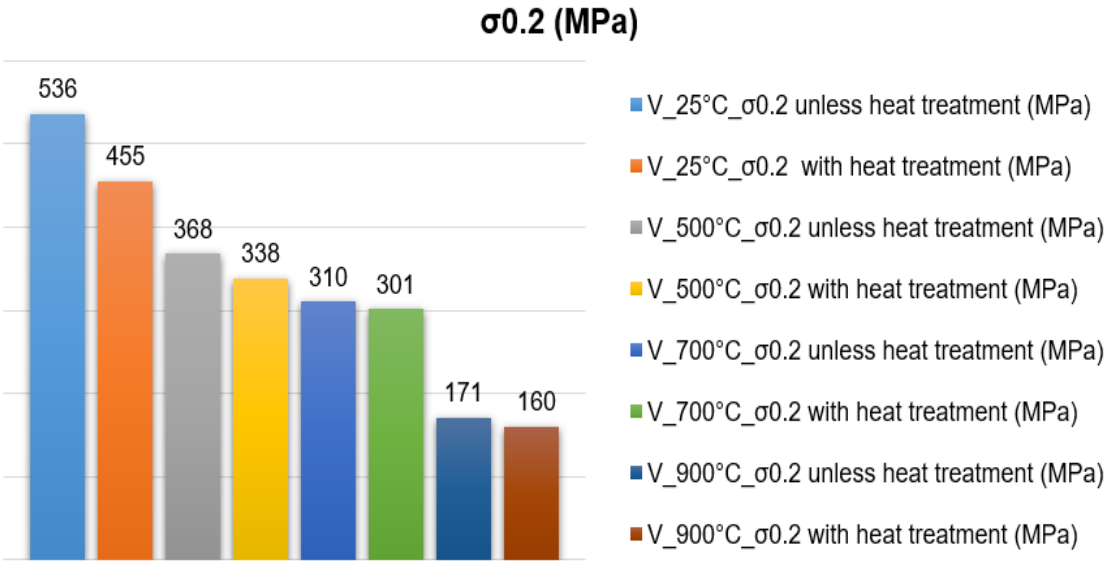

Figure 2.19. *Temperature influence with a constant vertical build orientation in $\sigma_{0.2}$ and in σ_{max} value*

If the σ_{max} value is considered, as shown in Figure 2.20 as there is not a consistent difference in its decreasing between 500°C and 700°C.

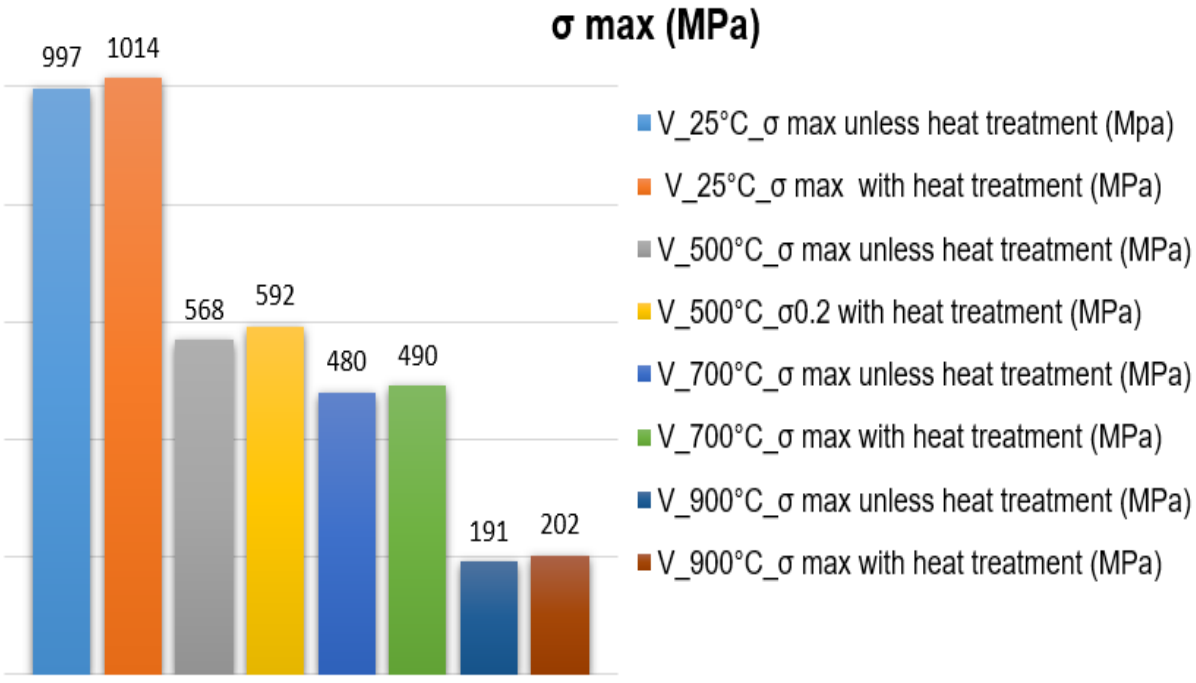

Figure 2.20. *Temperature influence with a constant vertical build orientation in σ_{max} value*

2.3.2 Tensile test

Room temperature tensile test

The compression test provides important data set about the process quality, nevertheless in this type of test the porosity has a small influence. For this reason, tensile test are necessary. Considering the specimen geometry in Figure 2.21, with a diameter of d = 6 mm and a practical length of 30 mm in agreement with the ISO 6892 – 1 standard tensile test can take place.

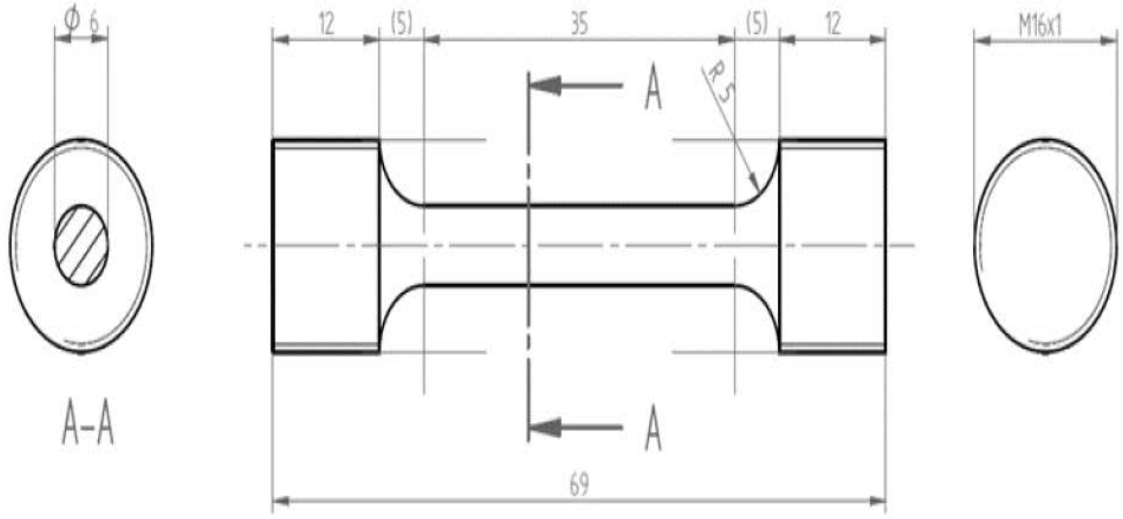

Figure 2.21. *Nominal geometry of the tensile specimens*

In Table 2.6 is possible to see the used parameters inside the range of the characteristics machine. The MYSINT100 is the model of a laser PBF machine produced by SISMA manufacturer (Italy).

Table 2.6. *Machine parameters used*

Laser power (W)	Laser spot size (µm)	Scanning velocity (mm/s)	Layer thickness (µm)	Hatch distance (mm)	Energy density (J/mm^3)	Preheating of build platform	Protective gas
150	70	700	50	0.07	61.2	No	Argon

If the tensile test results of a specimens group are plotted in diagram stress (MPa) – strain (%), it is possible to see in Figure 2.22 how the specimen with a 45° build direction (red) present for equal strains, highest stress values in comparison with the vertical build direction (green) and the conventional 316L (dark colour). The specimen manufactured with a vertical build direction shows a largest formability because the uniform deformation phase is until a 65% strain.

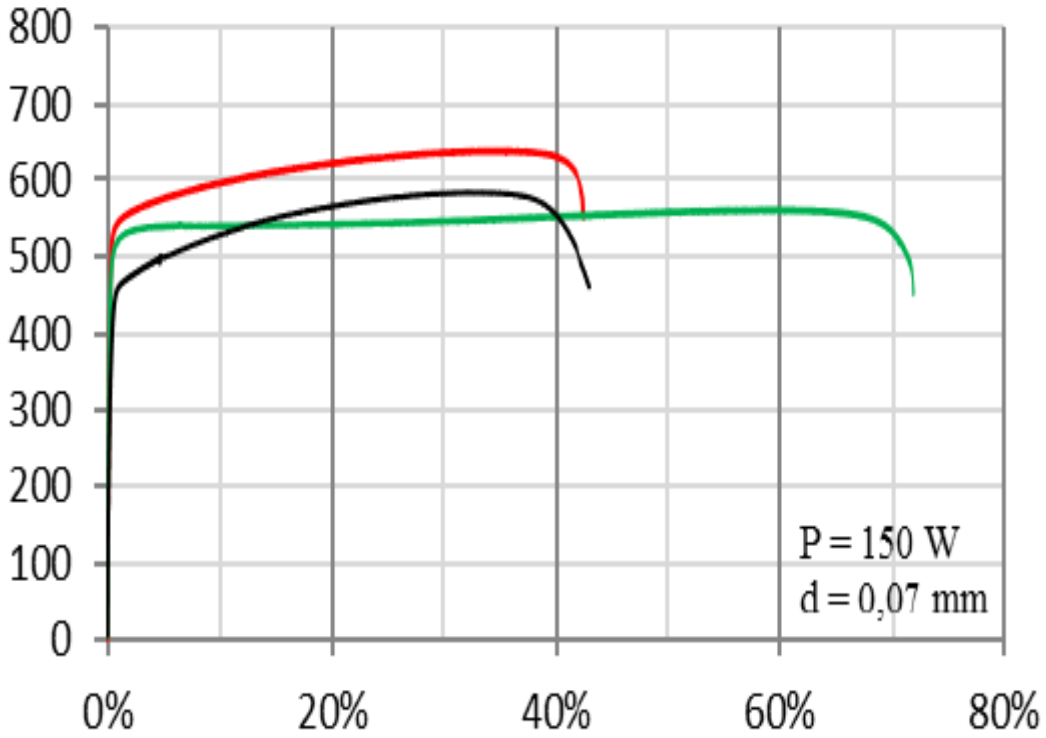

Figure 2.22. *Engineering stress – engineering strain diagram between conventional (dark colour) specimen and specimens with a 45°(red), vertical (green) build direction* [34].

Nevertheless, the vertical UTS is the slowest value, as shown in Figure 2.23. The best capability to absorb strain unless plastic deformations (yield strength), is however shown by the conventional material, but it is comparable with specimen manufactured with a 45° build direction.

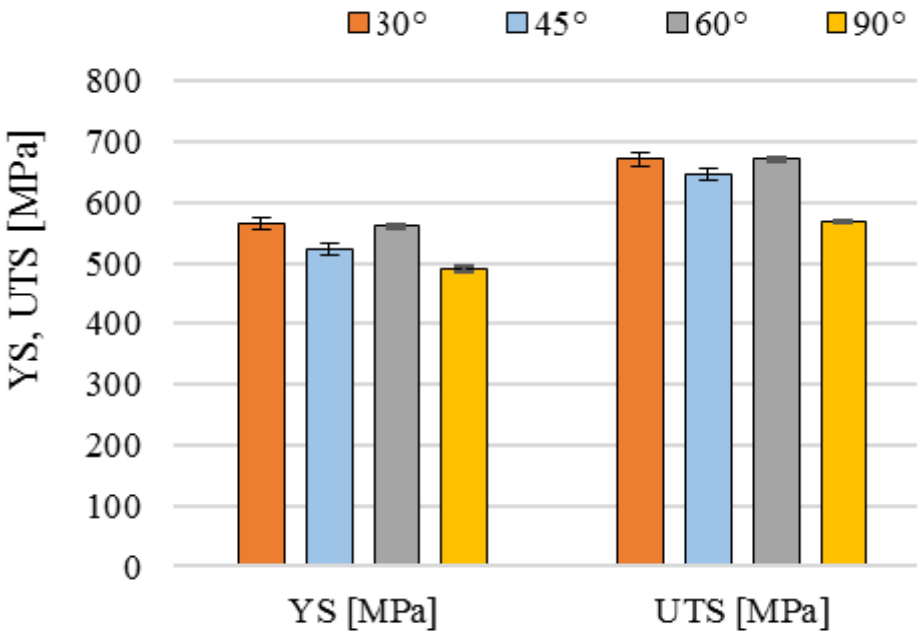

Figure 2.23. Comparison between the mechanical properties of specimens manufactured with a 30°, 45°, 60° and vertical build direction [34].

Others reflections can be done by considering PBF and conventional specimens manufactured with the geometry in Figure 2.24. Through the tensile test is possible to have information about

the material elastic and plastic properties under load.

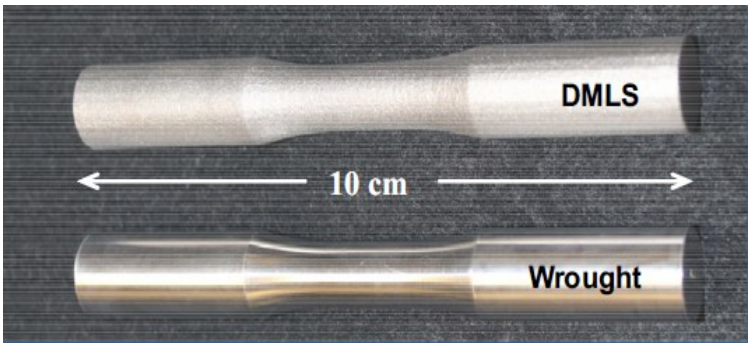

Figure 2.24. Nominal values in [mm] are respectively (h,d) = (100, 12,5) [36]

The PBF machine is a SLM 280 2.0 manufactured by the SLM Solutions Group AG (Germany). It provides a 280 x 280 x 365 mm^3 build envelope and presents two fibre lasers [35]. During the manufacturing process are used well calibrated process parameters, as shown in Table 2.7.

Table 2.7. *Used process parameters* [36]

Laser power (W)	Laser spot size (µm)	Scanning velocity (mm/s)	Layer thick-ness (µm)	Hatch distance (mm)	Energy den-sity (J/mm^3)	Preheating of build platform	Protective gas
195	100	750	40	0.07	93	Yes, 82°C	Nitrogen

The elastic modules are measured in flexure and stress-strain characteristics are analysed in tensile deformation [36].
When these experiments take place, it is necessary to take into account the effects of fabrication orientation, surface polishing and temperature upon mechanical behaviour.
By comparing the PBF specimens with the conventional materials, the data in Table 2.8 show that the stainless steel 316L presents stiffness nearly equal to that of conventional corresponding material, with specimens fabricated in the 45° direction exhibiting greater stiffness than the specimens fabricated horizontally.

Table 2.8. *Comparison between PBF and conventional 316L specimens* [36]

Material	Orientation	Module [GPa]	Yield [MPa]	UTS
Conv. 316L		187	345	563
PBF 316L	Vertical	180	496	717
PBF 316L	45°	193	473	680

Concerning the tensile deformation at room temperature for equal strain rate, the PBF 316L demonstrates nearly the same ductility, even if the yield strength PBF 316L (0.2% offset) is significantly higher (around 40%) than the conventional material, as seen in the stress-strain curves in Table 2.8.

Moreover the 45° direction specimens show a better Module and UTS than the conventional one and the horizontal cylinders have the highest UTS.
Another fundamental parameter is the layer thickness. Tensile strength and elongation at break also depend on the powder layer thickness during SLM. Samples horizontally built with 75 µm layer thickness demonstrate a little higher strength but with a really lower elongation at break than those built with 50 µm layer thickness, as shown in Figure 2.25.

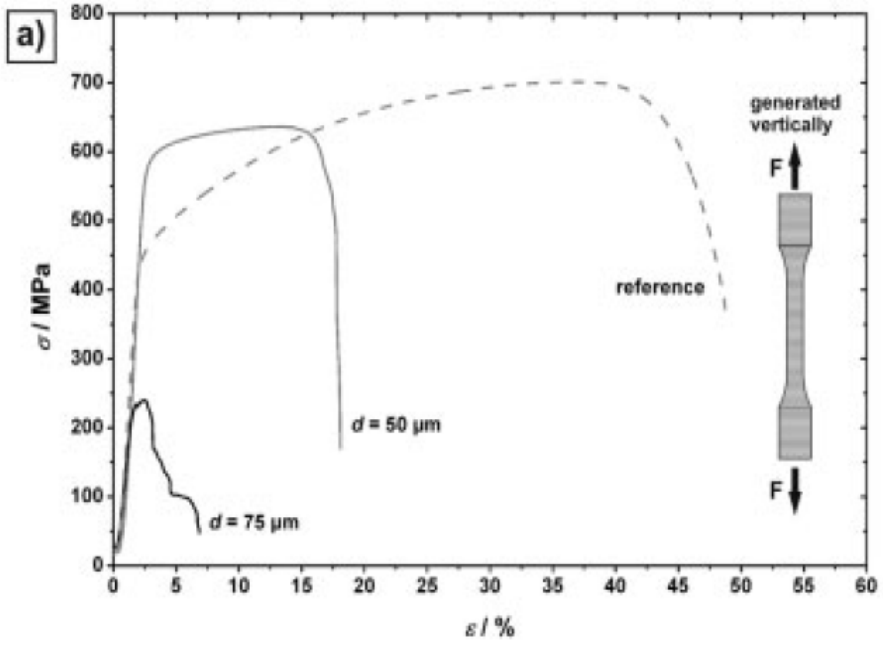

Figure 2.25. *Strain stress curves with tensile prove of 316L of vertically generated specimens. Machine laser power 100 W* [22]

Therefore, it is possible to find a trend where if d increases the mechanical properties improve but paying attention to the inferior limit with d<75 µm for the vertical direction.
It is necessary also taking into account that the horizontally built samples show higher strength properties and higher plasticity compared to the vertically built samples, as shown in Figure 2.26.

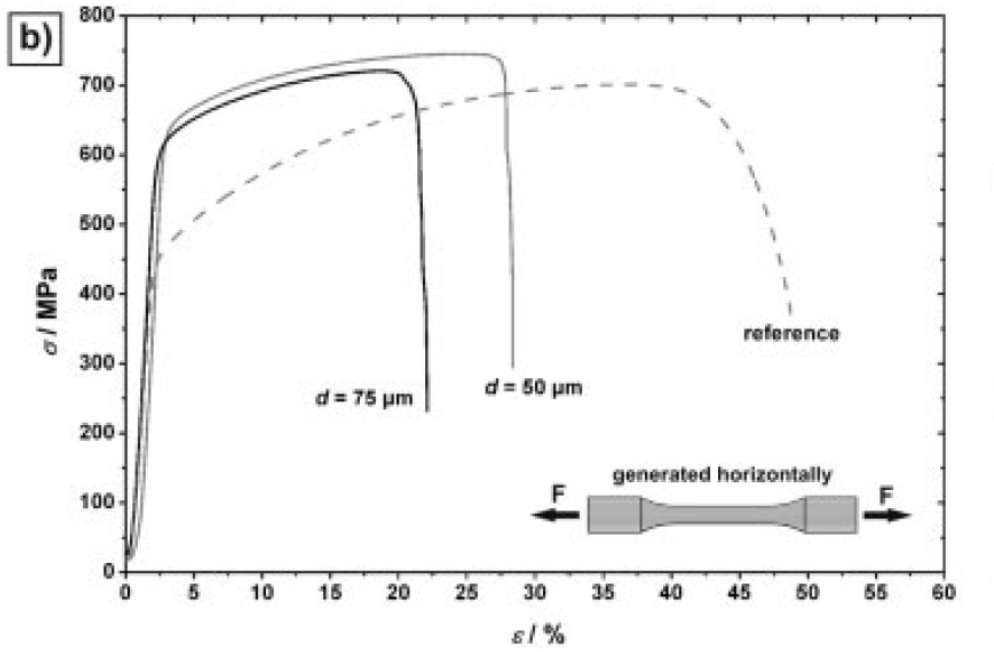

Figure 2.26. *Strain stress curves with tensile prove of 316L horizontally generated specimens. Machine laser power 100 W* [22]

Considering 316L stainless steel specimens manufactured in agreement with ASTM E606 standard through vertical, diagonal and horizontal build direction using the L-PBF Renishaw AM250 machine with the parameters in Table 2.9, several reflections can be done about the tensile tests.

Table 2.9. *Used process parameters* [37]

Laser power (W)	Laser spot size (µm)	Scanning velocity (mm/s)	Layer thickness (µm)	Hatch distance (mm)	Energy density (J/mm^3)	Preheating of build platform	Protective gas
400	65	1000	30	0.1	133.3	Not available	Argon

The tensile tests were performed at room temperature with a strain rate of 0.001 s^{-1} using a servo hydraulic MTS 858 testing machine with 25 kN load cells.
By watching the engineering stress strain curves in Figure 2.27, the horizontal building direction shows an higher yield strength but a smaller uniform elongation than the vertical building direction.

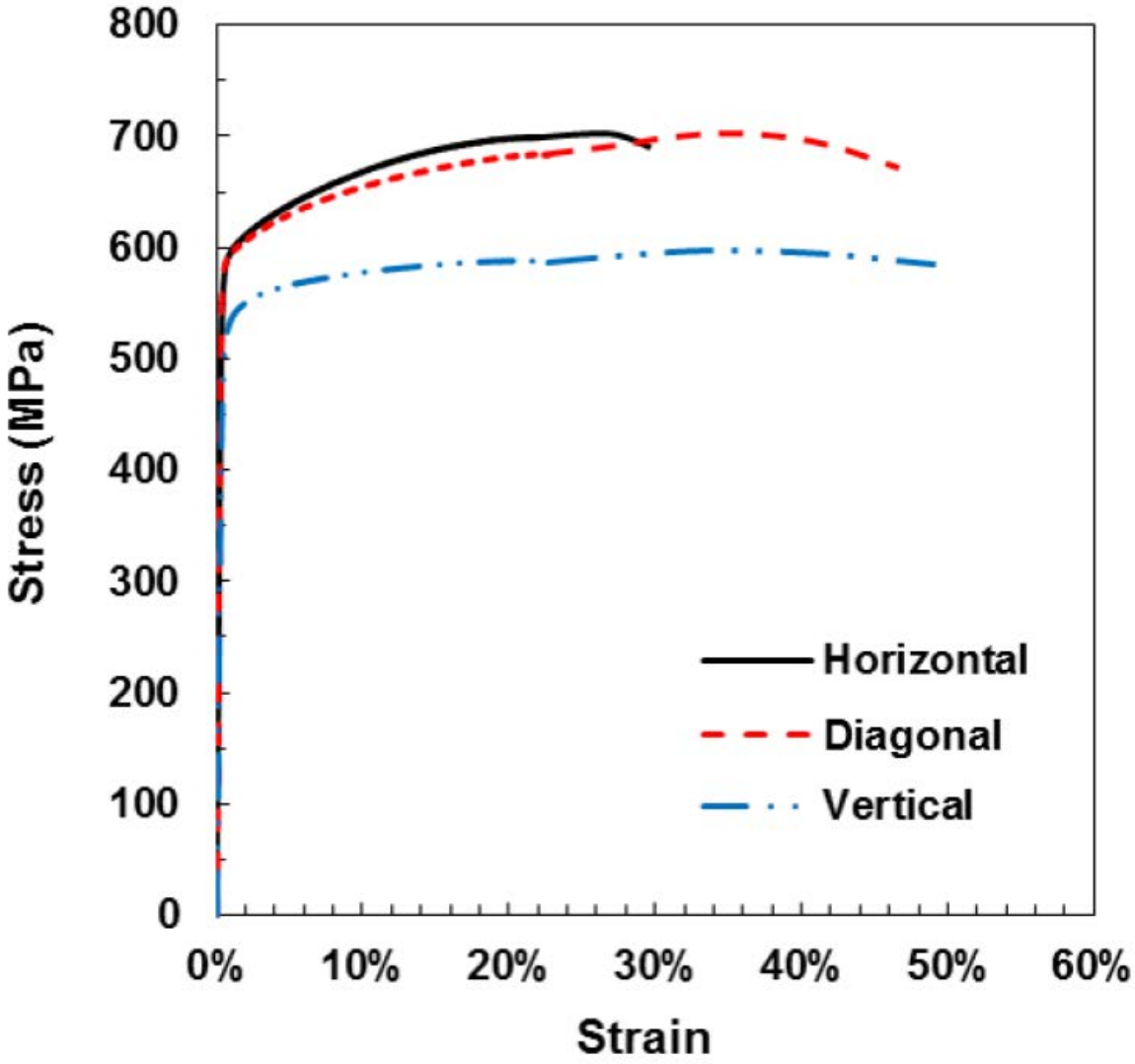

Figure 2.27. *Tensile engineering stress-strain curves for L-PBF 316L specimens built in horizontal, diagonal and vertical directions* [37]

Nevertheless, this knowledge level is not enough for 100% safe manufacturing parts.
It is necessary to carry out experiments to different setup conditions. This will be one of the goals of this thesis project.

2.4 Assessment of the State of art

The state of art regarding the mechanical properties of specimens manufactured with PBF process using 316L stainless steel, show a deep literature about room temperature tensile test. Nevertheless, data set about room temperature compression tests with 316L are limited and data with high temperature are rare. Almost absent result the 316L tensile test at high temperature. For this reason, this research work wants to explore the tensile and compression test at high temperature taking into account the temperature influence but also the orientation build direction of the specimens. Moreover, where it is possible, there will be a constant reference between the thesis results and the previous research.

3 Aims and methodology

The Thesis aim is the formability characterization of additively manufactured specimens with the Powder Bed Fusion process. The formability understanding, achievable with the mechanical properties' knowledge, allows to manage the forming processes, that take place after the Additive Manufacturing. The forming management means to find the compromise temperature between the force decreasing, at high temperatures, and the costs to achieve them. The AM process allows to manufacture close to the target geometry, with less material waste and a short process chain. This geometry will achieve the final shape after later forming processes.
A specific procedure including tensile and compression tests is used to assess the mechanical properties, the building direction influence and temperature influence of specimens manufactured with laser PBF. The 316L stainless steel parts are manufactured in three building directions: one perpendicular, one parallel and the last one with 45°. A good formability understanding, that is the material deformation quantity before the failure, depends by the assessment of factors influence. In this regard, the analysis of various preceding helps in the aim definition [38].
The formability is influenced from a:

- mechanical aspect, that is the process characteristics (applied state of tension, temperature variation);
- material aspect (mechanical properties evaluated taking into account the orientation for an AM material).

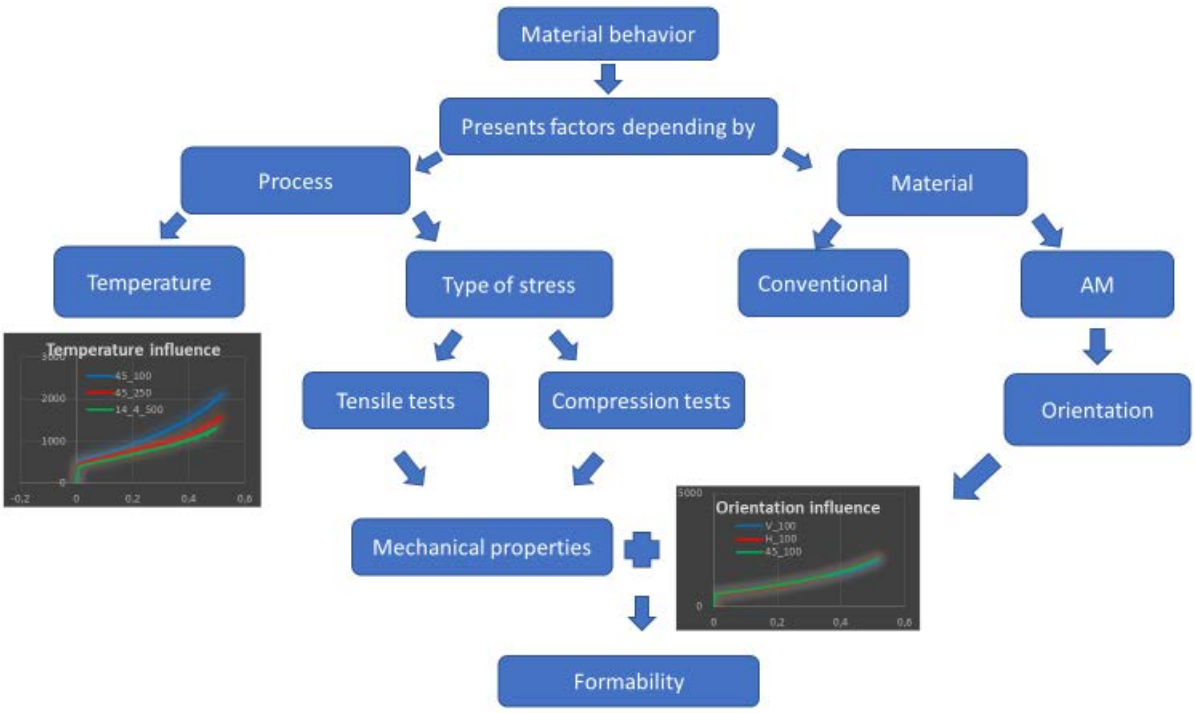

Figure 3.1. *Thesis task and goal summary*

In order to do this, both for the tensile and compression test, several specimens are produced in different orientation: vertically, 45° and horizontally. They are tested to different temperature (100°, 250°, 500°). By having these data set, are possible two comparisons:

- temperature influence;
- direction influence.

However the 316L has a high formability already at room temperature. For these reason, room temperature compression tests are needed. The specimens choice at room temperature is not random, but a strategy is followed: for every direction are selected specimens in different positions of the table machine in order to reduce the AM machine sistematic errors linked to the process.

4 Used machines and materials

4.1 Manufacturing phase

Specimens for the compression and tensile tests are built from 316L powder using Lasertec 30 SLM DMG Mori at the institute of manufacturing technologies at Friedrich-Alexander-Universität Erlangen-Nürnberg (Germany).

4.1.1 Lasertec 30 SLM DMG Mori

LaserTec 30, shown in Figure 4.1, is an AM machine working with the PBF process. This machine allows to realize mechanical parts with high density and optimum mechanical properties.

Figure 4.1. *LaserTec 30* [40]

It is especially suitable for productions with an high-mix, low volume parts and complex shaped workpieces. With the last improvements in the state of art, this model allows to achieve a recycling powder of 95%-98% [39].
The integrated CAM software is Celos, that with the RDesigner function carries out [40]:

- the CAD acquiring from Creo or SolidWorks;
- placement and orientation in the working table;

- support;
- slicing;
- hatching;
- copying;
- process control file generation;
- heat calculation.

As shown in Table 4.1, Lasertec 30 SLM DMG Mori can achieve highly accurate additive manufacturing of 3D parts with a layer volume of 300 x 300 x 300 mm, this means 3 axis with y-stroke, x-stroke and z-stroke from 0 mm to 300 mm.
The setup phase is slow because of the difficulty in the powder refilling: the powder has to go down completely from the table machine.

Table 4.1. *Lasertec 30 SLM nominal characteristics* [40]

Nominal tension	300 - 400	V
Frequency	50 - 60	Hz
Absorbed power	17.3	kVa
Required fuse	32	A
Required Power to the electrical circuit	250	KVa
Gas	Argon	
Purity degree	≥ 4.6	
Minimum gas consumption for production	1000	l
Average gas consumption	72	l/h
Minimum pressure	6	bar
Layer volume (x,y,z)	300 x 300 x 300	mm
Layer thickness	20 - 100	µm
Laser spot size	70	µm
Laser type	Fiber laser	
Max Laser power	600	W
Material	Ti, Cr-Co alloys, stainless steels	
Software	CELOS	
Machine weight	1200	Kg
Powder unit weight (vacuum)	540	Kg

4.1.2 Used materials and process parameters

The used material is the austenitic stainless AISI 316L steel with the chemical composition shown in Table 2.2, as already stated in the state of art..
The tensile and compression specimens, used for the tests, are built by Lasertec 30 with process parameters inside the recommended range by the manufacturer, as listed in the Table 4.2.

Table 4.2. *Used process parameters*

Laser power (W)	Laser spot size (µm)	Scanning velocity (mm/s)	Layer thickness (µm)	Hatch distance (mm)	Energy density (J/mm^3)	Preheating of build platform	Protective gas
219	70	744	50	0.11	53.5	No	Argon

After each layer, a contour parameter is used with two changings: laser power of 120 W and a scanning speed of 0.409 m/s.
The compression specimens have been manufactured before the beginning of this research work.
The scan pattern is a chess pattern with 2 mm by 2 mm of each field and alternating scan direction of 90 ° in each field, as shown with the arrows in Figure 4.2. For each layer the pattern is rotated by 67 °, in order to avoid too much repetitions of layer orientations with same alignment, minimize the internal defects [41] and increase the relative density [29].

Figure 4.2. Used scan pattern

4.1.3 Specimens geometry

In order to evaluate and compare the additive mechanical properties is necessary to conduct compression and tensile tests. To do these, the printed cylinder shapes for the compression and the parallelepiped shapes for the tensile, are worked with turning operations. In this way are obtained small cylinders and small tensile test pieces, that will be tested in agreement with respectively normative. Nevertheless, an additive evaluation needs a constant comparison with the conventional reference, therefore are manufactured directly thought turning operation also conventional specimens. This comparison needs the same shape specimens in order to do not have specific factor of influence.

Compression specimens

The compression specimens are obtained from long printed cylinders, that present a really high roughness. Their table placement, in threes as shown in Figure 4.3, allows to obtain a precise goal: minimize the machine systematic errors. In this regarding, if a table zone is critical for the printing machine, the defects due to a specific factor are not repeated in all the specimens: in this way some specific behavior will be limited in a few of specimens and not in the all specimens set.

Figure 4.3. *Compression cylinders arrangement in the machine table*

Focusing on the shape, as shown in Figure 4.4, the compression specimens present a cylindrical shape with a nominal diameter of 6 mm and a nominal height of 9 mm, in agreement with the normative.

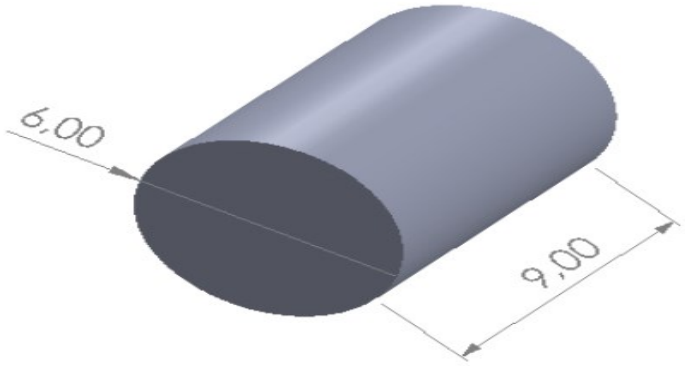

Figure 4.4. *Nominal measurements of compression specimens*

Tensile specimens

Similar but not same considerations have to be done for the parallelepipeds printed for the tensile tests. The printed components are placed only with vertical or horizontal build direction. This time a placement of vertical and horizontal parallelepipeds together in not possible because of the space optimization. In particularly, as shown in Figure 4.5, the parallelepipeds in group of three respectively in the upper left (UL), in the upper right (UR), middle (M), lower left (LL) and lower right (LR) table machine zones.

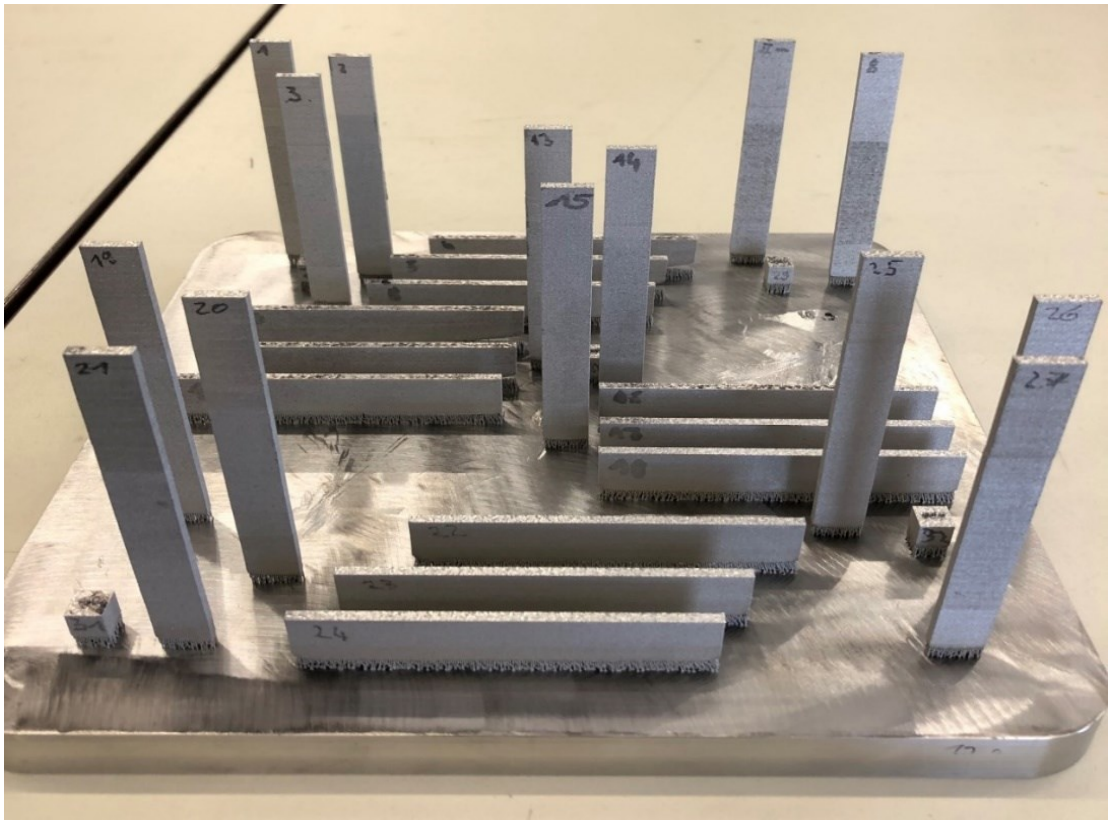

Figure 4.5. *Parallelepipeds arrangement in the table machine*

Once the parallelepipeds are printed and remove from the table, the turning operations take place. The parallelepipeds are transformed in small tensile specimens, as shown in Figure 4.6, in agreement with the normative. Also, in the tensile test, conventional specimens are manufactured for having a reference in the evaluation. They are manufactured with a 0° or a 90° rolling direction and with a 1.5 mm or 2 mm nominal thickness, in order to group from the minimum to maximum values the additive specimens.
The shape is the classical tensile test shape, with a L0 of 30 mm and a nominal width of 10 mm. The prove is done in agreement with the DIN EN ISO 6892-1.

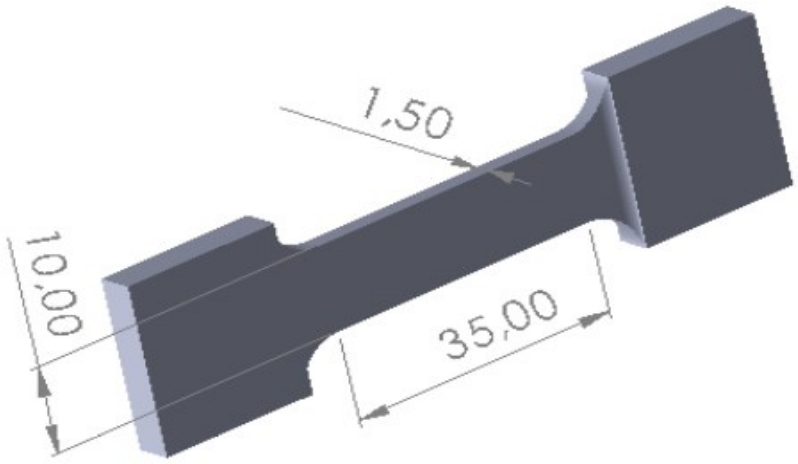

Figure 4.6. *Tensile specimen shape*

4.2 Testing phase

In order to conduct the compression tests are used two machine: the Thermo-Mechanical Simulator Gleeble 3500 (for high testing temperatures) and the Universal testing machine Walter+Bai 300 (for room testing temperature).

4.2.1 Gleeble thermomechanical simulator 3500

Gleeble machine can conduct compression and tensile test at different temperature. This machine is a fully integrated control mechanical and thermal testing system, as shown in Figure 4.7., combined with the software QuickSim. LVDT transducers, load cells and non-contact laser provide accuracy and measurements repeatability. It presents an hydraulic servo system capable to apply 10 tons of static force in compression or tension. The heating system can heat the specimens until rates of 10000 °C/s.

Figure 4.7. *Gleeble 3500* [42]

Machine setup

The compression tests are conducted at 100°, 250° and 500° to evaluate the formability. The tests have to conduct only after a deep understanding of the setup. In order to control the friction two tantalum foils between specimen and tool are used (one for each side), so the test can be considered to be an uniaxial compression test. Instead in order to have a correct heating transfer, graphite foils are placed. Looking the machine user manual, the recommended setup for steels in order to reach the isothermal condition is four graphite foils pieces of 0.25 mm in the R2 position and two pieces of 0.25 mm in R4 position [43], as shown in Figure 4.8 in agreement with ISO-T Anvils for Gleeble Systems, where:

- R1: cap and the interface;
- R2: graphite foils adjustable;
- R3: base and interfaces;
- R4: graphite foils adjustable;
- R5: copper disk and interfaces.

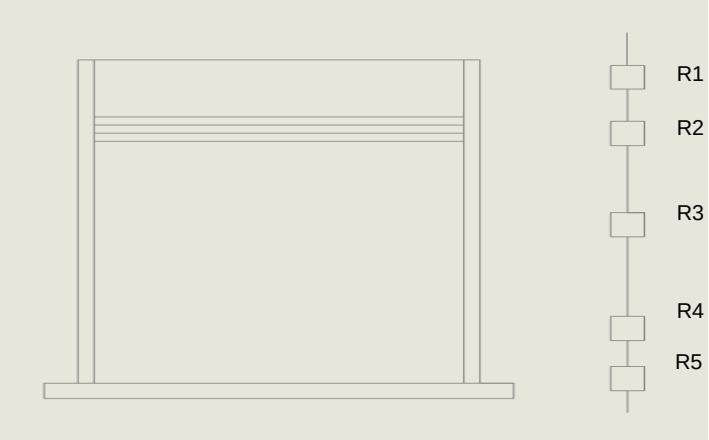

Figure 4.8. *Resistance of an ISO-T anvil assembly: from top to bottom R1, R2, R3, R4 and R5* [43]

The elastic deformation covers a fundamental role: the data set have to take into account a correct gauge length [mm]. In fact, it is necessary to use for the strain computing only the gauge length unless the elastic contribution due to the graphite foils.
The first tests take place with the conventional specimens in order to check the used setup. Once positioned between the punches, through two thermocouples the specimen can be received the heating, as shown in Figure 4.9. It is important that the cables are in the middle in order to have a temperature distribution in agreement with the target temperature.

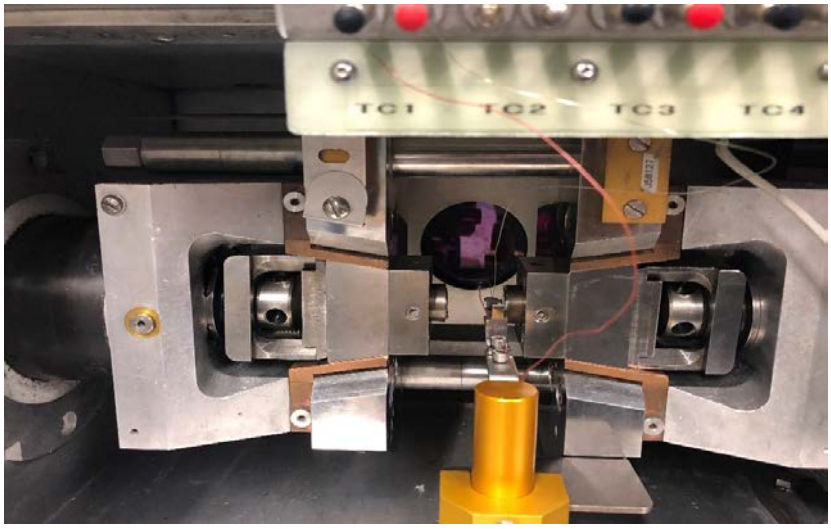

Figure 4.9. *Cylinder specimen placement between the punches*

As shown in Figure 4.10, the used setup together to suitable temperature gradients, allows a limited overshoot, this means good setup because there is an optimum overlapping between the target temperature and the actual temperature.

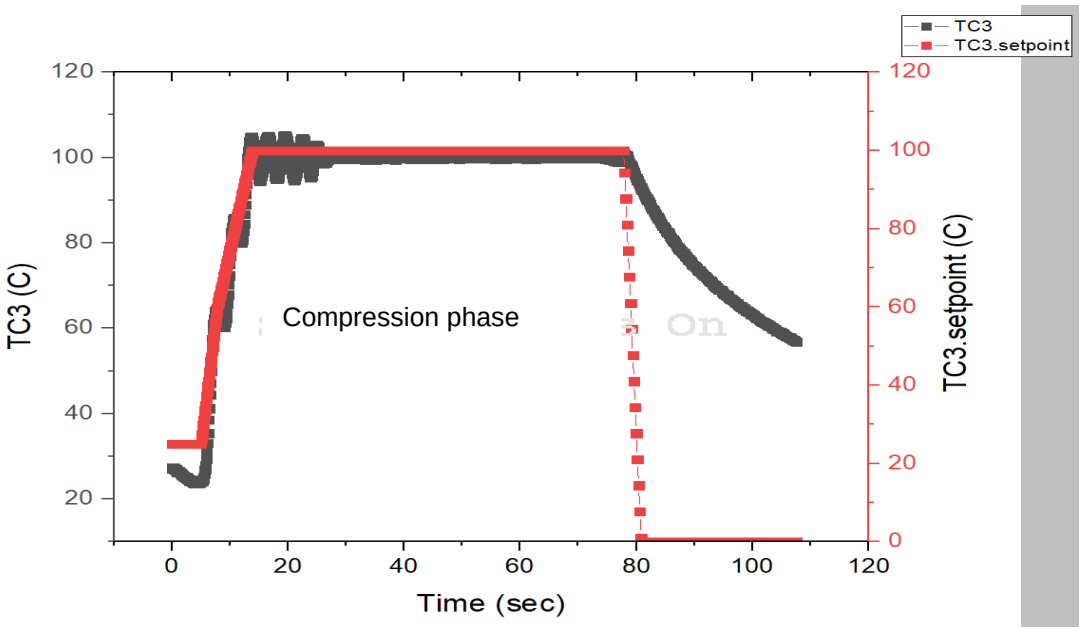

Figure 4.10. *T-t curves, where a correct heating transfer is obtained through different ∇ T*

A good overlapping means that the machine is fast with the heat transfer and it

is found taking into account several factors:

- ∇T;
- T target;
- PID controller;
- electrical resistance;
- specimen material;
- influence of the tool material;
- available heat power of the machine;

where the machine PID controller and the material electrical resistance represent the machine parameters. The ∇T management is possible through the software QuikSim linked to the machine, as shown in the equation and in Figure 4.11:
starting from the constant value $v = 12{,}5\ \frac{k}{s}$ is possible to manage the heating time with different gradients taking into account the equation:

$$time\ interval\ = \frac{T f\ - Ti}{v} \qquad \text{Equation 4}$$

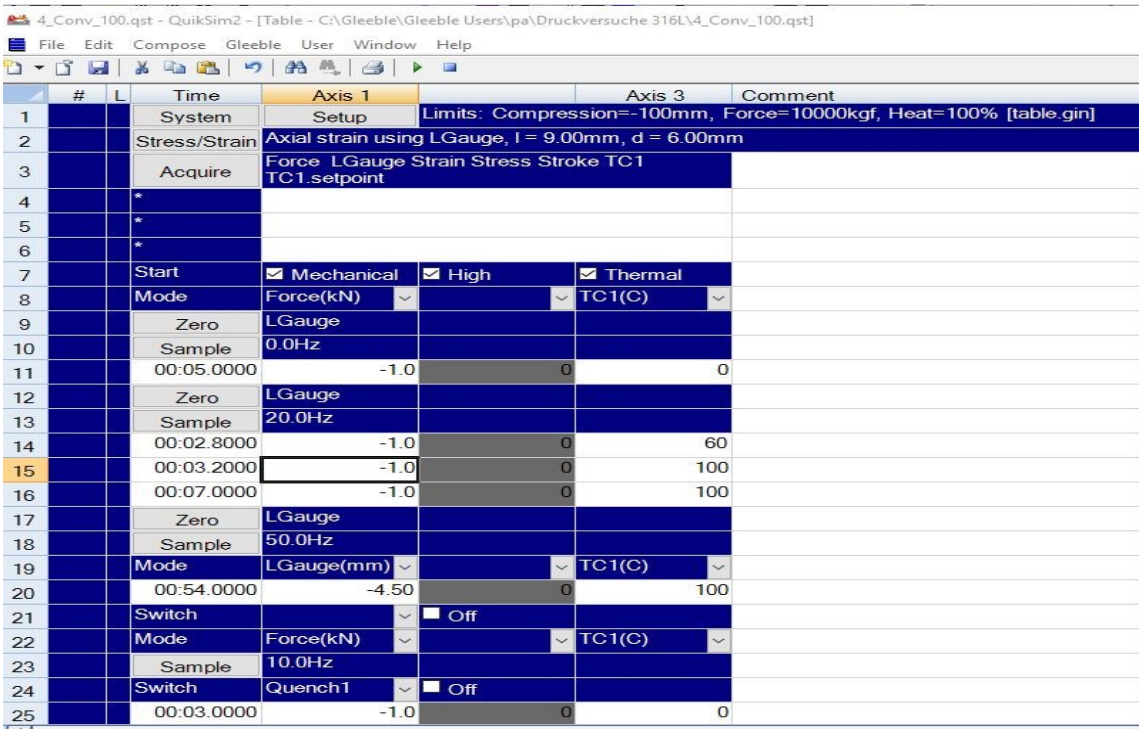

Figure 4.11. *In this script the heating time is managed as 00:02:8000 s (Tf =60°C, Ti=25°C), 00:03.2000 (Tf =100°C, Ti=60°C) and other 00:07:0000 in order to homogenise the temperature*

Once the data test is acquired by the QuickSim software, it is possible to export and then analysed them in an Excel format.

Scattering

Because of the necessity to warm the specimen, there is an initial phase where the data set about force and time do not increase in a constant way: the scattering. This cloud of data, as shown in Figure 4.12, has not to be analyse because it represents the data set from the environment temperature until the goal temperature of 100°C, 250°C or 500°C, therefore the data have to be cut. The Excel data set have to be acquired only when the force shows a monotone behaviour.

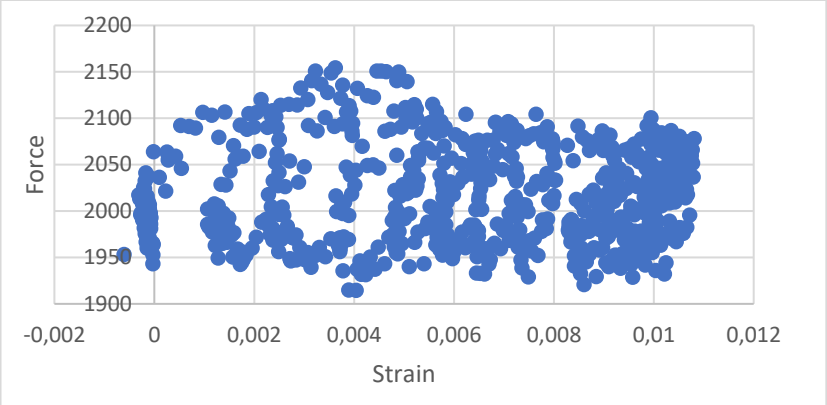

Figure 4.12. *Initial scattering of specimen 9_3_H_250°C*

In order to make easier the data set analysis, it is possible to plot a force-time diagram where is cleaner the beginning the monotone behavior. Nevertheless, the scattering is also a little bit provoked by the graphite foils film which is compressed in beginning phase.

4.2.2 Walter+Bai 300

In order to have a larger formability understanding, compression and tensile tests are carried out at room temperature with the Walter+Bai 300 machine manufactured by Zwick. For each test, a specific tool is placed together the main structure, as shown in Figure 4.13.

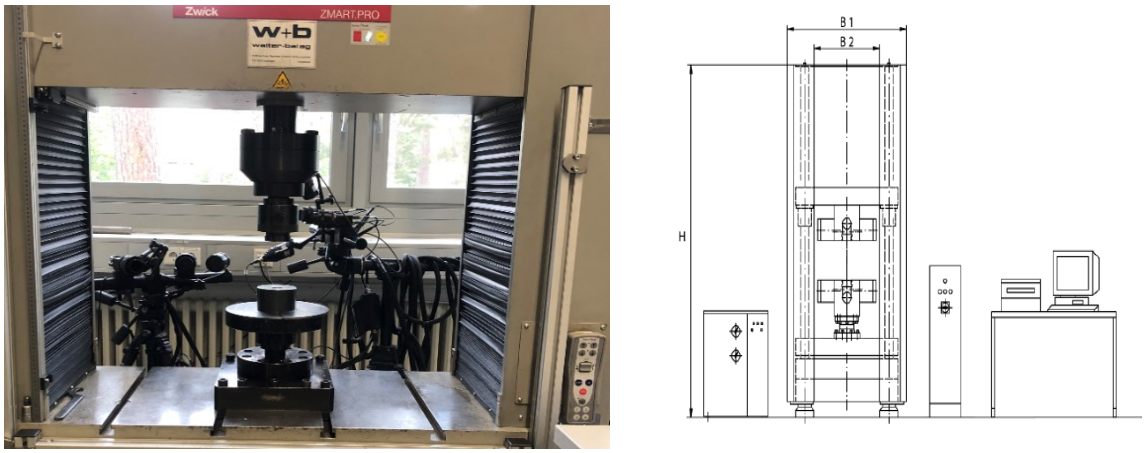

Figure 4.13 (a) *Compression tool* **(b)** *Software-machine bound* [44]

The traverse movement is controlled with a feed rate of 0,001 – 500 [$\frac{mm}{min}$] thanks to its altern current motor. Through a load cell, data set regarding the force and the stroke can be acquired, with a force range from from 0.6 kN to 300 kN [44].

The control software TestXpert 2.0 (as shown in the figure) enables to record the traverse stroke and the process forces during the formability process at a frequency of 50 – 500 Hz. Through the scripts of this software, the measurement can be exported and analyzed in Excel files.
The scattering is also present in a small quantity in the RT tests because of the Teflon film presence.

Clarified the machines and the setup used it is possible to analyze the results. Every specimen set presents the necessity to be optimize for the mechanical properties' evaluation. In order to do it, in the next chapters concerning the compression and the tensile tests will be done comparison only after a deep data optimization.

5 Results

5.1 Compression test

The tests are conducted in order to evaluate the temperature influence and the building direction influence.
Considering a constant strain rate, the stress strain curves are analysed for each orientation at each temperature: room temperature, 100°C, 250°C, 500°.
The influence understanding needs the fixing of one of two comparison parameters and the variation of the other: the building direction influence is evaluated for equal temperatures, instead the temperature influence is evaluated fixing a common build direction.
In the first instance, the temperature influence is analyzed: first the high temperature influence, then the room temperature curves.
In the second instance, the building direction influence is evaluated at high temperatures (500°C, 250°C, 100°C) and at room temperature.

For both the comparisons, is present a constant reference to the conventional material in order to focus on the best specimens, that is the specimens with mechanical properties greater or equal than the conventional one. The results are plotted with engineering stress strain curves, but in order to allow comparisons with the state of art in some cases are present also the true stress strain curves.
In the diagrams, above all with high temperature curves, the scattering curves is taken into account: the strain is normalized because the material does not present strain since zero stress.
From the results analysis, specific behaviours and conclusions can be found. Nevertheless, the plotted curves give only a qualitative point of view the mechanical properties. Therefore, in order to have a clear quantitative evaluation, the general test campaign evaluation is widely analyzed with tables and histograms taking into account the uncertainty. In this regarding, in the temperature comparisons are analyzed the elastic mechanical properties ($\sigma_{0.05,}$ $\sigma_{0.2}$), the mechanical properties after elastic limit (σ and ε with a 55% height reduction with the corresponding elastic ε_{el} and plastic ε_{pl} amount) and are inserted also the maximum σ and the maximum ε recorded in the test. Then with the build direction comparisons are described the elastic ε_{el} and plastic ε_{pl} values in percentage terms. For every strain value is necessary to take into account the elastic and plastic amount, also considering the values with or unless the scattering contribution.
It is better to evaluate the room temperature curves singularly in other diagrams because of the different machine and different test setup used compared to the high temperature curves.
For each parameter combination (number of repetitions n = 3) only one mean representative curve is shown. In this regarding, only after the build orientation comparison for equal temperature values analysed in section 5.1.2, it will be possible to have a clear overview.

5.1.1 Temperature influence for equal building direction

Temperature influence with horizontal building direction

In order to analyse the temperature influence with horizontal specimens build direction, in Figure 5.1 are plotted the mean engineering stress-strain curves of horizontal specimens tested at high temperatures. Before is done a qualitative analysis of the curves focusing on their diagram position and then a more quantitative understanding is possible through histograms and tables.

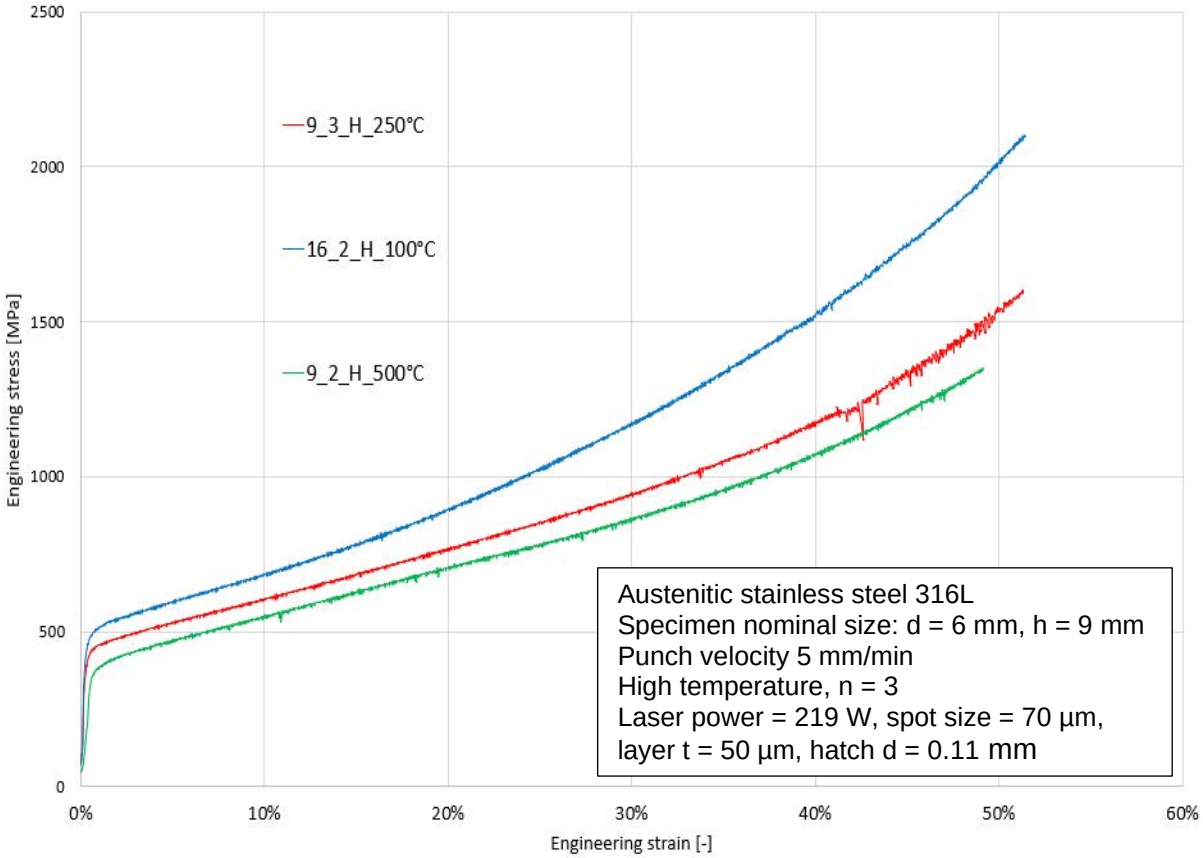

Figure 5.1. *High temperature influence for equal horizontal building direction*

As shown in Figure 5.1, the 100°C stress-strain curve is the highest one, in agreement with a common metal material behavior in the presence of a temperature increasing.

In this regarding, if a forming operation has to be done, the 500°C $\sigma_{0.2}$ is clearly the lowest therefore the material will start flow before.

Moreover, for equal stress the 100°C curve shows smallest strain compared to 250°C and 500°C. One of the most interesting result is that 250°C and 500°C curves are not so far between them, therefore even if there is a working condition changing until 500°C, the additive workpiece will maintain a deformation energy comparable with 250°C. In fact, in agreement with Equation 3 [32] of the state of art, the deformation energy amount represented by the area below the red curve is not so larger compared to the green one.

Considering other tested specimen set, with the same comparison method as shown in Figure 5.2, interesting comments can be done.

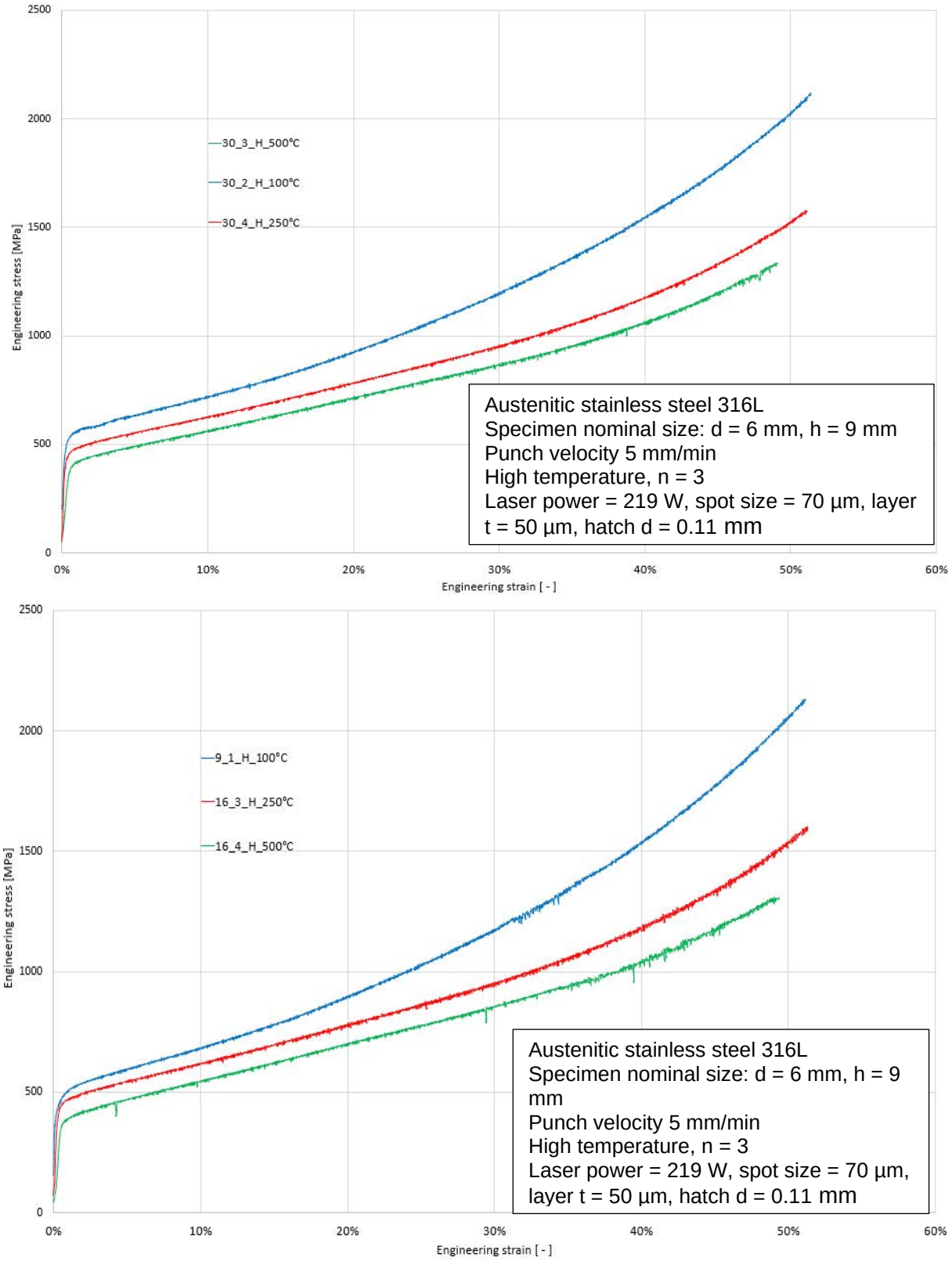

Figure 5.2. *High temperature influence for equal horizontal building direction*

Focusing on low strain values, the 30_2_H_100°C specimen shows an high gradient, while the 9_1_H_100°C specimen is really close to the 250°C specimen because of its slower gradient. The 30_2 specimen present also a stress decreasing during the passage between elastic and plastic part. The green and red curves continue also in this specimen set to be closer compared

to the distance between the 100°C and 250°C.
A constant reference with the conventional specimens is necessary. Regarding this, a good approach is the evaluation of each additively manufactured specimen taking into account the respective conventional one, that averagely better represents the conventional behavior for that specific temperature. For this reason, in Figure 5.3 are plotted each additive specimen at high temperatures (100°C, 250°C, 500°C) and RT together the corresponding mean conventional curve.
The diagrams allow only a qualitive overview of the results. In order to have a quantitative analysis is necessary to consider the average mechanical properties of the all specimen sets manufactured with an horizontal building direction. For this reason are summarized in Table 5.1 all the mechanical properties at different high temperatures for equal build direction. Later, in the section 5.1.2, the data will be also described with histograms.

Table 5.1. *Horizontal mechanical properties at high temperature*

	(MPa)	$\sigma_{0.05}$	$\sigma_{0.2}$	σ, 55% h reduction	σ max
H_100°C	Average	417	475	1759	2087
	±	33	35	11	46
H_250°C	Average	375	434	1334	1595
	±	14	14	9	14
H_500°C	Average	356	383	1195	1334
	±	9	15	18	22
Conv_100°C	Average	432	490	1697	2061
	±	5	30	14	22
Conv_250°C	Average	429	480	1247	1513
	±	11	8	10	11
Conv_500°C	Average	425	475	1237	1321
	±	8	5	36	20

As it is possible to see, the qualitive results are confirmed from the a decreasing of the $\sigma_{0.05}$ and $\sigma_{0.2}$ with the temperature increasing. The same trend of stress decreasing with temperature increasing is also present with the sigma in correspondence of a 55% height reduction and for the maximum stress recorded in the prove. If the conventional materials are considered, interesting comments can be done. The conventional specimens maintain higher $\sigma_{0.2}$ at low deformation values, instead for high deformation values the specimens manufactured with an horizonal build direction present higher σ, 55% h reduction value. This means the presence of a changing point in the stress strain diagram. For this reason is useful to evaluate the trend looking in Figure 5.3.

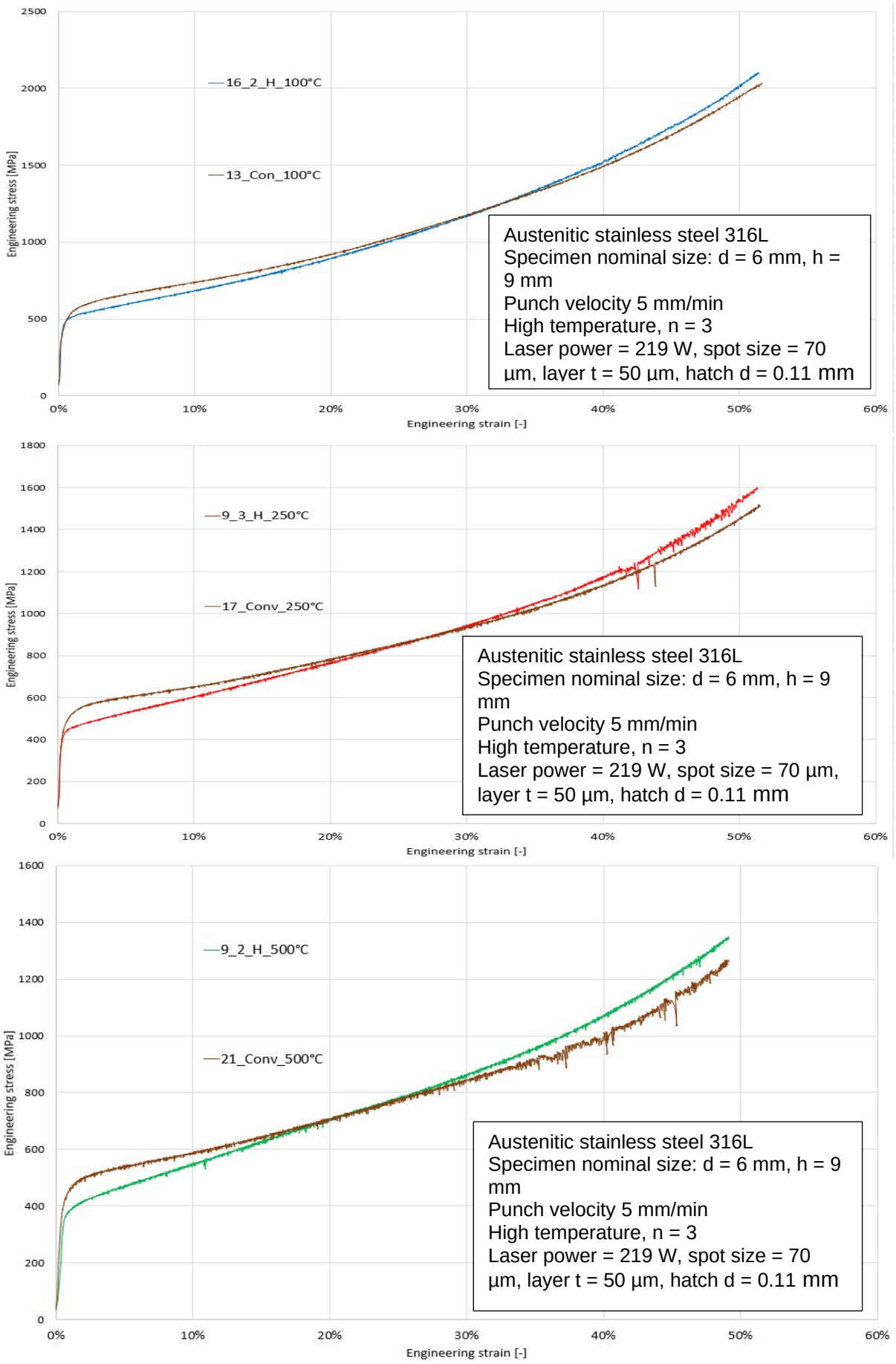

Figure 5.3. *Horizontal and conventional building comparison for each high temperature*

Starting from the high temperatures, until 20% ÷ 30% the conventional specimens show a higher resistance to the deformation, but after 30% the higher energy deformation is given by the additively manufactured specimens.
If the room temperature curves are plotted, as shown in Figure 5.4, a different behaviour is present.

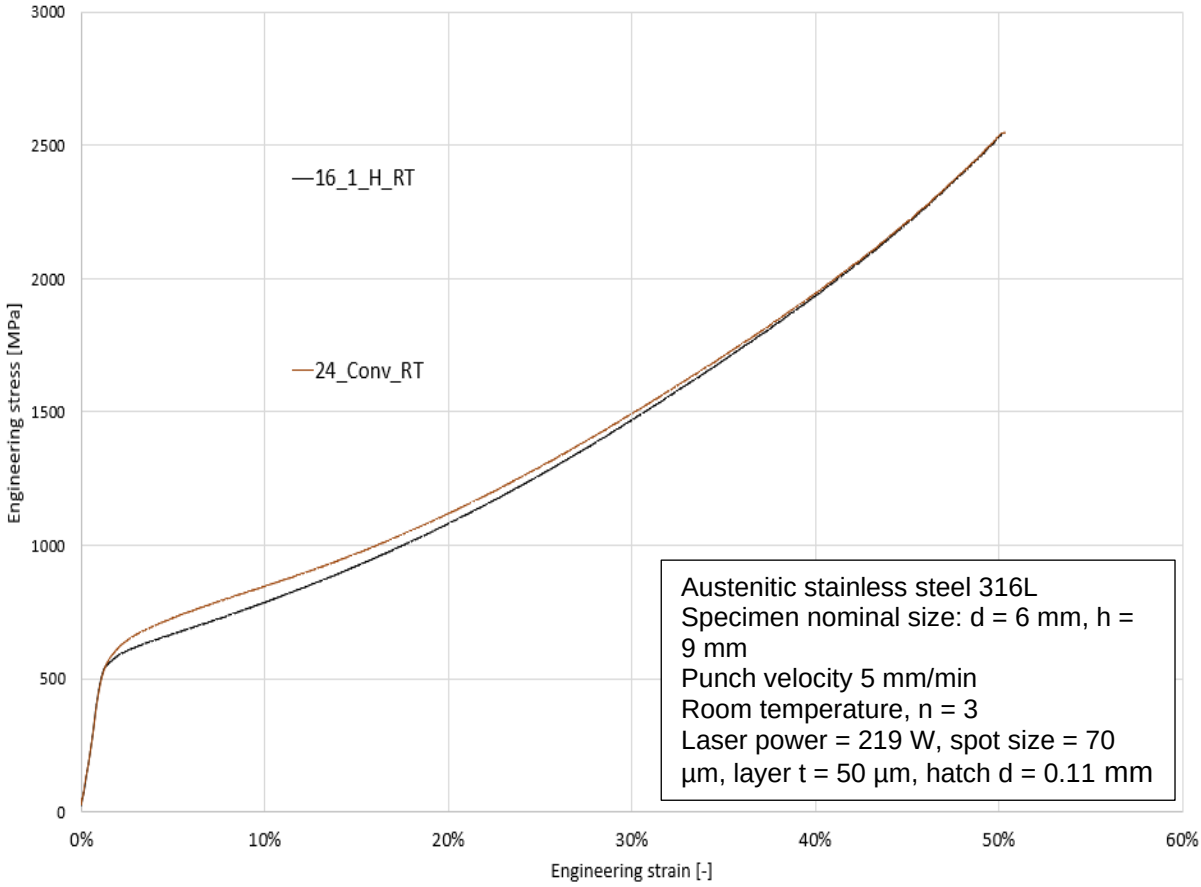

Figure 5.4. *Horizontal additive and conventional specimens at room temperature*

The conventional curve is ever higher, both for small and high strain values. So, there is not a changing in the strain around 30% as in high temperature curves. This means the conventional shows ever a higher general resistance compared to the corresponding additive. Nevertheless, the additive and conventional specimens tested at room temperature present a smaller yields strength difference compared to the specimens at high temperatures.
Focusing on the fitting, the room temperature additive curve shows the best fit with its corresponding conventional, while the 500°C presents the highest deviations between conventional and additively manufactured material. Therefore, seems to be present a variability increasing with the temperature increasing in the additive fitting compared to the conventional.
Finally the room temperature values are considered, as shown in Table 5.2.

Table 5.2. *Horizontal and conventional mechanical properties at room temperature.*

		σ0.05	σ0.2	σ, 55% h reduction	σ max
H_RT	Average	409	527	2208	2548
	±	5	27	6	3
Conv_RT	Average	503	547	2207	2537
	±	19	18	9	11

As with the high temperature, for low strain values the conventional presents higher values. Instead for high strain values, the additive mechanical properties are not clearly higher than the conventional, but basically the same.
If the state of art is considered, the room temperature horizontal curves of specimens manufactured by LaserTec 30 Machine present a really higher value of σ0.2 compared to the Table 2.5 in section 2.3.1: 527 ± 27 MPa instead of 489 ± 32 MPa.

Temperature influence with 45° building direction

The second comparison takes place with the diagonal building direction, as shown in Figure 5.5.

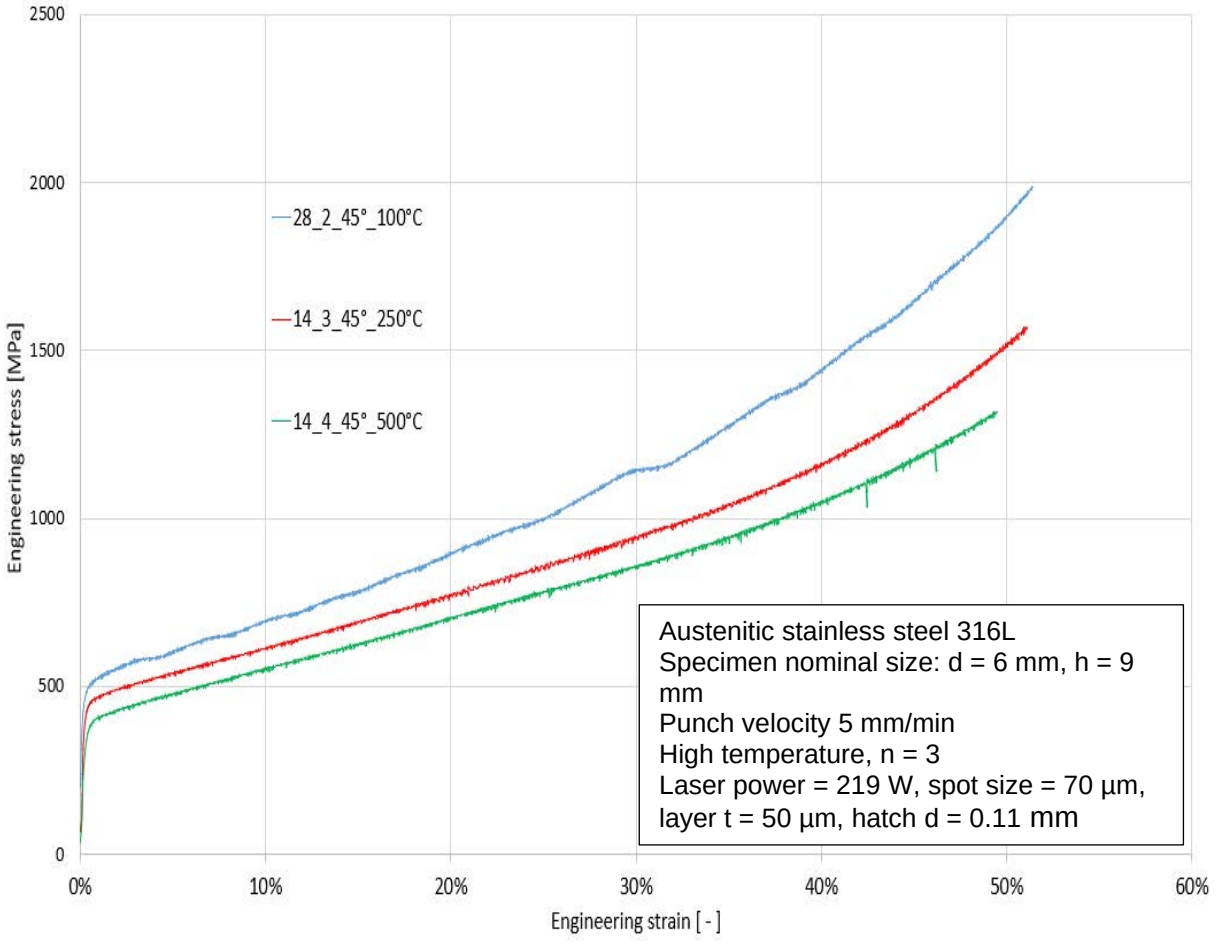

Figure 5.5. *High temperature influence for equal 45° building direction*

The mean curves position once again respect the hot metal material behaviour. They show a regular passage from the elastic to the plastic part. Nevertheless, the 100°C curve present an instability, due to an inhomogeneous heating process, that increases with the strain increasing. This can happen because a setting of a component in the tool, that provokes a wrong temperature therefore an irregular material resistance.
Focusing on the quantitative values, the mechanical properties can be seen in Table 5.3.

Table 5.3. *Diagonal mechanical properties at high temperature*

		σ0.05	σ0.2	σ, 55% h reduction	σ max
45_100°C	Average	419	479	1669	2086
	±	18	4	84	83
45_250°C	Average	403	435	1305	1568
	±	21	1	7	8
45_500°C	Average	336	374	1166	1340
	±	48	9	29	26

The elastic mechanical properties at high temperature are ever lower compared with conventional, as shown in Figure 5.6. An orientation building direction comparison with the horizontal additive specimens will be done in section 5.1.2.
Analyzing instead the $\sigma_{55\%}$ h reduction and the σ_{max}, seem to be present the same horizontal trend, where the additive max stresses are higher than the conventional.
In this regarding, if the Figure 5.6 is considered, it is possible to see that the stress strain curves for additively manufactured material is ever lower than the conventional. Nevertheless, the specimen analyzed, that is the number 28_2_45°_100°C, present an irregular behavior as already mentioned. Therefore, by considering the average value of the Table 5.3, it is possible to say that also the 100°C specimens manufactured with a diagonal build direction present mechanical properties higher at high strain values.
Analyzing the additive engineering stress strain curves at high temperature in Figure 5.6, they intersect the conventional curves for the same strain values of the horizontal additive curves, that is around 25% strain.

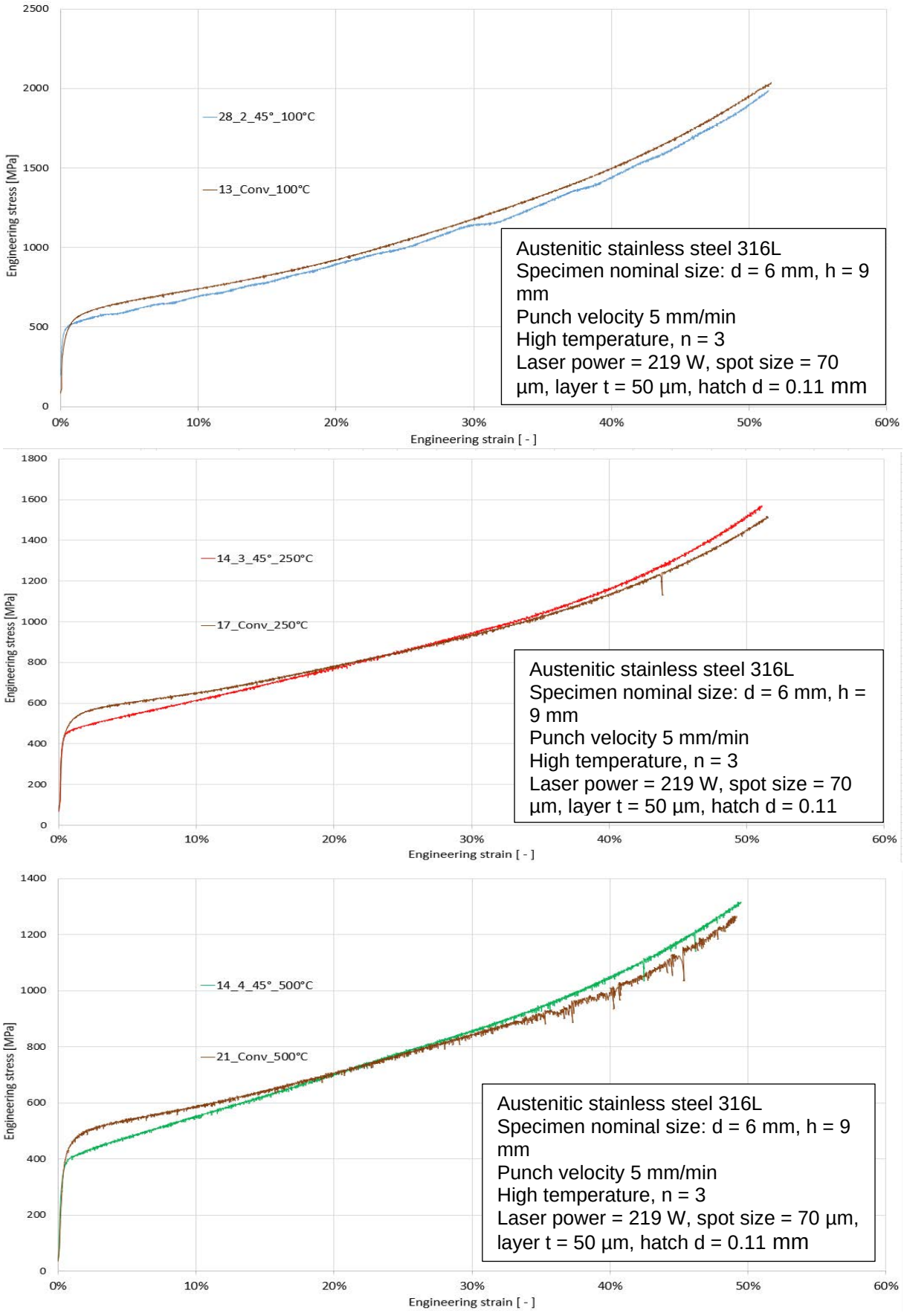

Figure 5.6. *45° additive and conventional building comparison for each high temperature*

If the room temperature specimens are analyzed, as shown in Table 5.4, it is not possible to state if the sigma 0.2 is higher or lower for AM or Conventional material, since the mean values are too close together and the deviations ±14 or ±18 overlap.

Table 5.4. *Mean diagonal mechanical properties at room temperature*

		σ0.05	σ0.2	σ, 55% h reduction	σ max
45_RT	Average	509	552	2066	2396
	±	16	14	46	53
Conv_RT	Average	503	547	2207	2537
	±	19	18	9	11

In this regarding, Figure 5.7 illustrates the mean curves with really close values. The same values can be seen also in the state of art in Table 2.5 in section 2.3.1. The state of art presents a $\sigma_{0.2}$ of 522 ± 17 MPa.

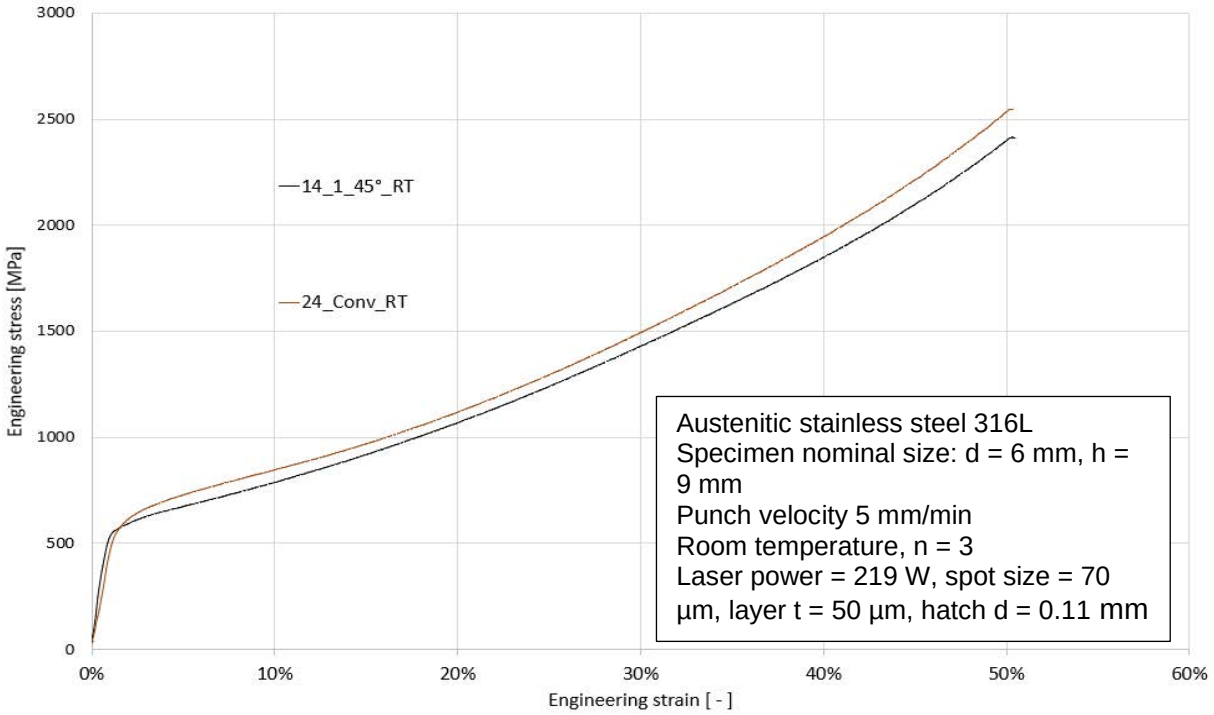

Figure 5.7. *45° additive and conventional specimens at room temperature*

Nevertheless, the plastic mechanical properties are lower, so a really different behaviour from the high temperature tests where the additive plastic properties for high strain values are ever higher than the conventional. Moreover, the difference regarding the stress values, that is the stress difference between the black and brown curves, is nearly constant for all the test.

Temperature influence with vertical building direction

Considering the vertical build, as shown in Figure 5.8, the influence temperature is totally analyzed. The curves in the engineering stress strain diagram follow the behaviour already found with the horizontal and the diagonal specimens. The transition from the elastic to the plastic part is with an equilibrated gradient. Nevertheless, a stress decreasing is present in the specimen 12_3_V_250°C around 45% strain, but it is really limited, therefore probably it does not depend

by a material defect.

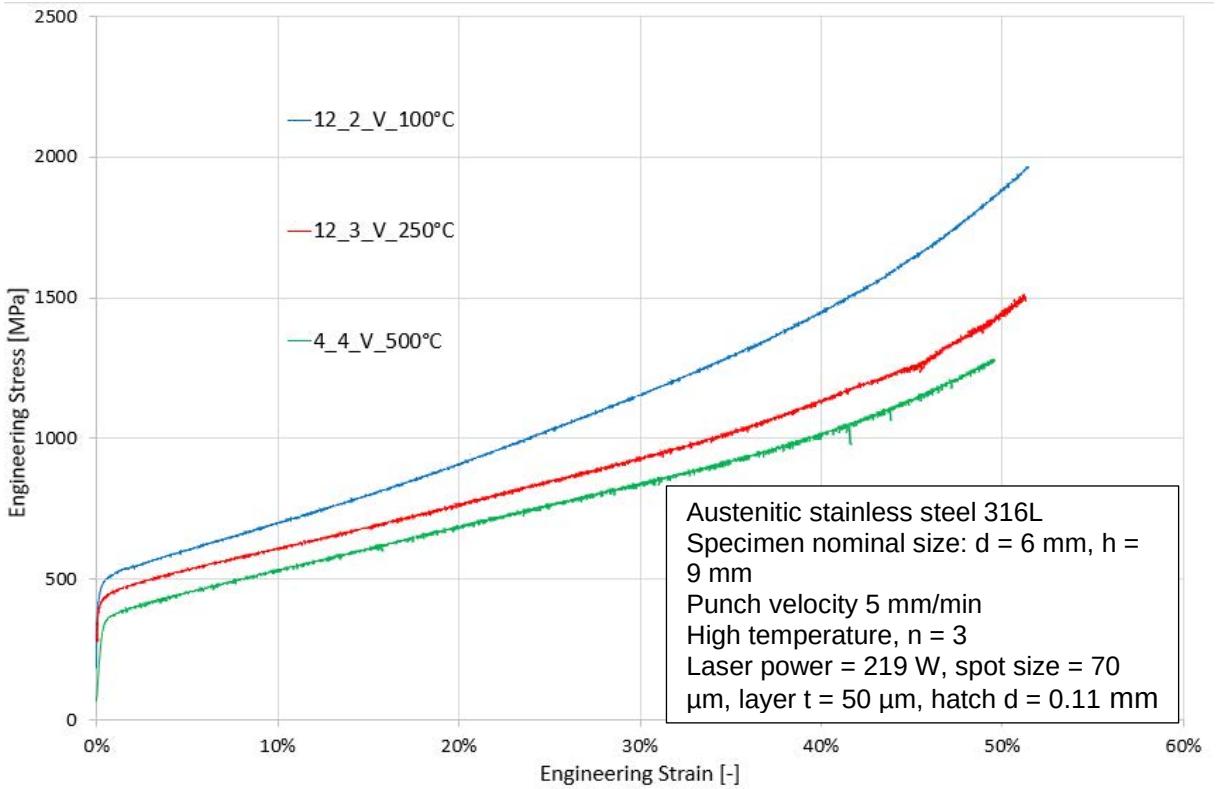

Figure 5.8. *High temperature influence for equal vertical building direction*

Analysing the quantitative values, as shown in Table 5.5, taking into account also the Table 5.5, the $\sigma_{0.05}$ at 100°C is higher than the corresponding conventional. This can be also seen in Figure 5.8, where the specimen 12_2_V_100°C present a really high gradient at the test beginning. The rest of the additive elastic properties remain lower than the conventional as for the previous horizontal and 45° specimens.

Table 5.5. *Plastic and elastic vertical mechanical properties at high temperature*

		σ0.05	σ0.2	σ, 55% h reduction	σ max
V_100°C	Average	438	483	1586	1951
	±	36	31	49	25
V_250°C	Average	427	446	1291	1586
	±	56	47	108	165
V_500°C	Average	352	374	1133	1256
	±	45	28	49	63

Nevertheless, the plastic mechanical properties are different than before. For high values of strain the curves are never higher than the conventional as shown in Figure 5.9. In particularly the 100°C curves are lower, instead the 250°C and 500°C show a perfect fitting. Moreover, focusing on the uncertainty budget, a strong variability is present for the 250°C tests in the values of the σ, 55% h reduction and the σ max.

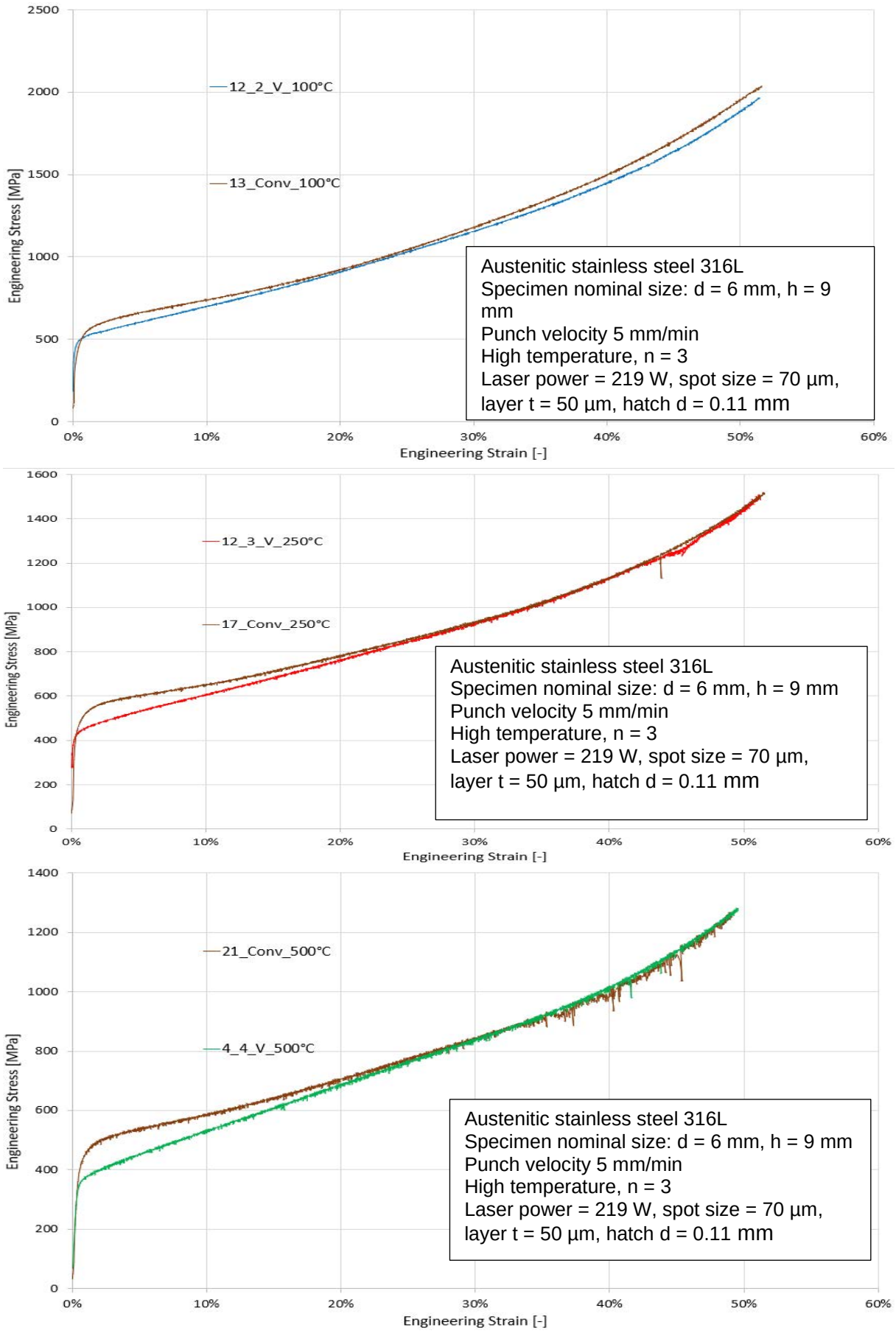

Figure 5.9. *Vertical and conventional building comparison for each high temperature*

Once again, the room temperature allow to have a deeper overview of the temperature influence, as shown in Figure 5.10.

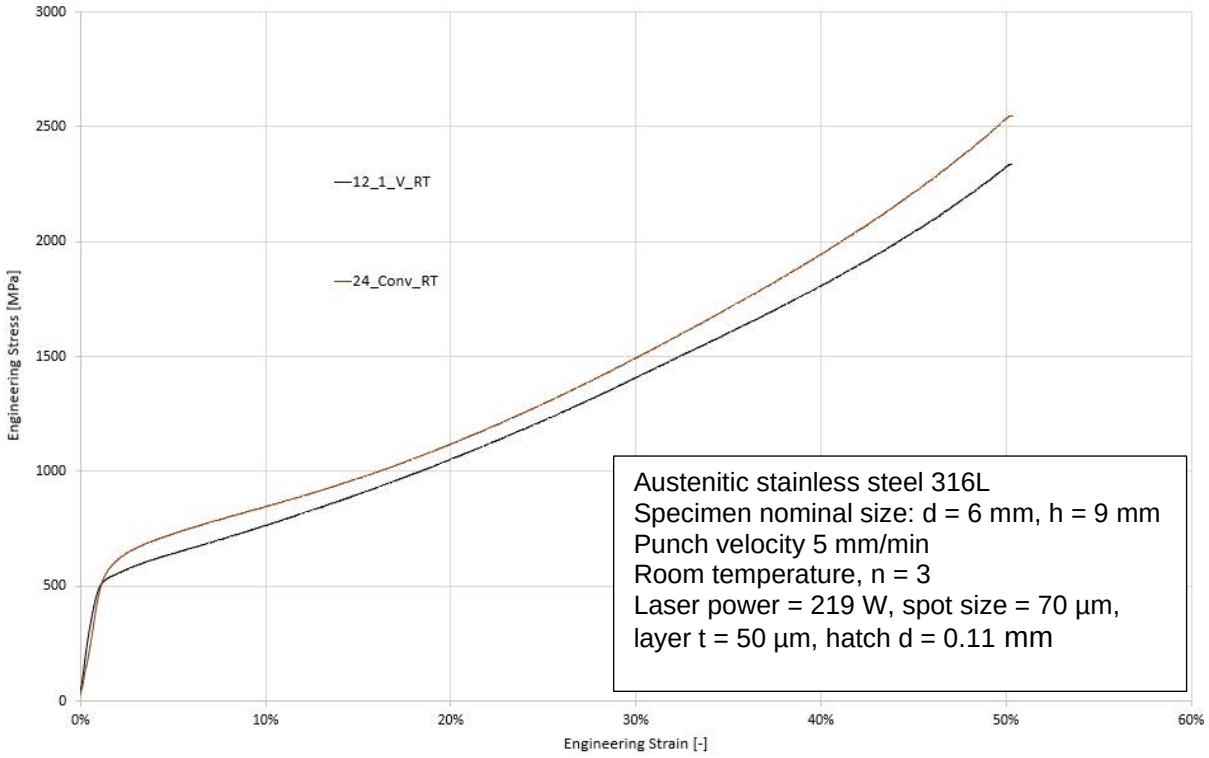

Figure 5.10. *Vertical additive and conventional specimens at room temperature*

The additive curve overlaps the conventional one in the elastic part but for all the plastic part is costantly inferior. This is also shown in Table 5.6, where the σ for a 55% height reduction and the σ max are strongly lower compared to the conventional specimens.

Table 5.6. *Plastic and elastic vertical mechanical properties at room temperature*

		σ0.05	σ0.2	σ, 55% h reduction	σ max
V_RT	Average	483	522	2035	2331
	±	10	2	26	29
Conv_RT	Average	503	547	2207	2537
	±	19	18	9	11

Once again, if the Table 2.5 in section 2.3.1 is taken into account, the Lasertec $\sigma_{0.2}$ is higher compared to the corresponding value in the state of art: 522 ± 2 instead of 403 ± 6.
Both in the Lasertec data set and the state of art, the values show the smallest uncertainty than the other build direction, therefore averagely the vertical build direction presents values range smaller.

Comparison with the true stress strain curves of the state of art

Regarding the comparisons with the state of art, this last one allows to have complete data set both with high temperature both with the room temperature only with vertical building direction. Moreover in the state of art the curves are given only with true strain stress curves, therefore in order to do a comparison for equal conditions the mean curves of thesis vertical build direction are analyzed in Figure 5.11.

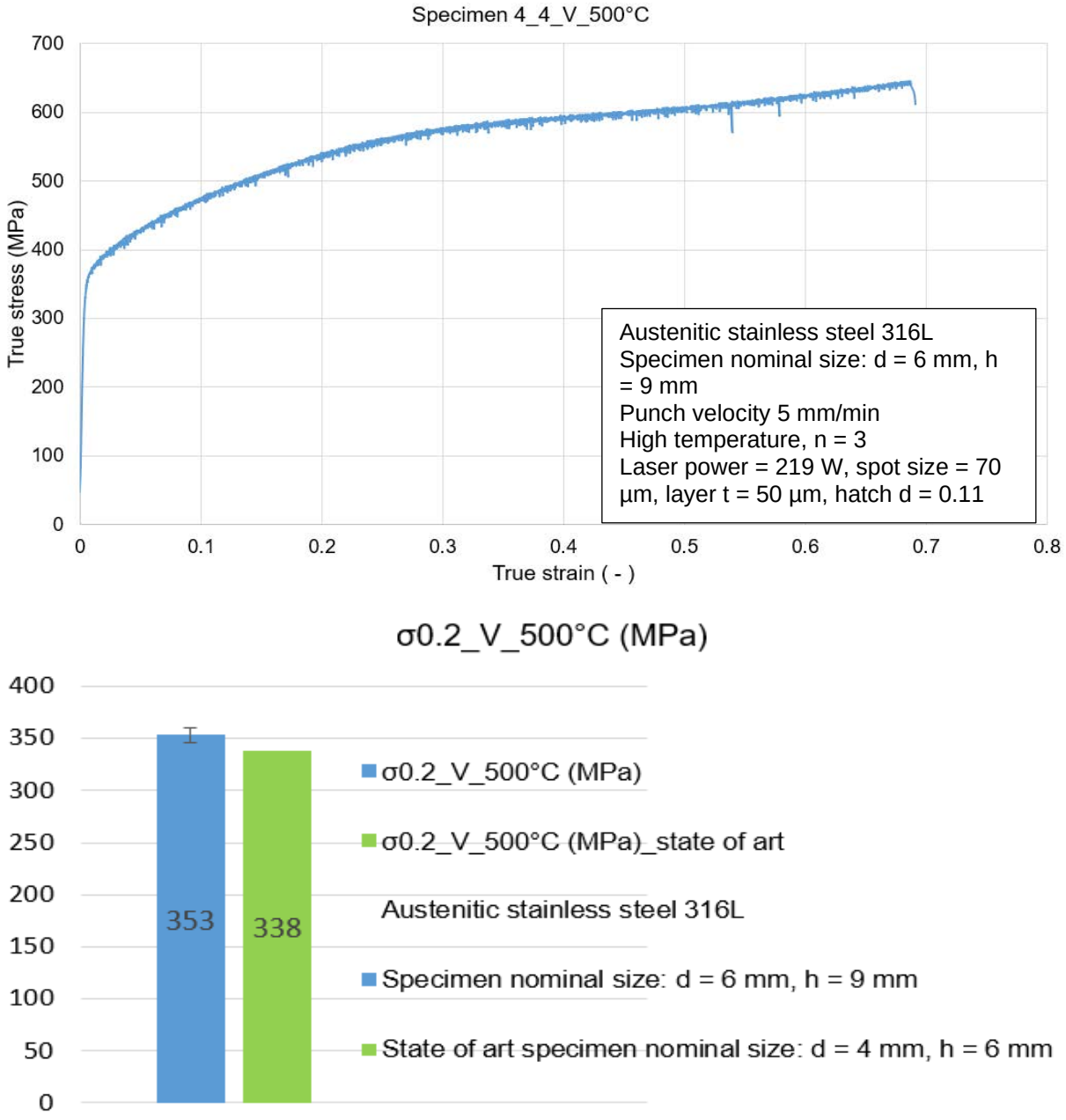

Figure 5.11. *Mean true stress strain curves of vertical build direction at 500° and $\sigma_{0.2}$ comparison with the state of art*

As shown in the histograms, at 500°C the Lasertec $\sigma_{0.2}$ is comparable with the corresponding in the state of art for equal vertical building direction, however because of the uncertainty lack in the state of art data is not possible to state which one setup and manufacturing conditions are better.

If the true stress strain curves at room temperature are considered, as shown in Figure 5.12, the same trend is found.

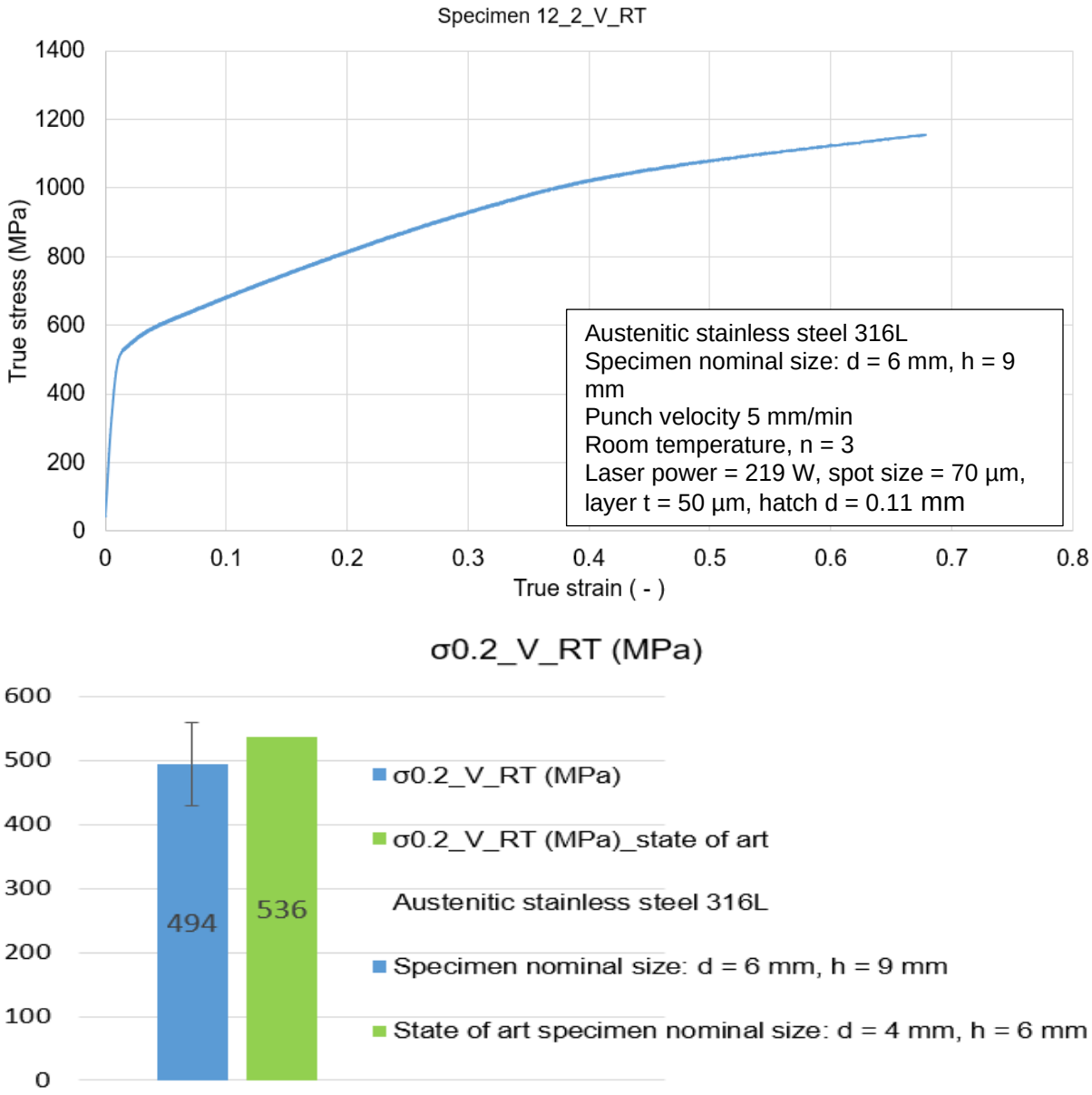

Figure 5.12. *Mean true stress strain curves of vertical building direction at room temperature and $\sigma_{0.2}$ comparison with the state of art*

The state of art and the Lasertec $\sigma_{0.2}$ once again are comparable, but the uncertainty lack continues to be an obstacle for a deeper analysis.

The comparison done in section 5.1.1, allows to have an overview of the additive characteristics in correspondence of temperature changings. The formability understanding is intimately linked to stress strain curves: if the deformation energy will be higher, then will be necessary a larger press size in order to work the component. With the temperature influence comparison, the main important stress strain values are now known, nevertheless it is not possible to state what build direction prevails. For this reason a building direction comparison is needed.

5.1.2 Building direction influence for equal temperature

Building direction influence at high temperature: 500°C

The second comparison focus on the build orientation influence. Starting from the high temperature, in particular from the highest test temperature is possible to evaluate the hot forming behavior with the building direction variation. The Figure 5.13 shows a specimens set (4_4_V, 9_2_H, 14_4_45°) tested at 500°C, representing the mean curves between all the specimens sets. Each specimen plotted, is manufactured with a different building direction: vertical, 45° and horizontal. In the Appendix is shown each specimen alone in order to allow an individual point of view.

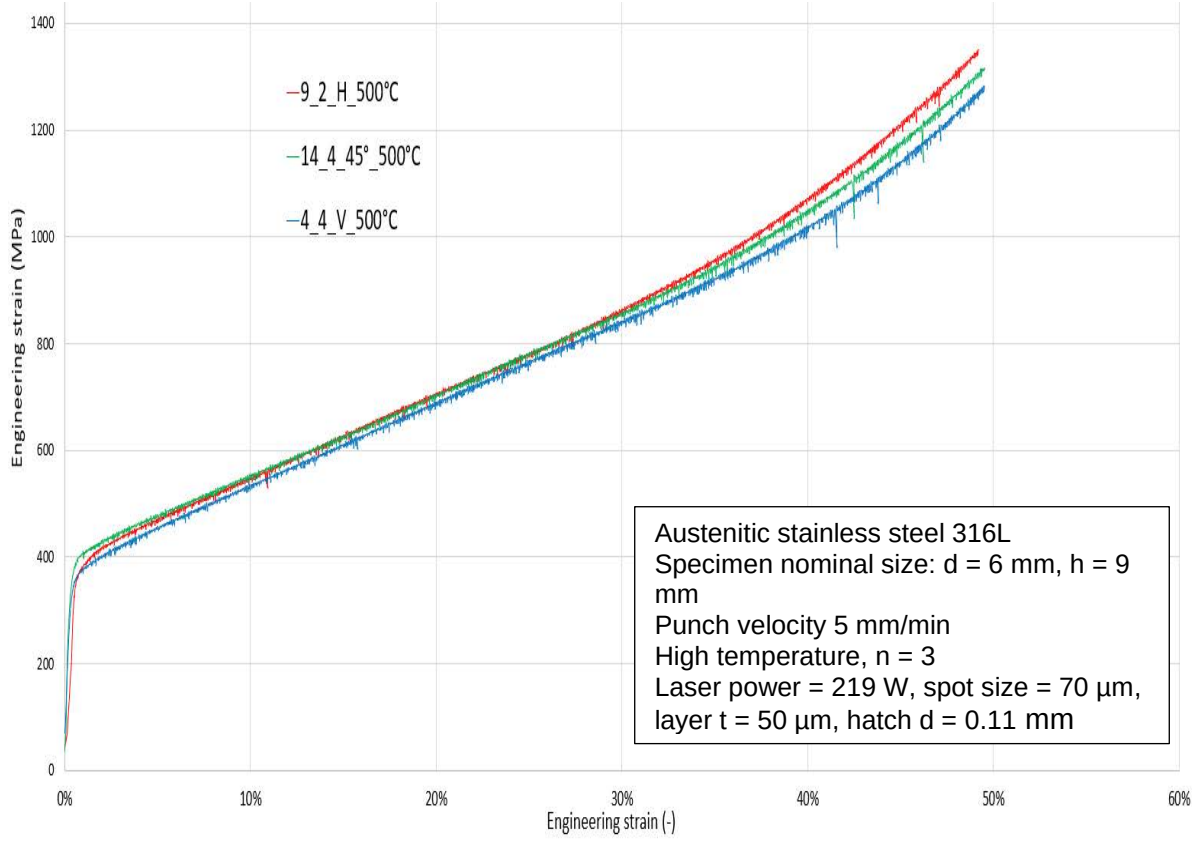

Figure 5.13. *Building direction influence at 500°C*

If it is considered the specimens set in Figure 5.13: between 0 % ÷ 20% of strain the 45° build direction is the highest curve, between 20% ÷ 30% of strain the 45° and the horizontal present the same fitting, instead after 30% of strain the horizontal becomes the highest. Therefore, the diagonal 14_4 specimen present a better resistance for elastic stress, that is a better static behaviour, nevertheless far from the elastic conventional properties as shown in Figure 5.6.

Concerning the vertical building direction, it presents an elastic part with a higher gradient of the horizontal one, but in the high strain values it is clearly the lowest curve.

As before, a qualitive overview is not enough for a correct understanding. In this regarding, are now widely analyzed through histograms all the three additive build directions in order to realize clear comparisons.

Mechanical properties at 500°C to vary the building direction variation: $\sigma_{0.05}$ and $\sigma_{0.2}$

As seen in Figure 5.14, considering the average value the vertical and the horizontal build directions show comparable $\sigma_{0.05}$ (strain 0.05%) while the diagonal building direction present the inferior value.

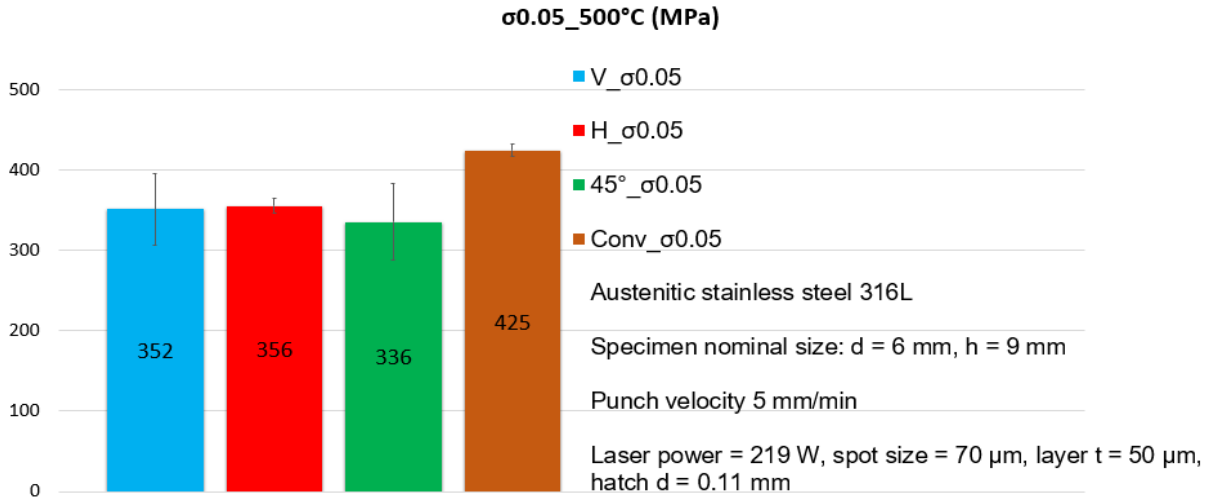

Figure 5.14. *$\sigma_{0.05}$ comparison at 500°C*

On average, the vertical building direction present the nearest value to the conventional specimens, that is if the uncertainty is considered: the vertical direction present the highest specimens number with a $\sigma_{0.05}$ really close to the conventional set.

A second fundamental elastic mechanical property is the $\sigma_{0.2}$ (strain 0.2%).

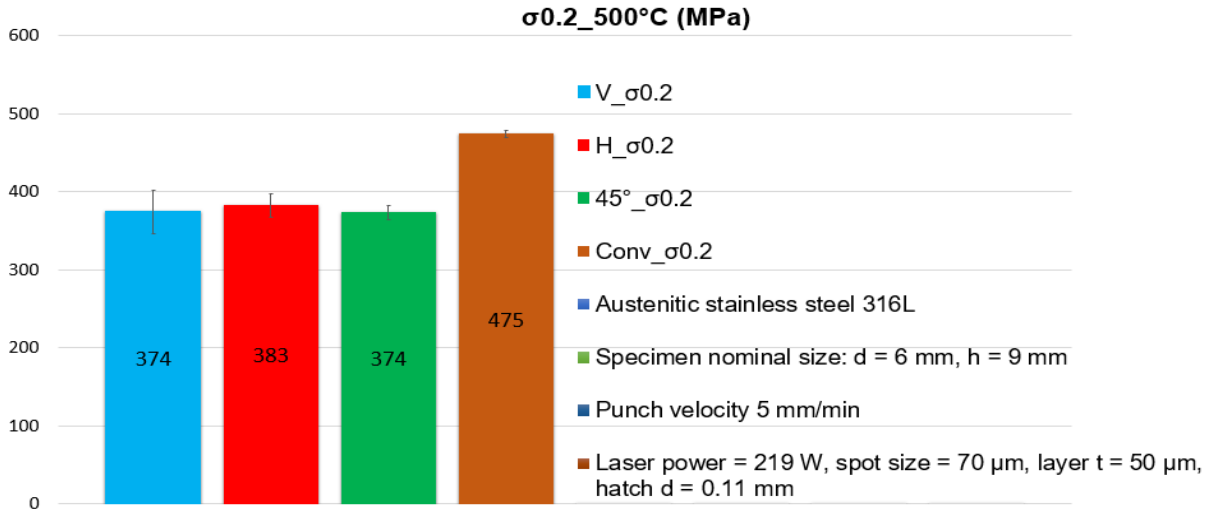

Figure 5.15. *$\sigma_{0.2}$ comparison at 500°C*

As shown in Figure 5.15, the yield stress of conventional manufactured material is higher than for additively manufactured material. This is also independent from the building orientation. As regards deviation, no one clear trend is shown, however a clear difference compared to the conventional material is visible.

Mechanical properties at 500°C to vary the building direction: $\sigma_{max,}$ σ and Ɛ with a 55% height reduction and the corresponding elastic $Ɛ_{el}$ and plastic $Ɛ_{pl}$ amount

Focusing on the other mechanical properties, the sigma in correspondence of a 55% of height reduction is now analyzed in a clear comparison with the other directions, as shown in Figure 5.16.

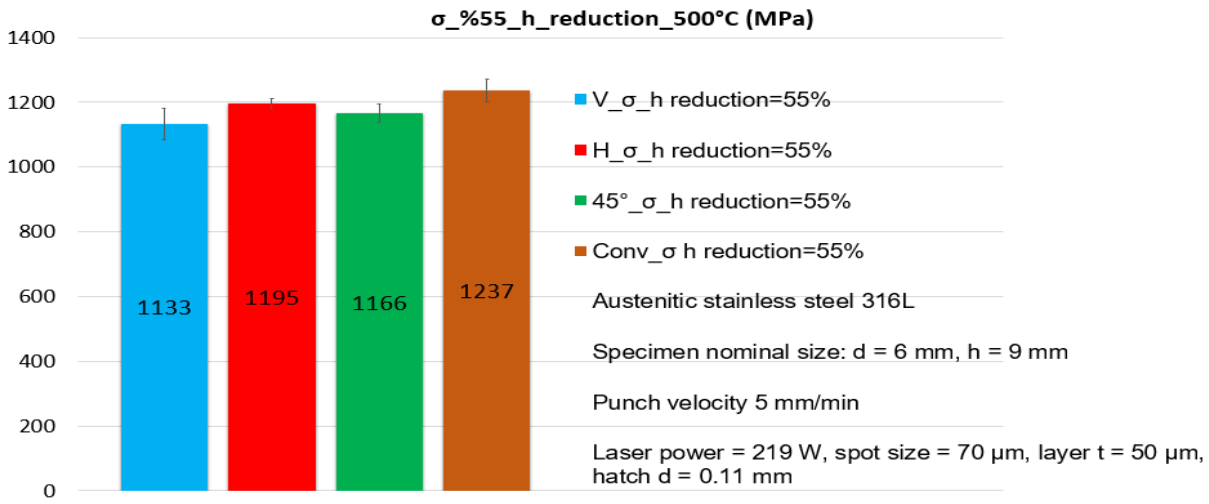

Figure 5.16. *Stress comparison in correspondence of a 55% height reduction*

The horizontal direction presents averagely a clear supremacy compared the other two build direction. Even if, averagely it remains lower than the conventional, there are some specimens with higher stress value taking into account the red uncertainty budget.

If the maximum stress in the test is analyzed, an important behavior is found.

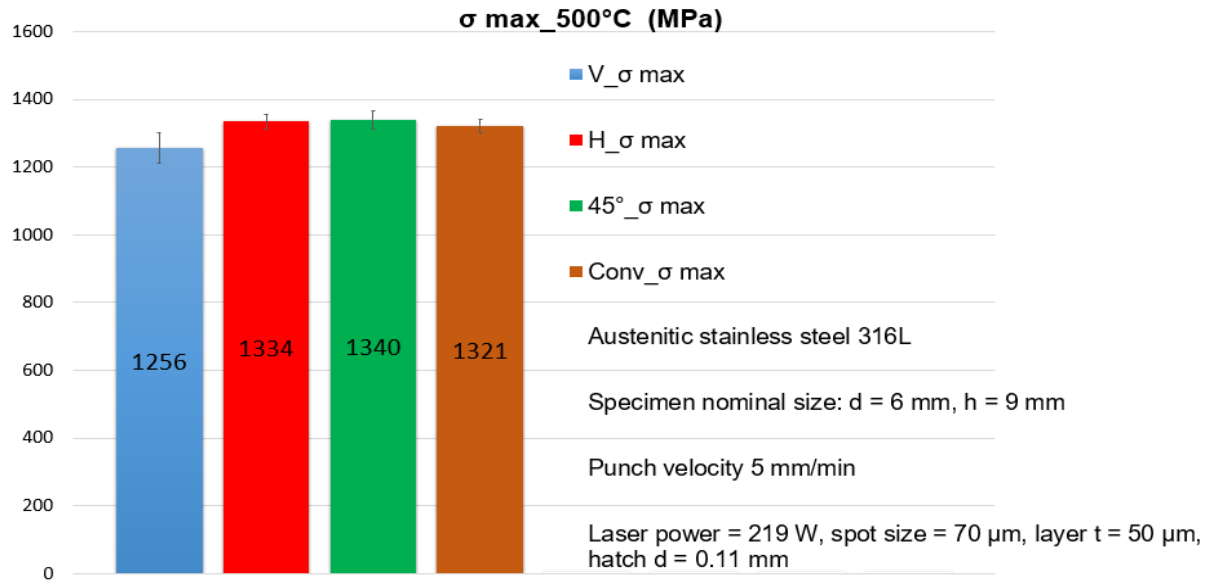

Figure 5.17: *Stress comparison before the material failure*

As shown in Figure 5.17, for a consistent height reduction, the horizontal and the 45° building directions are averagely higher compared to the conventional property. Moreover both the building direction are really close between them, instead the vertical is strongly inferior.

Focusing on the strain values in percentage terms, other comments take place. Figure 5.18 illustrates the elastic strain amount comparison.

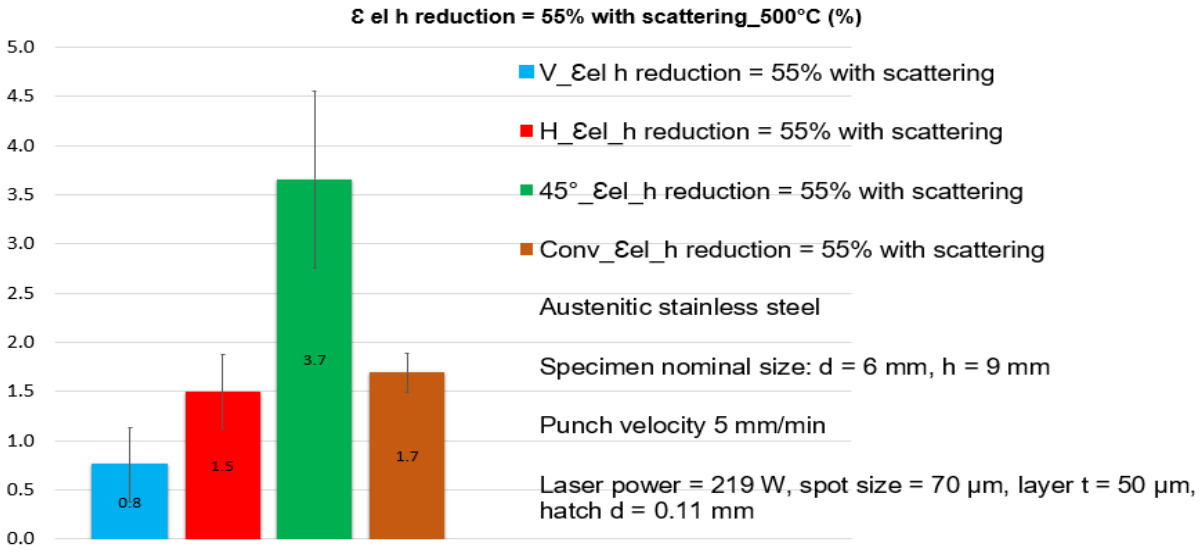

Figure 5.18. *Elastic strain comparison in correspondence of a 55% height reduction*

In the comparison, the diagonal build direction shows a consistent elastic strain for a 55% height reduction. This means a static behaviour for a longer time, that is a positive behaviour.
Finally, in Figure 5.19, is shown the maximum strain.

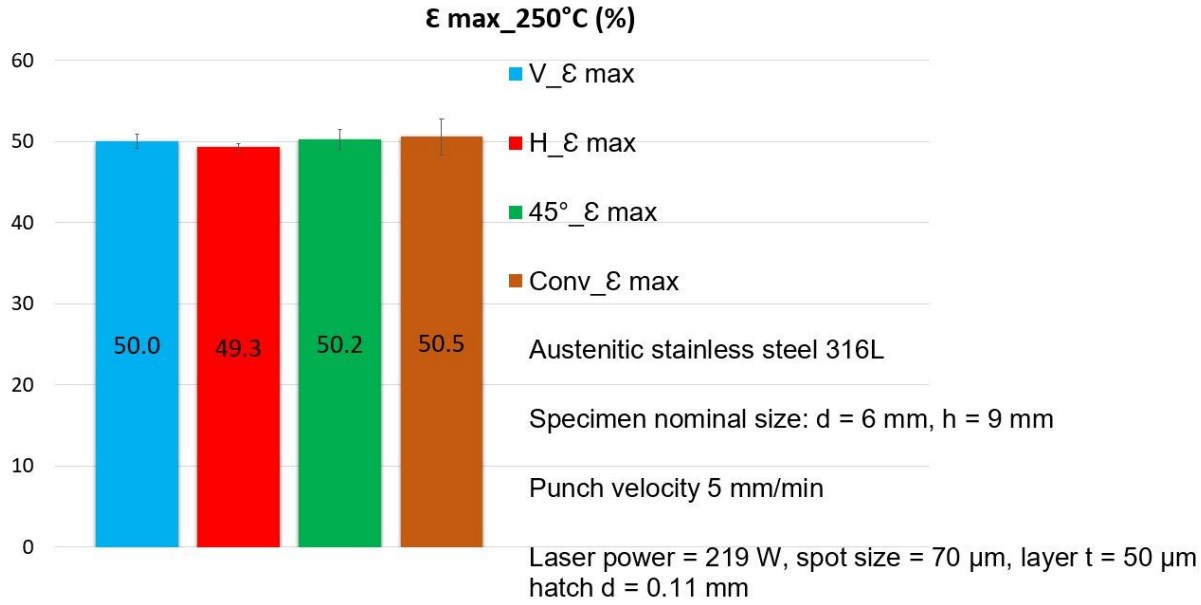

Figure 5.19. *Strain comparison before the material failure*

This value together the maximum stress in Figure 5.17, bring to consider that, for equal stress between the horizontal and the diagonal build direction, the best building direction seems to be the horizontal one thanks to a smaller maximum strain. Taking into account the comparison done, the 45° build direction averagely seems to show the best compromise behaviour at 500°C.

Building direction influence at 250°

At 250°C a qualitative trend of the three building direction is given by Figure 5.20.

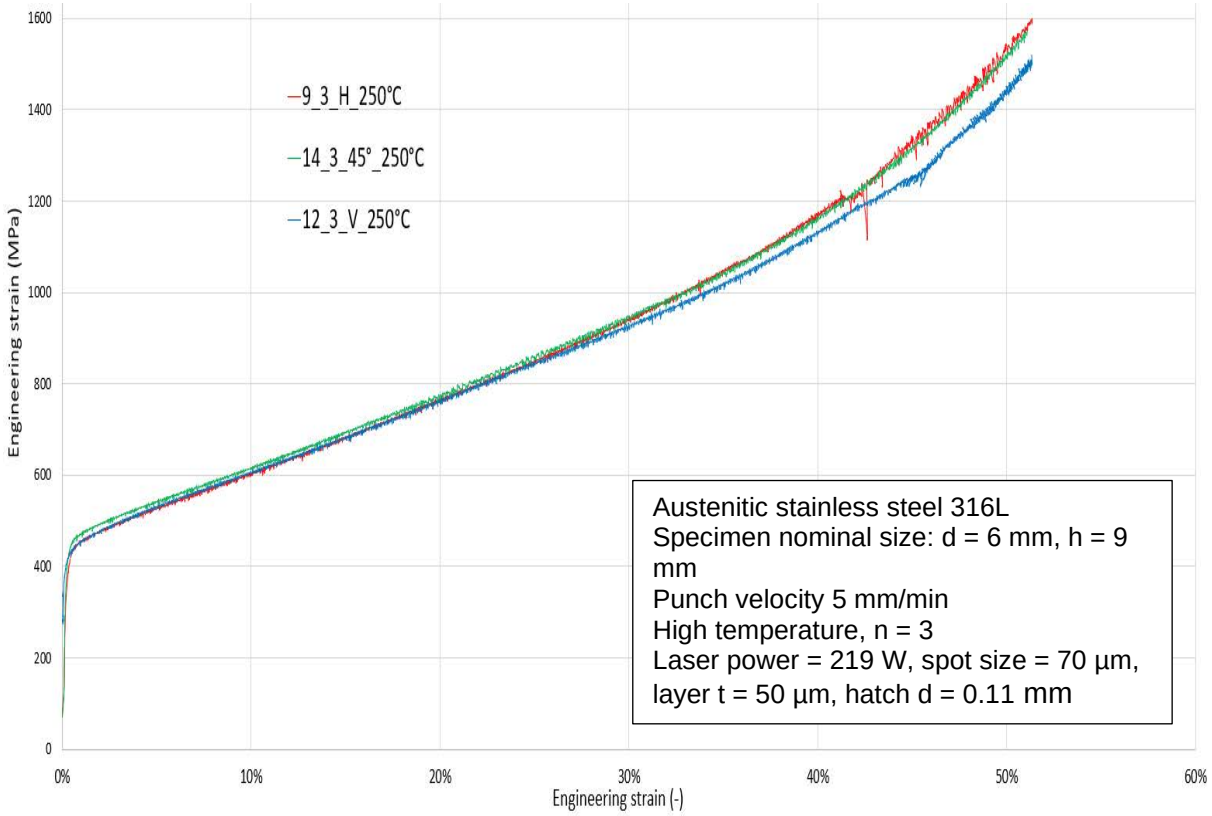

Figure 5.20. *Building direction influence at 250°C*

Once again by considering the specific specimens set, the 45° build direction overlaps perfectly the horizontal building direction.

Mechanical properties at 250°C to vary the building direction

In order to have a wide overview is better to consider the average values, as shown in Figure 5.21.

In the histograms, the elastic mechanical properties are really similar between them, but the vertical averagely overcomes, a little, the conventional specimens. Focusing on the stress in correspondence a 55% height reduction, the behavior is different. All the additive specimens overcome clearly the conventional specimens set. In particular the horizontal build direction presents also a small uncertainty, therefore averagely the horizontal specimens can show a high resistance for consistent strain values.

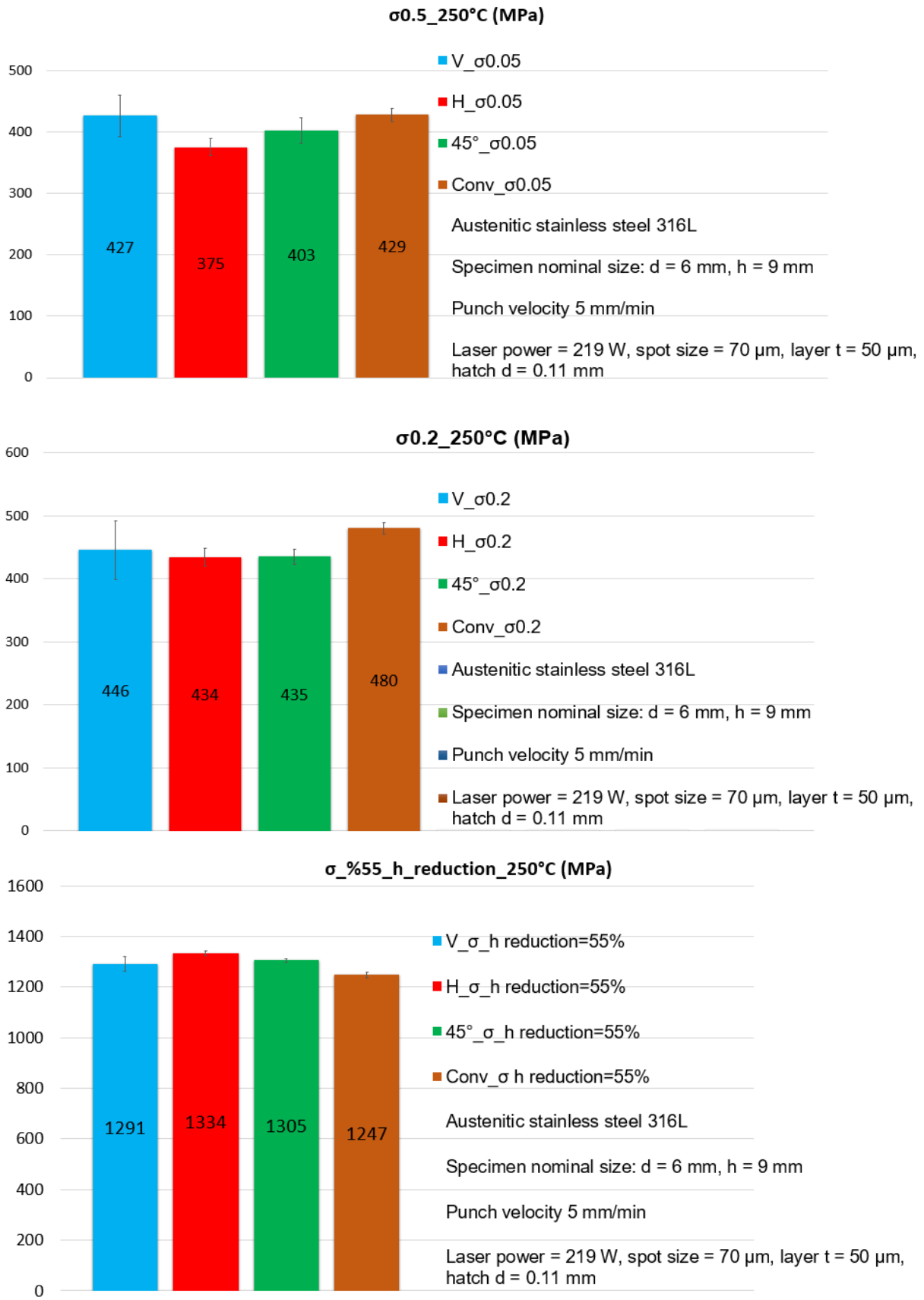

Figure 5.21. *Elastic and plastic mechanical properties at 250°C*

Nevertheless, the trend is different for the highest strain as shown in Figure 5.22. The horizontal

at the ending of the test, averagely overcomes yet the conventional specimens, but in turn is overcome by the vertical building direction, that shows the highest deformation. Concerning the elastic part at a 55% height reduction, the diagonal build direction presents a really large amount compared to the other two additive build direction. Therefore, also at 250°C the best build direction averagely seems to be the 45°.

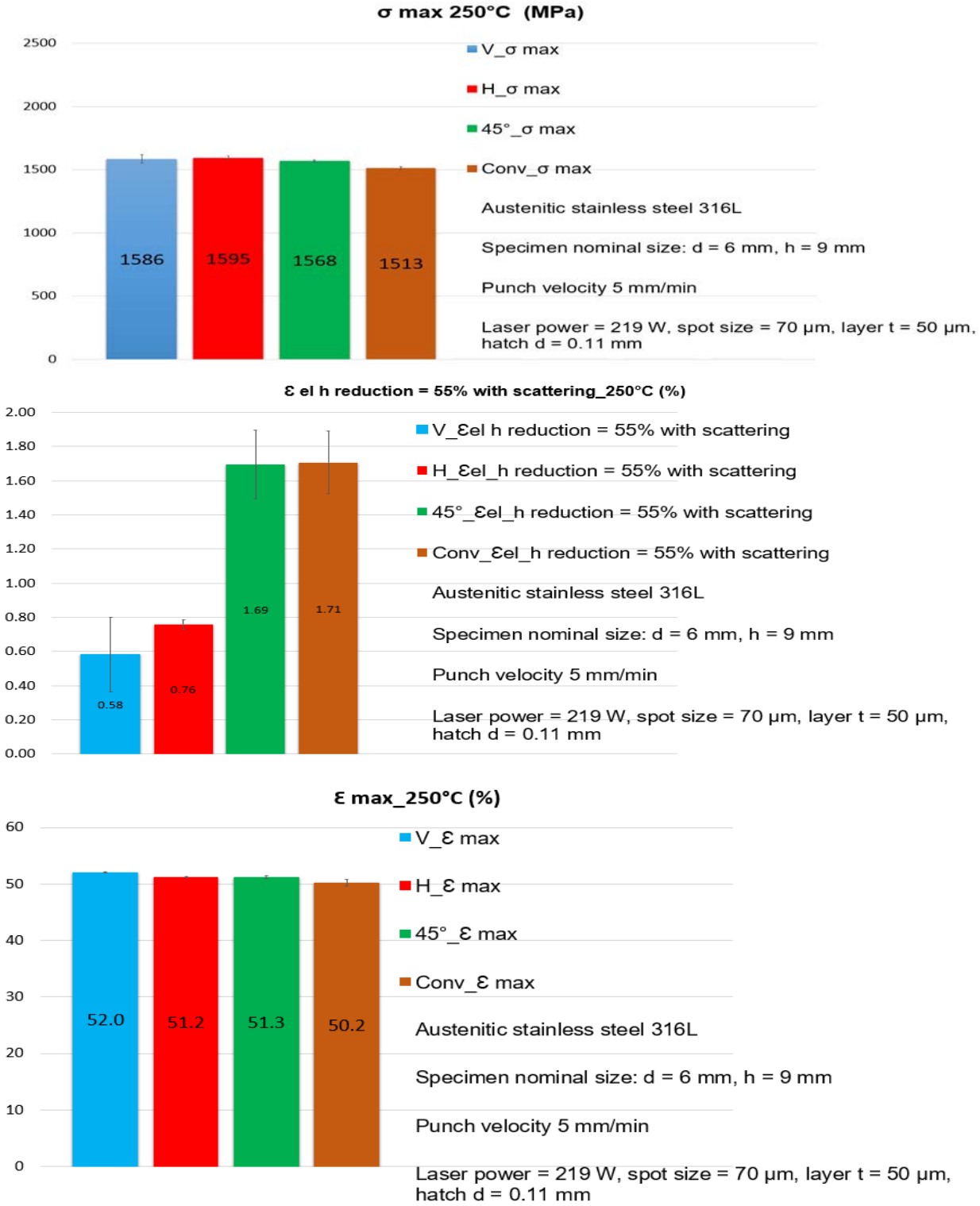

Figure 5.22. *Elastic and plastic strains at 250°C*

Building direction influence at 100°

Once again a qualitative stress strain curves trend is shown in Figure 5.23.

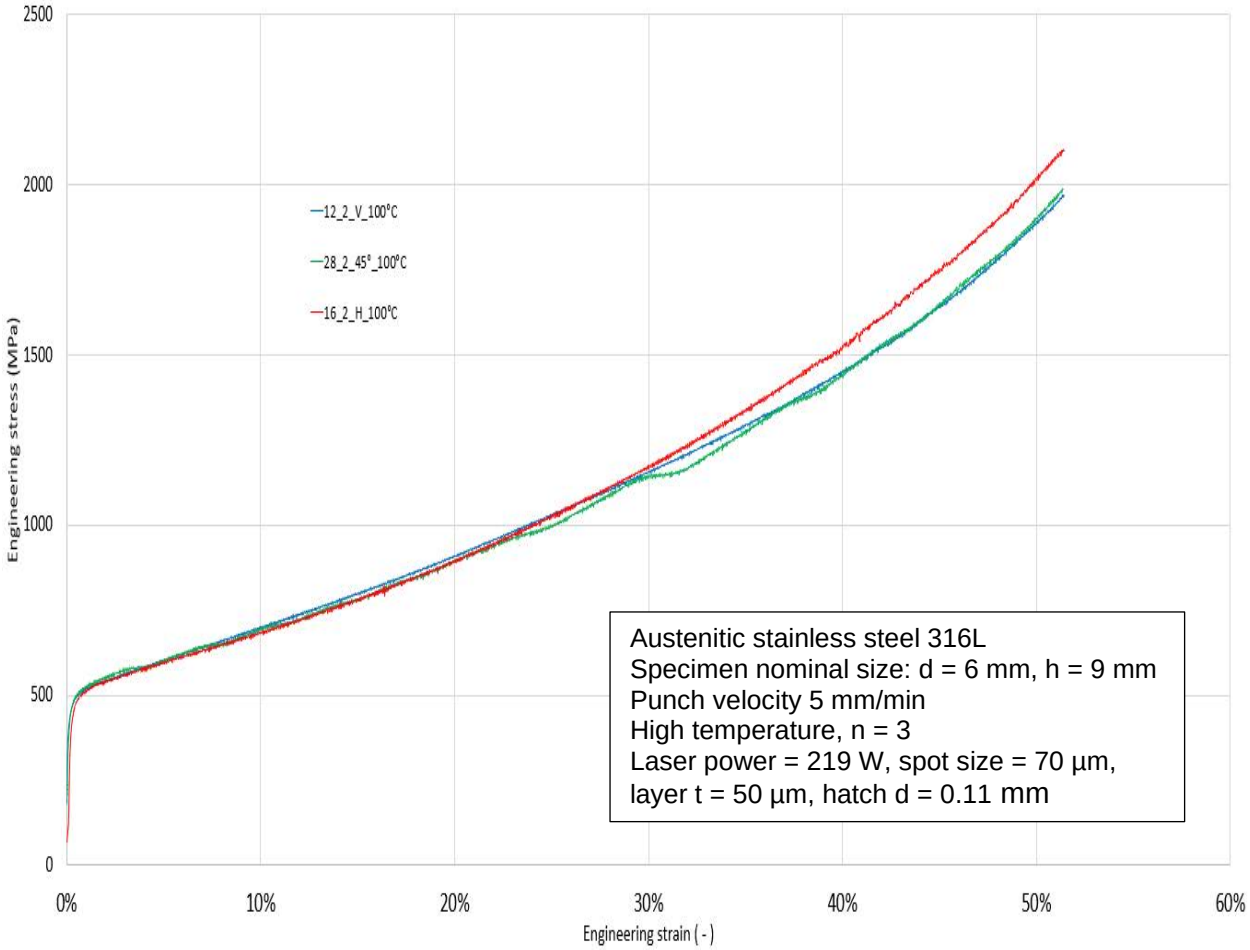

Figure 5.23. *Building direction influence at 100°C*

Mechanical properties at 100°C to vary building direction

Taking into account the histograms regarding the mechanical properties in Figure 5.24, all the additive specimens show good $\sigma_{0.05}$ and $\sigma_{0.2}$, close to the conventional.

With a 55% height reduction, the horizontal building direction shows clearly the best resistance, nevertheless the 45° direction maintains a stress endurance close to the conventional.

Considering instead Figure 5.25, all the additive specimens present maximum strains at the prove ending lower than the conventional. Moreover, the 45° build direction averagely presents also the largest elastic strain amount as shown ever in Figure 5.25, therefore once again the 45° building direction seems to be the best at 100°C.

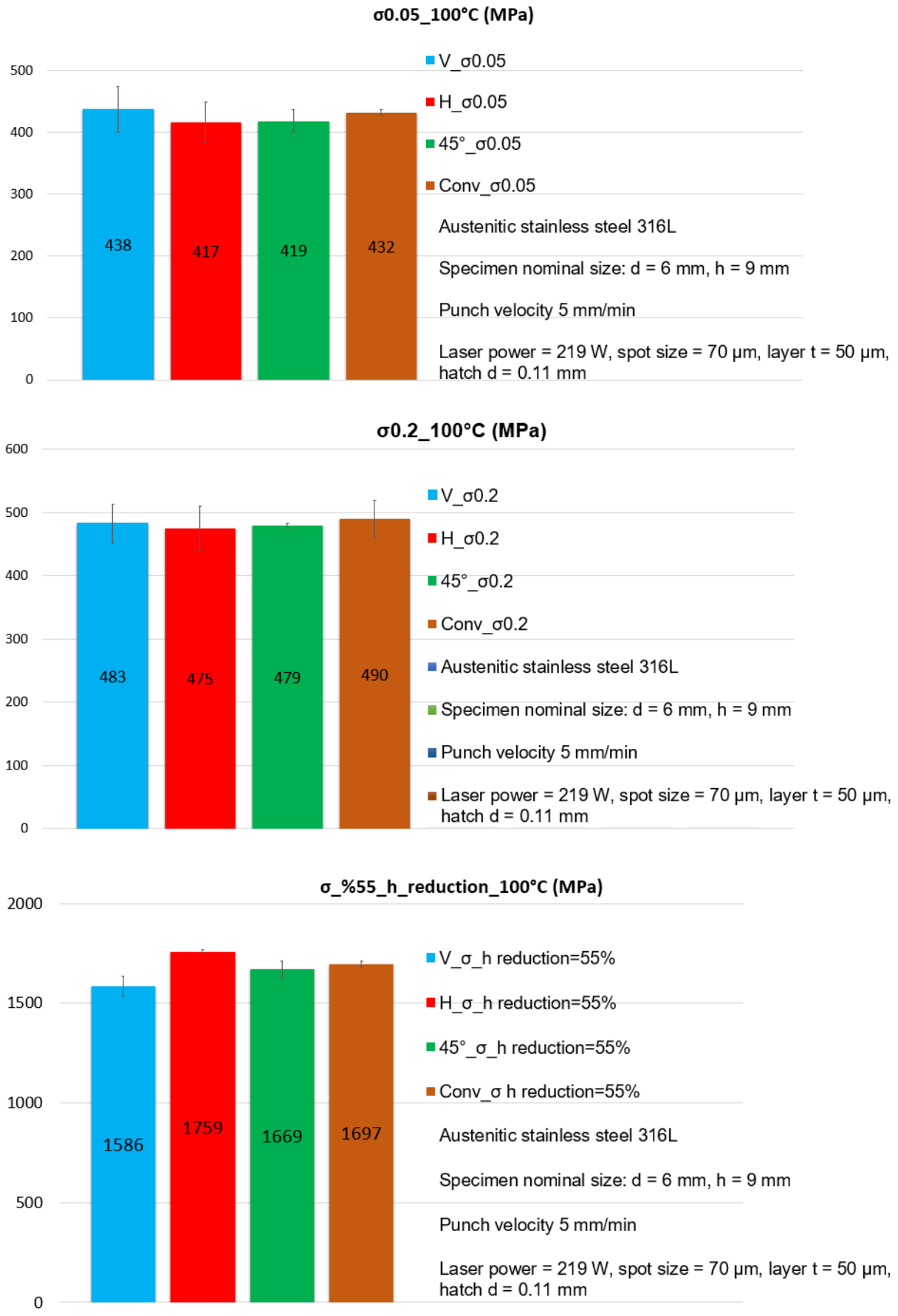

Figure 5.24. *Elastic and plastic mechanical properties at 100°C*

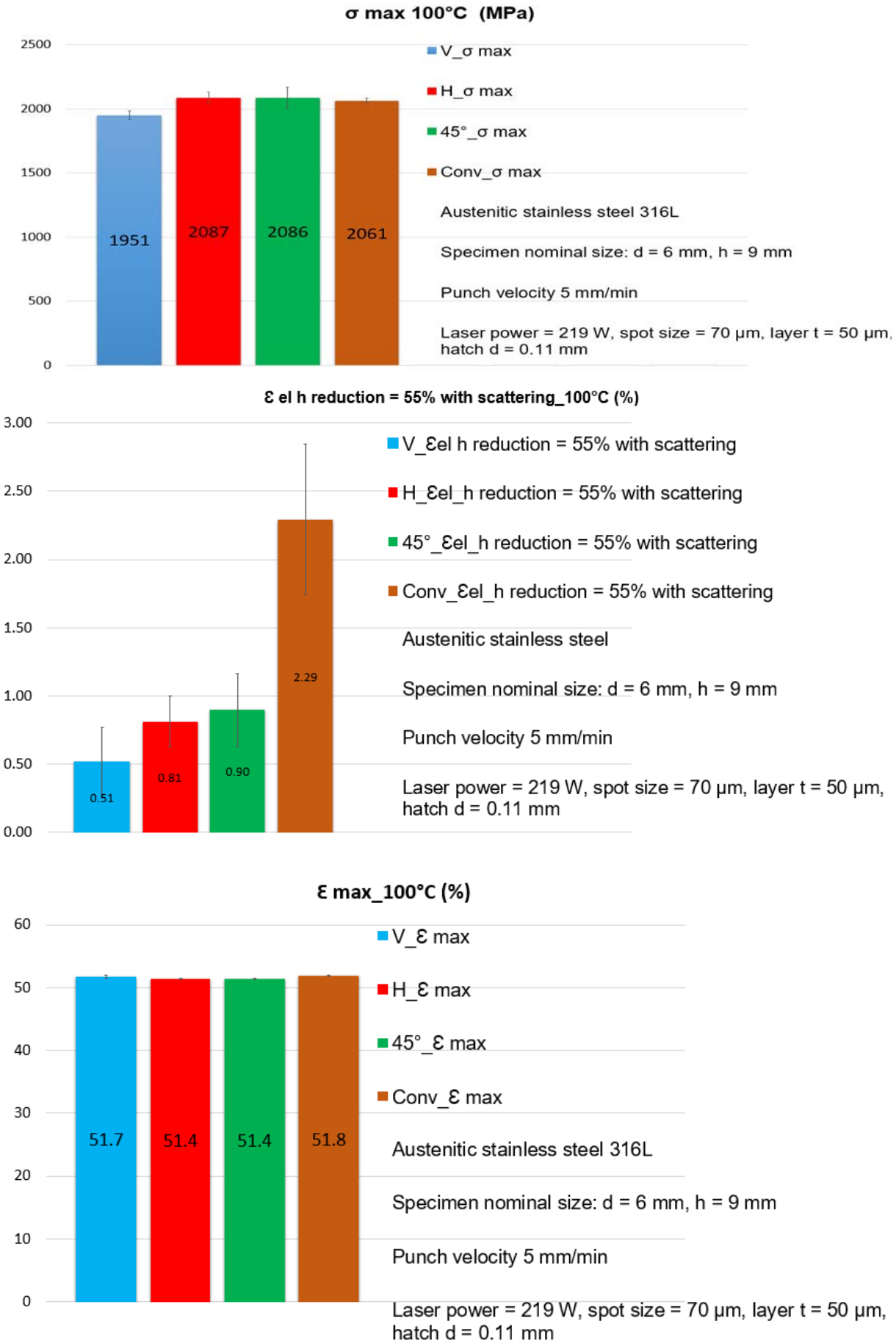

Figure 5.25. *Elastic and plastic strains at 100°C*

Building direction influence at RT

The 45° build direction influence at room temperature in the specimens set in Figure 5.26 is clearly in the middle between the other two building direction at high strain values.
Instead in the elastic zone the 45° building direction seems to have the highest gradient.

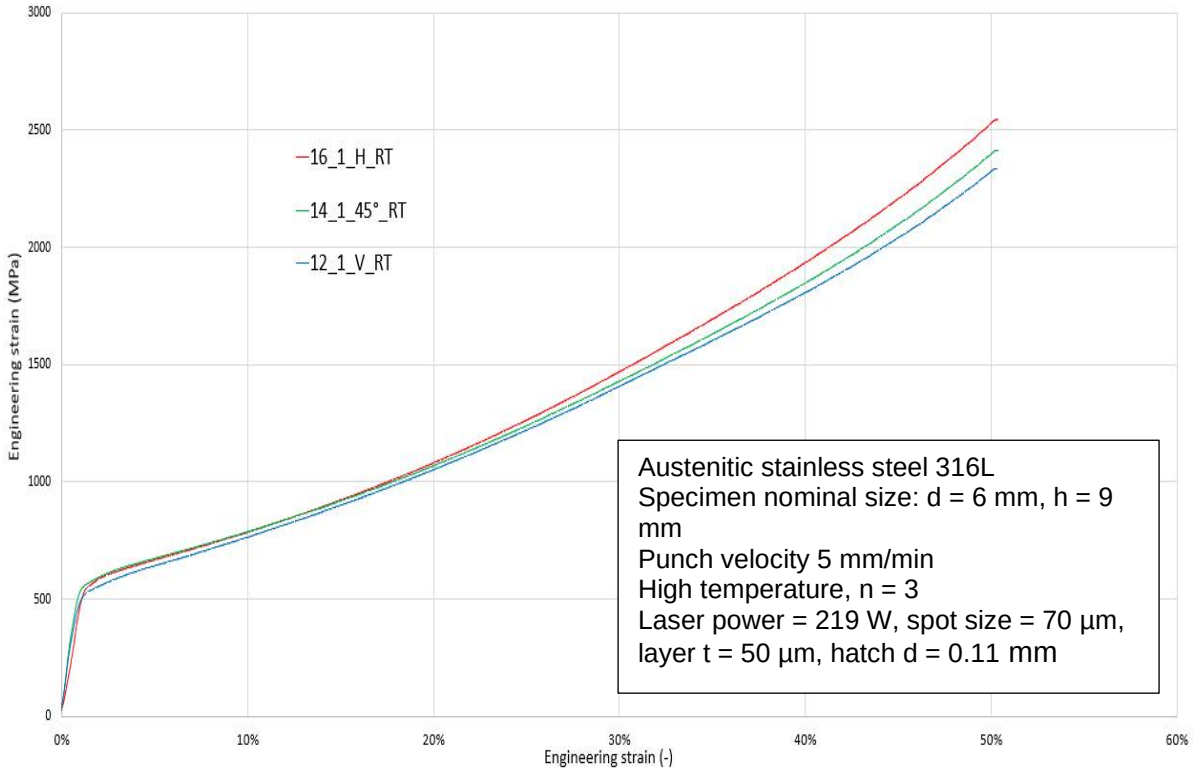

Figure 5.26. *Building direction influence at 500°C*

These considerations about the gradient in the elastic part are confirmed for all the specimens tested, as shown in Figure 5.27. In fact, the 45° building direction shows the highest $\sigma_{0.05}$ and $\sigma_{0.2}$, even if a little.
Another fundamental value is regarding the stress for a 55% of height reduction. Concerning this, the best endurance is shown by the horizontal build direction, averagely better than the conventional. However, the 45° building direction presents a good resistance and is clearly higher than the vertical also thanks to its small uncertainty.
Analysing instead the mechanical properties for high strain values, the best properties are shown once again by the horizontal build direction, because as shown in Figure 5.28: this build direction presents the highest elastic amount for a 55% of height reduction and it has lowest maximum strain around the additive specimens, even if it rests higher from the conventional maximum strain at the test ending.

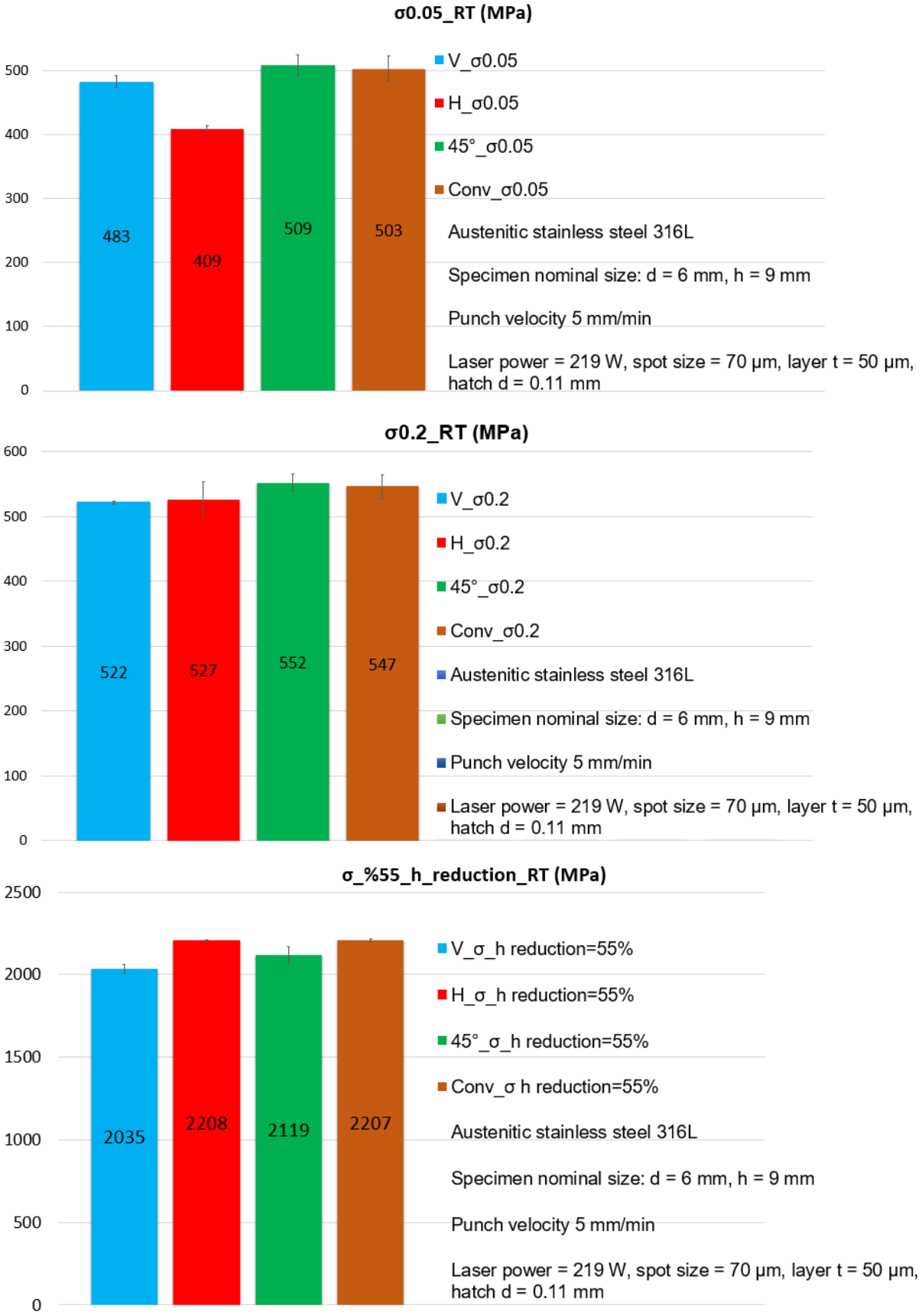

Figure 5.27. *Elastic and plastic mechanical properties at room temperature*

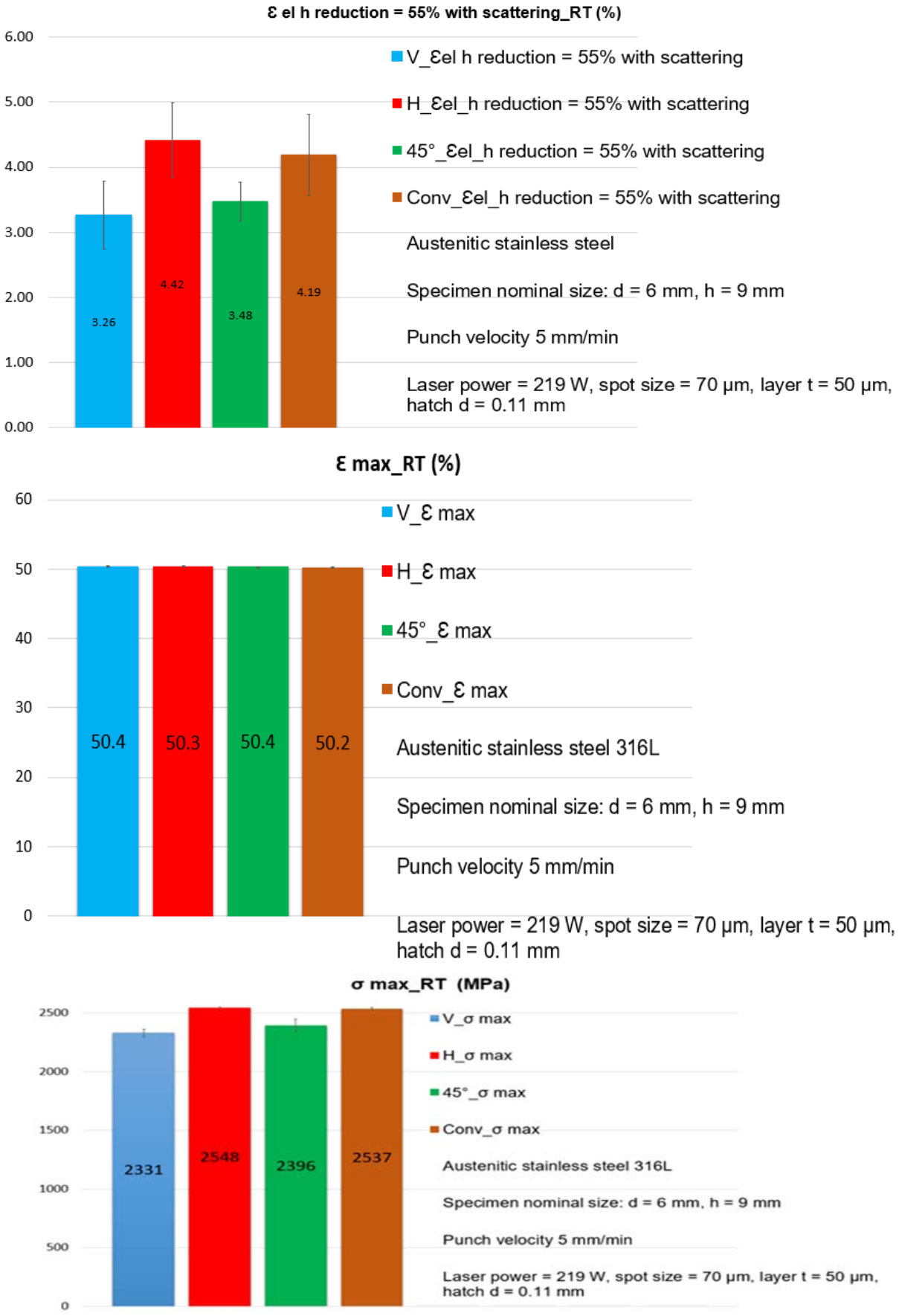

Figure 5.28. *Elastic and plastic strains at room temperature*

With the second comparison the additively manufactured specimens are analysed deeply. From the results analysis, seems to be present a superiority of the horizontal building direction at the room temperature. Nevertheless, ever at the room temperature, the 45° build direction maintains good mechanical properties, remaining ever over the vertical direction. Moreover, if the temperature increases, the mean best mechanical properties at low and high strain values are shown by the 45° build direction. Therefore, averagely for compression load situations, the diagonal building direction seems to be the most suitable.

5.2 Tensile test

For a metal material, the tensile test represents the most significant analysis for having wide resistance data set ($R_{0.2}$, R_m) together to the uniform elongation (A). In every engineering structural design phase, the first material resistance controls focus on the static security based on the comparison between the total ideal stress and the $R_{0.2,}$ where the ideal stress is found by a combination of the Navier's flexion σ distribution, Jourawsky's flexion τ distribution and Coulomb's torsion τ distribution [45] through Guest, Bach or Von Misses criteria, in order to find a safety coefficient greater than 1.5, as shown in Equation 5:

$$\frac{\mathrm{Rp0.2}}{\sigma \mathrm{id}} > 1.5 \qquad \text{Equation 5}$$

Instead for metal forming applications the attention is addressed towards the uniform plastic deformations zone. Finally, the local deformations zone presents factor of interest for Neuber's principle. This last one zone ends with the failure.
For these reasons is necessary the tensile mechanical properties analysis of the additive material, maintaining a constant comparison with the conventional reference. There are two type of conventional specimens as mentioned in 4.1.3: the first presents a 1.5 mm of thickness, the second 2 mm. Then each one is manufactured with a 0° or 90° rolling direction, because of the material anisotropy. Even if the tensile specimens are milled before the prove, remains a visible waviness on the along L_0 stretch, therefore a breaking of sharp edges and a further cleaning phase is necessary before the measurements otherwise the results could be affected.
The tensile mechanical properties calculated are:

- yield strength, where the metallic material exhibits a yield phenomenon, that is the stress corresponding to 0.2 % plastic strain;
- tensile strength (R_m), that is the stress corresponding to the maximum force (F_m) divided by the initial surface $A_0$of the specimen;
- elongation in percentage after fracture (A), that is the permanent elongation of the gauge length after fracture (L_u - L_o), expressed as a percentage of the original gauge length (L_o).

Regarding the last listed mechanical property, is necessary to do a specification. The A, corresponding to R_m, is the only % plastic strain excluding the scattering amount since the deformation does not start from zero stress. In diagrams are plotted the engineering stress strain curves.

5.2.1 Building direction influence at room temperature

Regarding the tensile tests results, the only build direction comparison is conducted since the proves are only at room temperature. As already mentioned in 4.1.3, the tensile additive specimens are tested together two types of conventional: 1.5 mm and 2 mm of thickness. In order to do a well-organized comparison, at the beginning are analysed singularly all the horizontal specimens and all the vertical in two different diagrams. In this regarding, the meanest curves are then considered together compared with the 1.5 mm conventional in first instance, and in second instance with the 2 mm. Also, the conventional will represent the mean curves.

Specimens manufactured with a horizontal building direction

Starting from the horizontal specimens, they are built in the upper, medium left, medium right and lower table machine zones as shown in Figure 4.5 in section 4.1.3.

If they are plotted in the same diagram, as shown in Figure 5.29, it is possible to see as the AM_H_MR_16 specimen presents comparable $R_{p0.2}$ to the others but the highest uniform plastic zone. Instead the AM_H_U_4 specimen shows the shortest uniform elongation. For these reasons, the mean representation of the horizontal building direction is given by the AM_H_ML_10 and the AM_H_L_24 specimens.

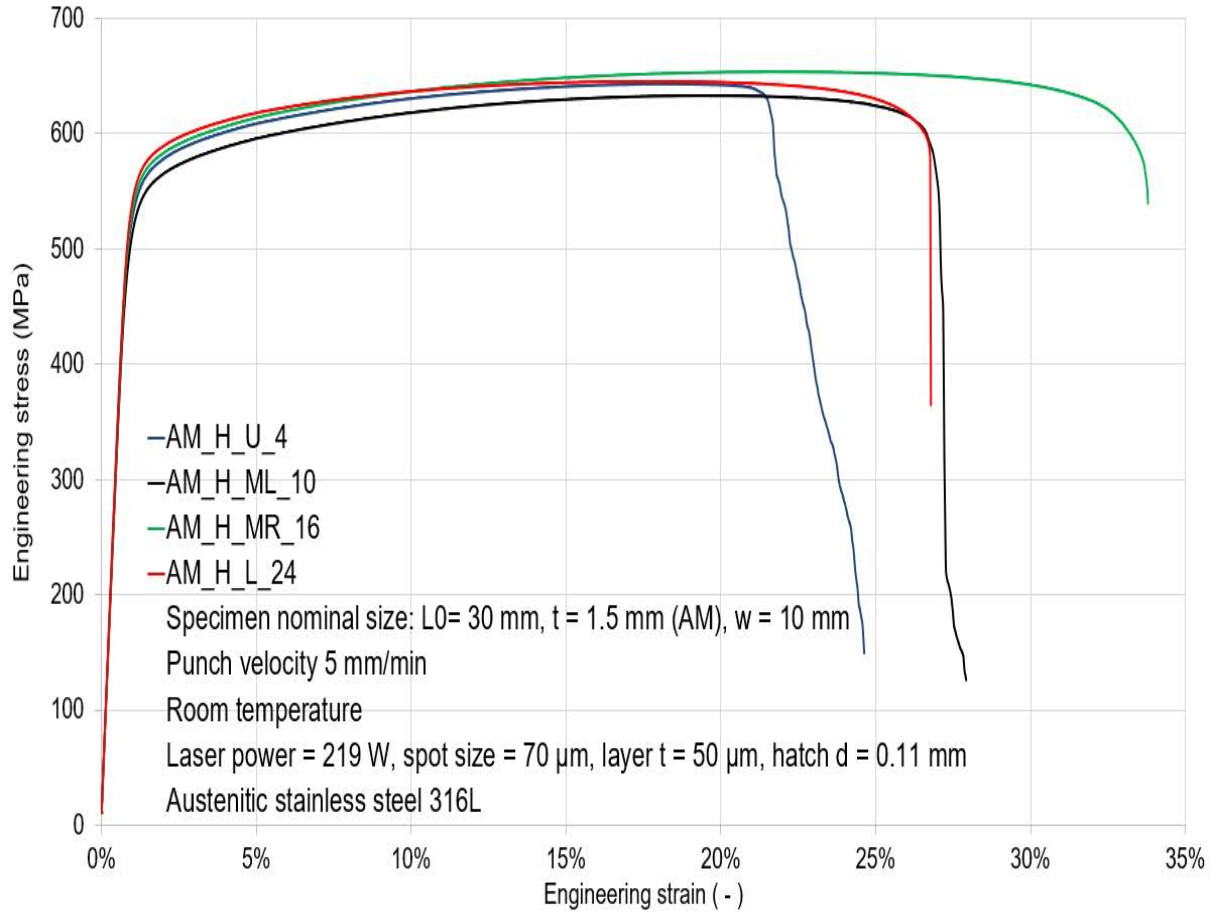

Figure 5.29. *Comparison of additive specimens manufactured with an horizontal build direction*

Focusing on these last one specimens, as shown in Figure 5.30, it is possible to do a further comparison.

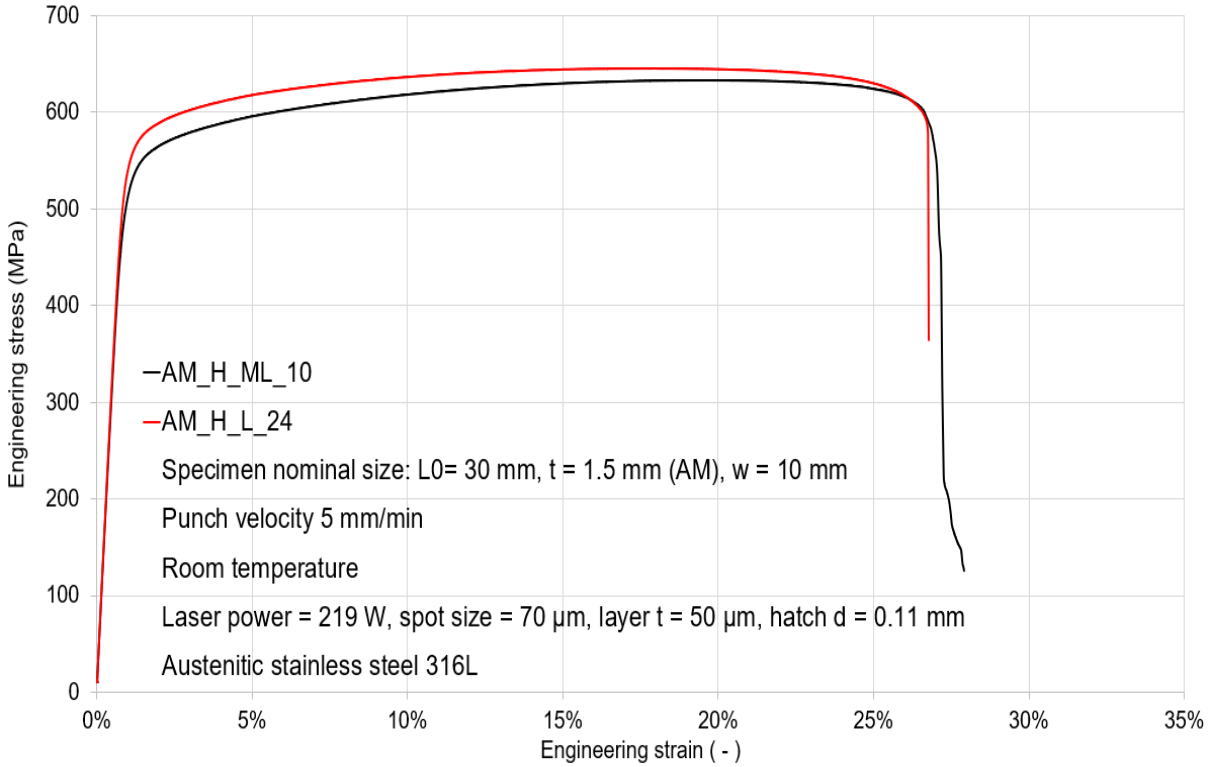

Figure 5.30. *Mean curves of the horizontal specimens set*

The AM_H_L_24 specimen can be considered superior to the other because they both present the same uniform elongation but the blue one has an higher yield stress. If all the horizontal specimens set is considered, is possible to see in Figure 5.31 a quantitative description through histograms.

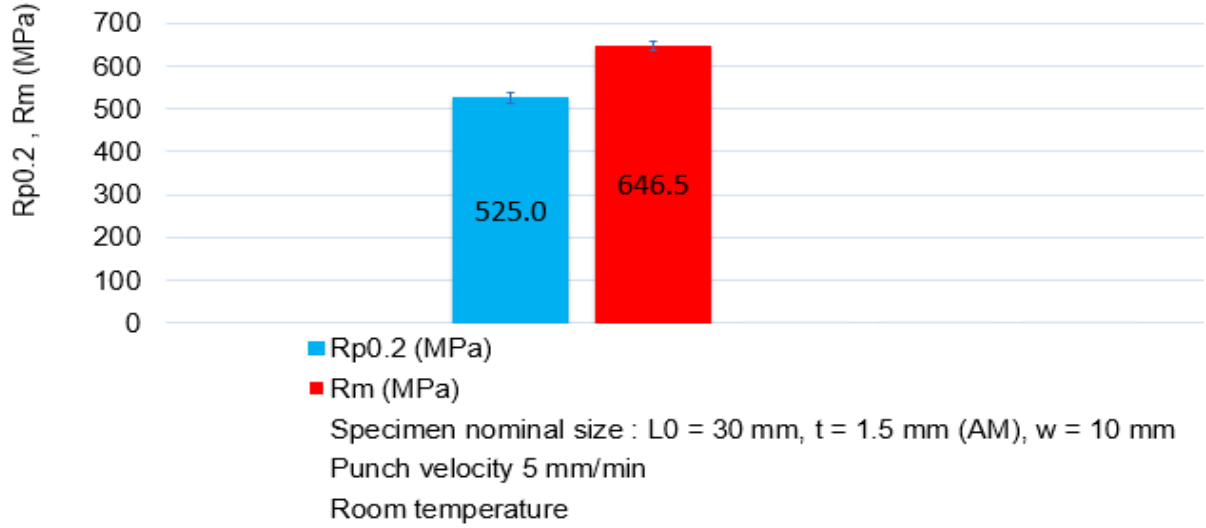

Figure 5.31. *$R_{p0.2}$ and Rm mean values of horizontal building direction*

Specimens manufactured with a vertical building direction

If the specimens manufactured with a vertical building direction are analysed, as shown in Figure 5.32, it is clear as the AM_V_LR_25 specimen represents the good compromise between the entire vertical specimens set.

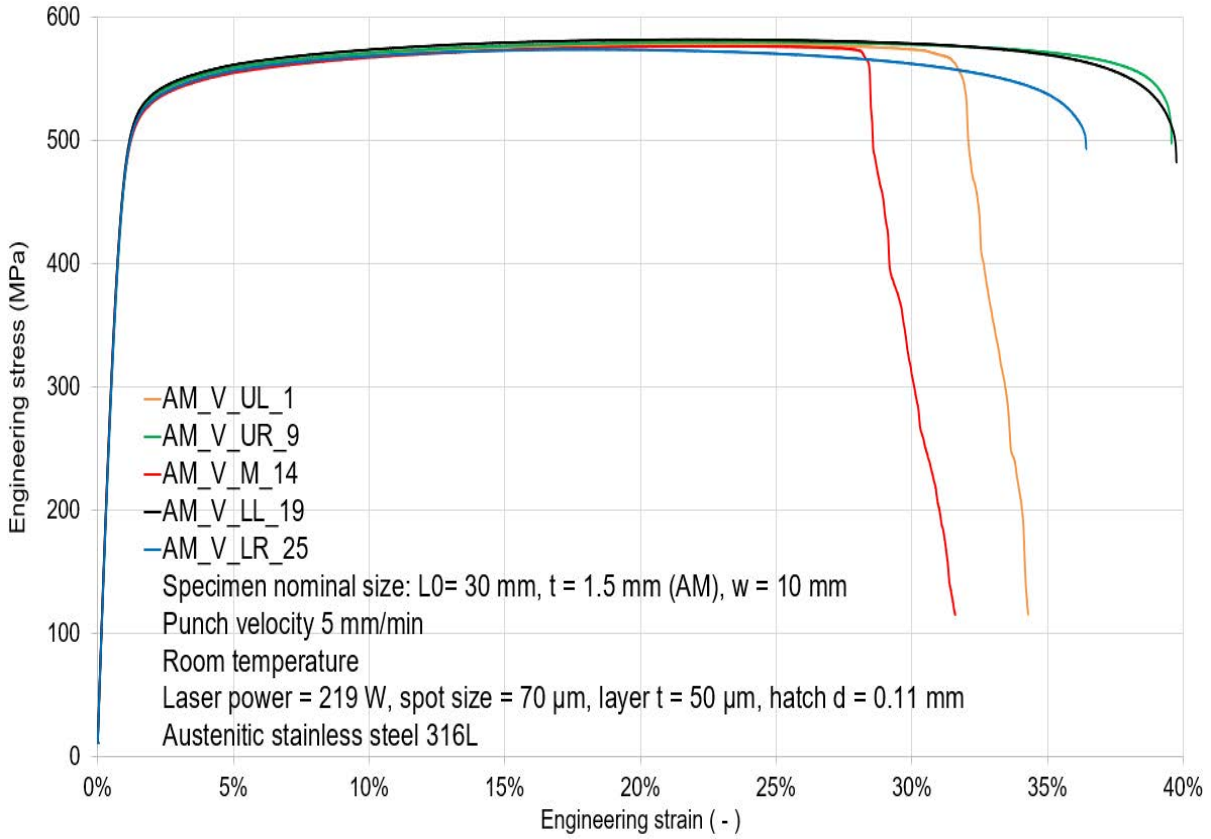

Figure 5.32. *Comparison of additive specimens manufactured with an vertical building direction*

Compared to the horizontal specimens, the vertical is closer between them in the $R_{p0.2}$ value.
Considering the state of the art, in particular section 2.3.2, the $R_{p0.2}$ and Rm of Figure 5.32 are comparable with the engineering stress strain curves of the specimen manufactured with a vertical build direction of Figure 2.22.
If the qualitative results of the diagram are summarized in a histogram, it is possible to evaluate with accuracy the yield stress and Rm values.
If a comparison with Table 2.8 in section 2.3.1 is done, the vertical specimens manufactured with Lasertec PBF machine show, in Figure 5.33, a consistent slower yield stress: 434 ± 14.1 MPa instead of 496 MPa (state of art uncertainty value not available), and a lower Rm: 577.9 ± 9.6 MPa instead of 717 MPa (state of art uncertainty value not available). Therefore, the only yield stress is comparable.

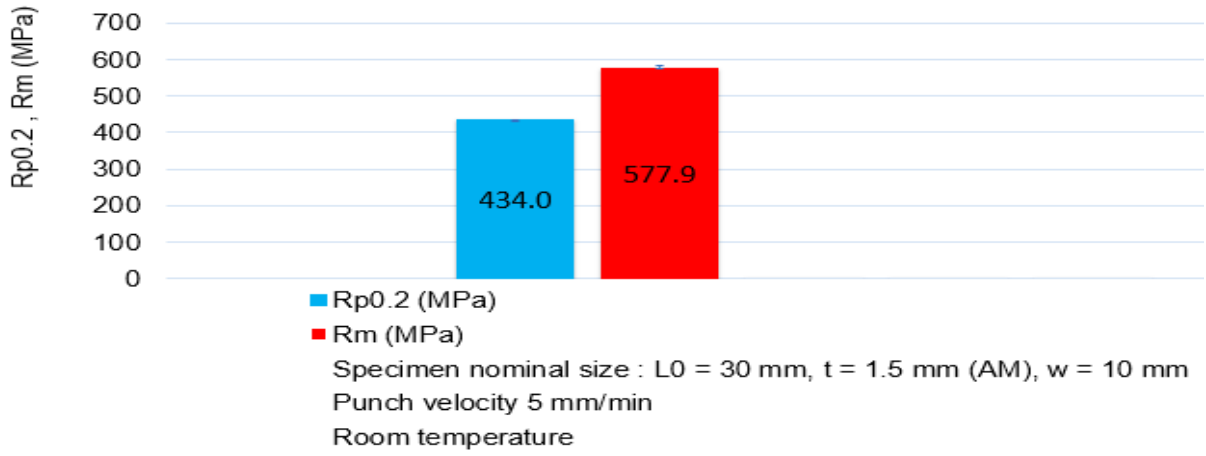

Figure 5.33. *$R_{p0.2}$ and Rm mean values of vertical building direction*

The uncertainty of vertical specimens is smaller than the state of art and also of the horizontal specimens, nevertheless the specimens number considered is limited, therefore the statistical analysis is strongly affected.
In Figure 5.34, is shown singularly the mean engineering stress strain curve of the vertical specimens set.

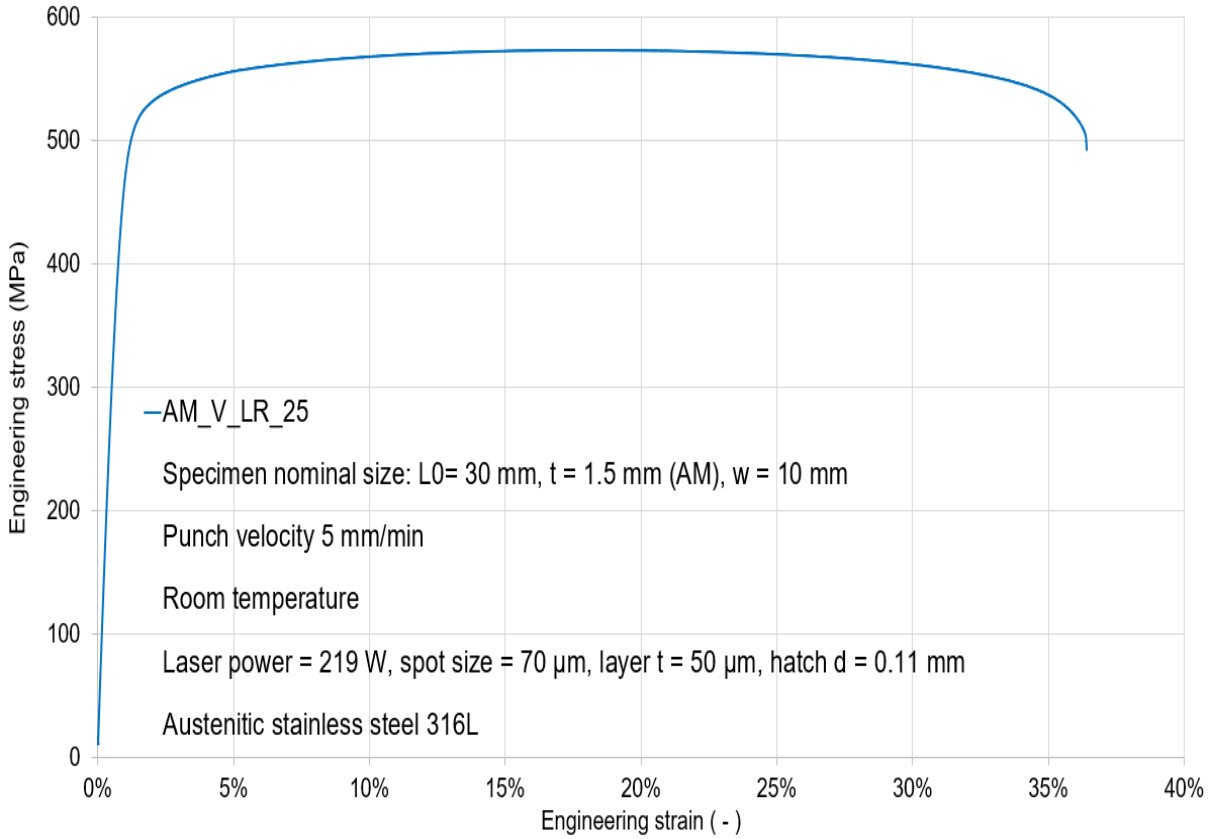

Figure 5.34. *Mean curve of the vertical specimens set*

Once the mean curves are found, respectively the AM_H_L_24 and the AM_V_LR_25, a comparison between the different build direction can be done. As shown in Figure 5.35, the horizontal specimen present a longer elastic zone, but a smaller zone of uniform plastic

deformation.

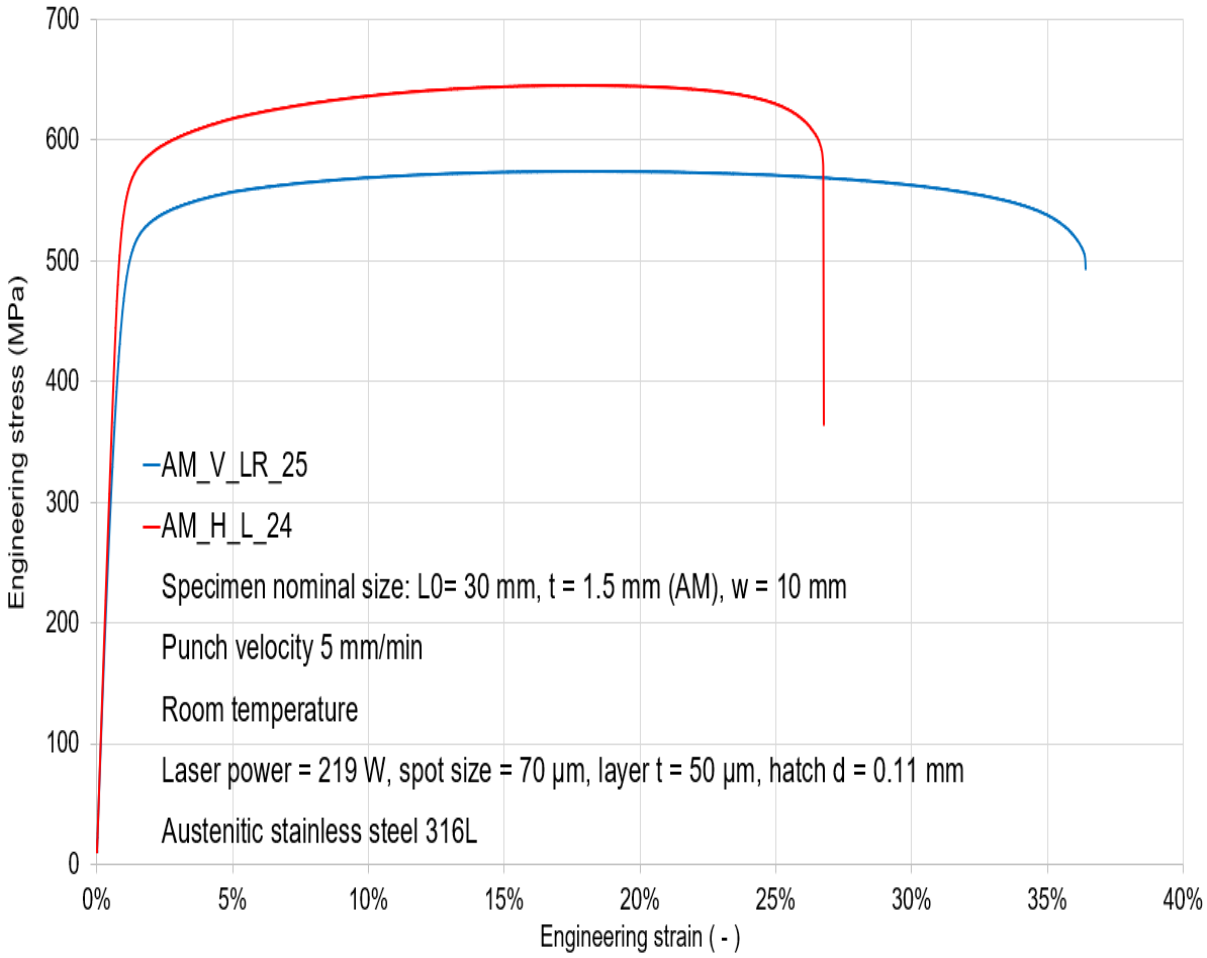

Figure 5.35. *Mean curves of horizontal and vertical building directions*

Moreover, the horizontal $R_{p0.2}$ is clearly higher than the vertical that brings the horizontal building direction to show a higher Rm, therefore the AM material shows a strong influence of the building direction on the stress strain curve. This can be reasoned by the different alignment of weld beads due to the manufacturing process; where, as in case of vertical direction, the maximum strain is higher than in case of horizontal direction.

Nevertheless, as for the compression tests, a constant reference has to be done with the conventional. As mentioned in section 4.1.3, the conventional specimens used present same L_0 and width but a different thickness.

As shown in Figure 5.36, the first conventional specimens considered present a 1,5 mm of thickness. Once again in the diagram are plotted the mean curves, that is the most representative of the conventional specimens set. The conventional specimen worked with a 90° rolling direction, presents a little higher yield stress but a really larger uniform plastic zone compared to the 0° rolling direction.

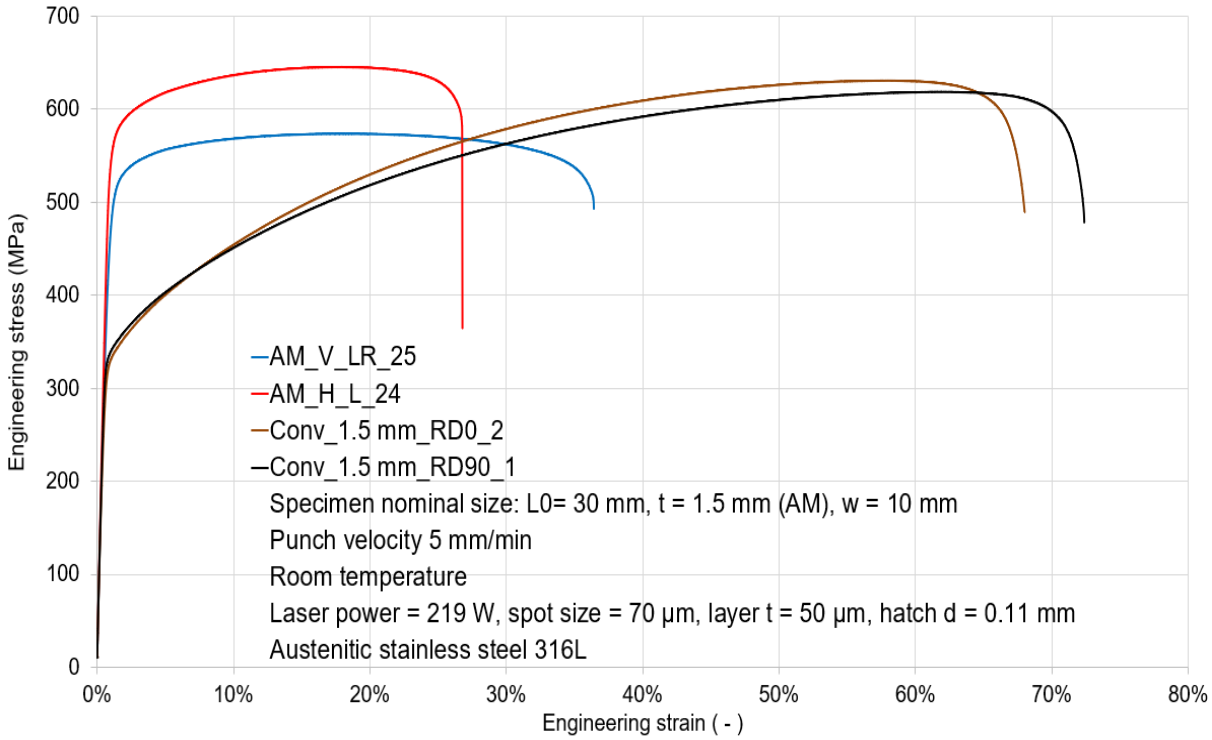

Figure 5.36. *Horizontal and vertical mean curves compared with the conventional specimens having thickness of 1.5 mm*

The yield stresses of AM material are higher than for the conventional material. But the Rm values is not higher in every case. Furthermore, the strain of conventional material is much higher than for AM material.

As already introduced, the horizontal specimens present a longer elastic zone, but a smaller zone of uniform plastic deformation. This means that for static applications the additive, above all the horizontal build direction, is superior compared to the conventional. Nevertheless, both the additive specimens show a really limited uniform plastic zone than the conventional. Even if plastic zone is synonymous of forming, nevertheless it is not possible to make a clear interpretation for the sheet metal material, since the manufacturing process is completely different and the anisotropy is reasoned by a another phenomenon, which is the rolling process.

If the 2 mm conventional specimens are considered as in Figure 5.37, it is possible to see the same trend of before: the 90° rolling direction allows to have a little higher elastic zone and an important increasing in the uniform plastic zone.

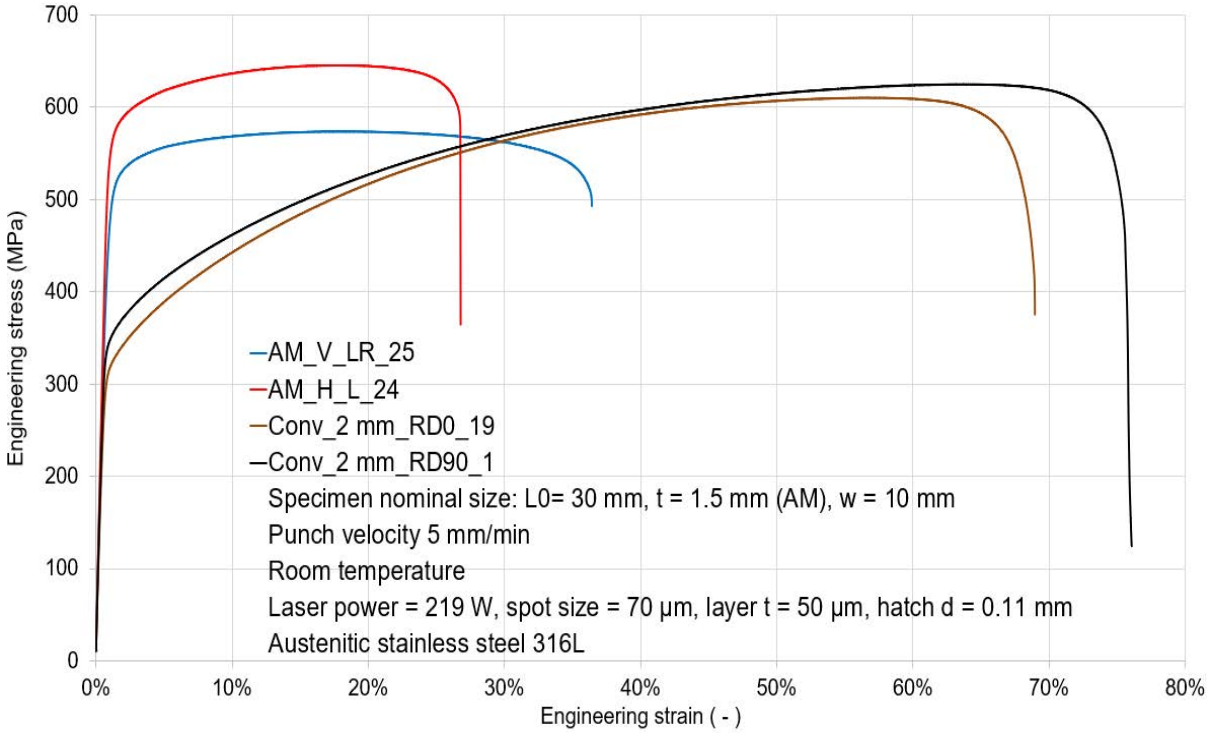

Figure 5.37. *Horizontal and vertical mean curves compared with the conventional specimens having thickness of 2 mm*

After a qualitative overview, quantitative results with a reference to the conventional material are necessary in order to conduct a correct evaluation. For these reasons are considered additive specimens together all the conventional. Nevertheless, the uncertainty amount calculation is not ever possible because of the limited specimens' number.

Until now the results found are in agreement with the state of art. Nevertheless, after a qualitative overview, quantitative results with a reference to the conventional material are necessary in order to conduct a correct evaluation. For these reasons are considered the entire additive specimens set together all the conventional. As shown in Figure 5.38, the horizontal build direction presents the highest $R_{p0.2}$ value. This value is consistently higher than the vertical build direction and both the additive $R_{p0.2}$ values are positively far away from the conventional. These last two show an improvement only in the rolling direction changing and not with a higher thickness.

Finally if also the thesis conventional values are compared to Table 2.3 in section 2.2, they are really close to the state of art.

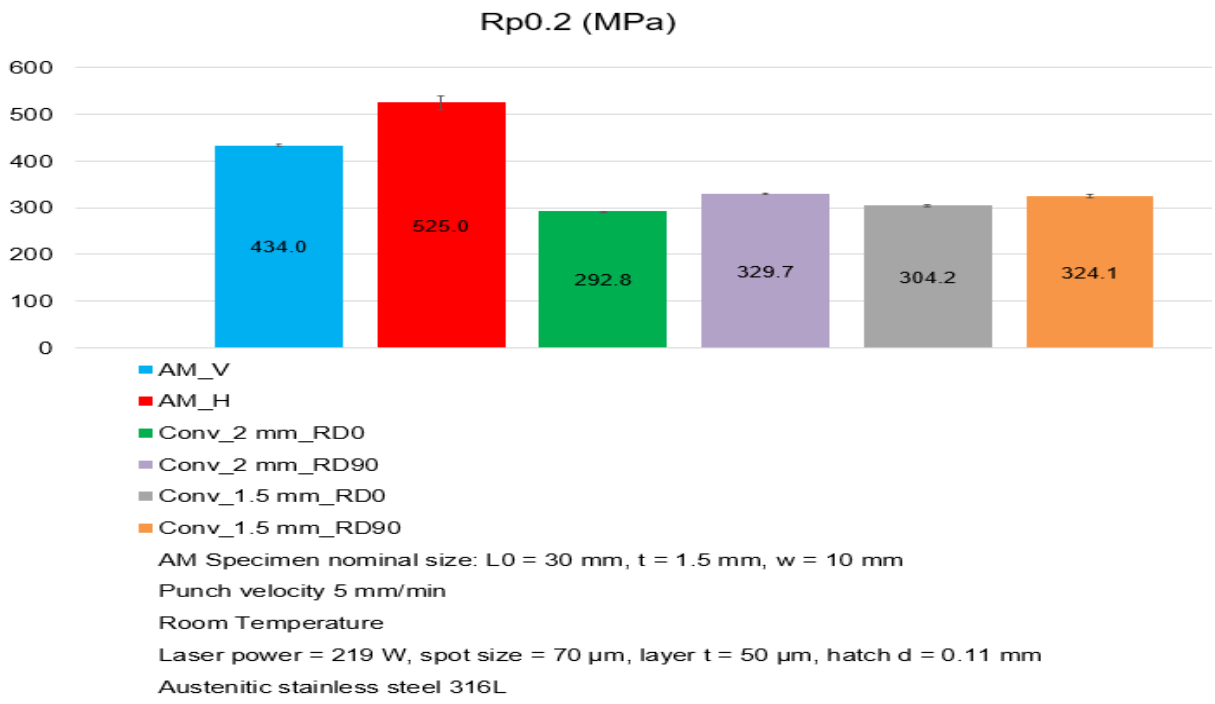

Figure 5.38. *Building direction influence on $R_{p0.2}$ value*

If the Rm (UTS) is analyzed as shown in Figure 5.39, a different trend is found. Once again, the horizontal build direction presents the highest value, even if no so far away from the conventional. Nevertheless, it is necessary to speak of different trend, because the vertical build direction shows an inferior value compared the conventional.

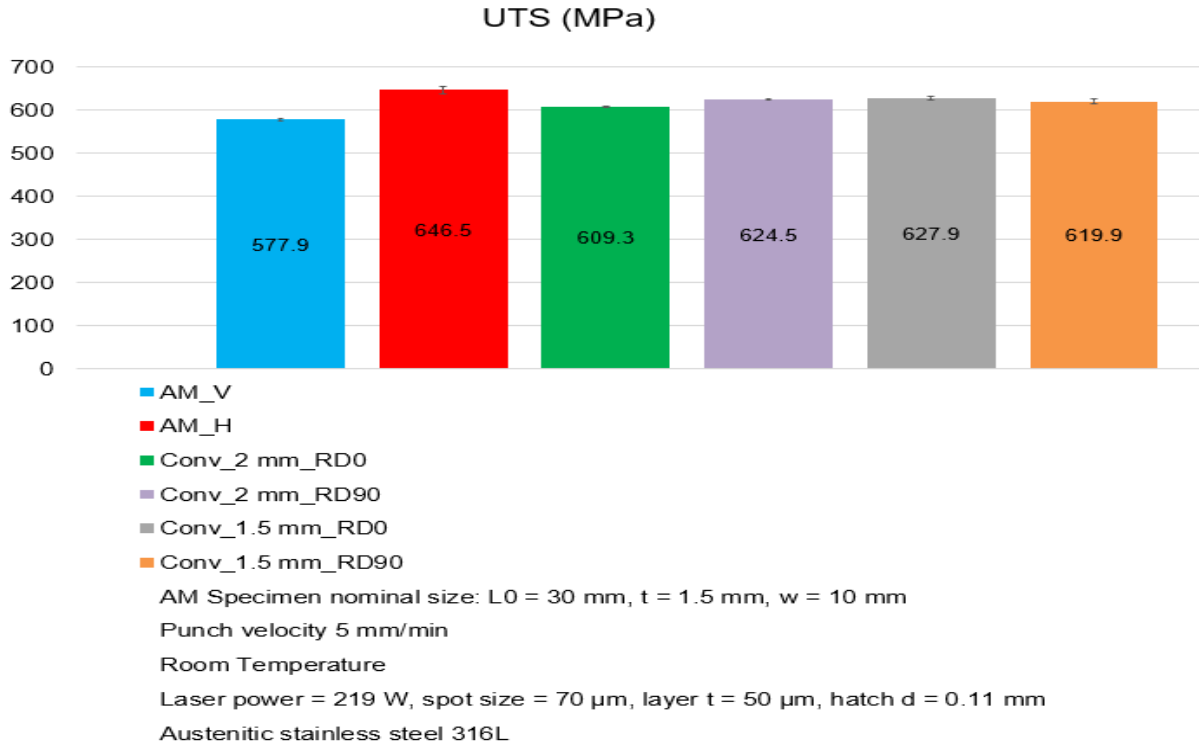

Figure 5.39. *Building direction influence on Rm value*

Moreover, there is not an improvement in the different rolling direction as before with the $R_{p0.2}$ value. The Rm value covers an important role in the forming evaluation. Until now the additive specimens, above all the horizontal, seem to show higher mechanical properties. Nevertheless, in order to have a clear forming overview it is necessary to consider also the uniform elongation zone, that is the plastic strain in correspondence of Rm value.

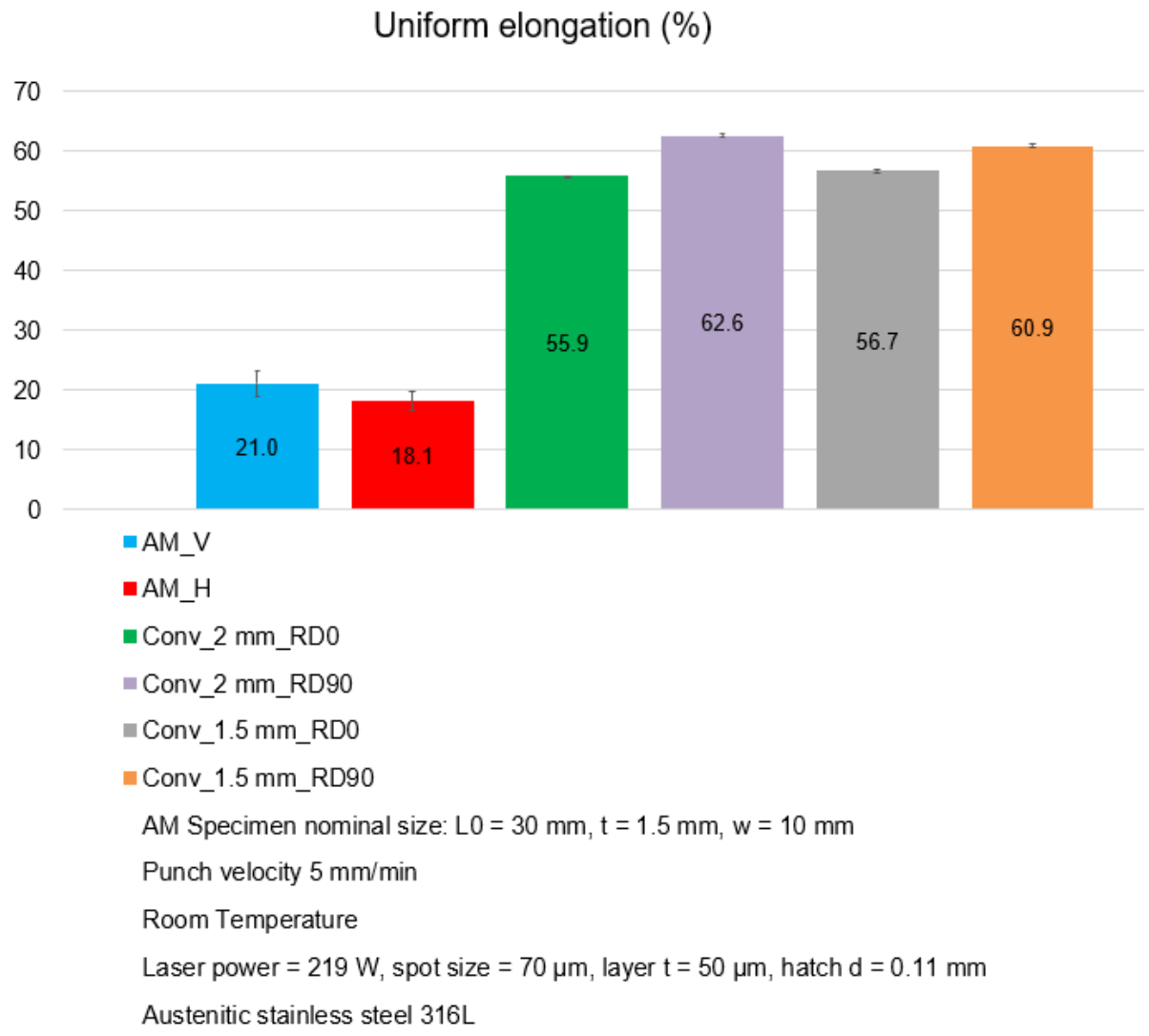

Figure 5.40. *Building direction influence on A value*

In this regarding, Figure 5.40 illustrates as both the additive uniform elongation is less than half compared to the conventional. This means the presence of a weakness in the additive specimens that balances negatively the positive additive mechanical properties found until now.
Concerning the conventional, returns a clear improvement in the value if the specimen is worked with a 90° rolling direction, as also found for $R_{p0.2}$ value.
Finally, in order to show clearly all the comments found, coming from the data set analysis, in the Appendix is possible to find singularly the $R_{p0.2}$, Rm and uniform elongation values of all the specimens set.

6 Summary and outlook

The formability knowledge allows to manage the forming processes after Additive Manufacturing. In this research work, the formability of 316L, manufactured with L-PBF, is being investigated at different temperatures in order to define the compromising temperature between the force decreasing, at high temperatures, and the increasing costs to achieve them.
The extrapolated data, coming from the material flow curves, is used in numerical simulations for modelling the following forming operations, in order to predict the real forming process. The flow curves are useful to implement mathematical flow curve approaches.
From the tests flow curves were derived for describing and modelling the forming behaviour.
The elevated temperature reduced the yield strength, which meant that material started to flow at lower stresses. This resulted to be beneficial for the formation of lower forces. Nevertheless, 316L has a high formability even at room temperature.
The results that were found are in agreement with the State of art and often higher, in terms of resistance: from the experimental data, the compression with a vertical build direction at 500°C shows higher values of $\sigma_{0.2}$ than in the State of art; respectively 353 ± 7 MPa (Thesis) instead of 368 MPa [33].
Regarding the tensile test, comparable values of $R_{p0.2}$ at room temperature are discovered between the vertical building direction of Thesis and the State of art: 434 ± 2 MPa (Thesis) instead of 496 MPa [36].
Nevertheless, even at room temperature, different values are displayed in the compression $\sigma_{0.2}$ between the vertical build direction of Thesis and the State of art, respectively: 494 ± 66 MPa (Thesis) instead of 403 ± 6 MPa [29] and regarding the tensile Rm: 577.9 ± 9.6 MPa (Thesis) instead of 717 MPa [29].
Focusing on the compression tests, there is a clear superiority in the diagonal building direction compared with the two other building directions, whereas from the tensile one can see a dominance of the horizontal building direction.
The analysis of the results focuses on the investigation of mechanical properties by varying:

- The temperature for equal building direction
- The building direction for equal temperature

Regarding the compression tests:

- at 500°C the additive $\sigma_{0.05}$ and $\sigma_{0.2}$ show comparable values between them but clearly inferior to the conventional material. Nearly same values can be found between AM and conventional for the sigma in correspondence of a 55% height reduction. Additive horizontal and diagonal deformation in correspondence of UTS is a little superior to the conventional. The deformation in correspondence of UTS is around 50% for all the materials while the elastic deformation in correspondence of 55% height reduction shows a consistent dominance of diagonal AM material than both the conventional and the vertical and horizontal AM material. A high elastic deformation means a static behavior for a longer time. Therefore, on average, we can state that the best choice at 500°C is represented by the diagonally built AM material. Therefore, the best compromise at

500°C is represented by the diagonal building direction, even better than the conventional.

- At 250°C vertical and diagonal AM $\sigma_{0.05}$ is comparable to the conventional one and clearly higher than the horizonal. AM $\sigma_{0.2}$ is in general a little inferior to the conventional, whereas AM sigma in correspondence of a 55% height reduction is in general higher than conventional. Once again, the AM diagonal elastic deformation in correspondence of 55% height reduction is more than twice as high as the AM horizontal one, more than the three times as the AM vertical and comparable with the conventional material. The AM UTS deformation is in general a little higher than the conventional. At this temperature, the specimens showing the best mechanical properties are built in a diagonal direction. Nevertheless, they do not overcome the conventional.
- At 100°C, AM $\sigma_{0.05}$ and $\sigma_{0.2}$ are on average the same between each other and between the additive material. The horizontal AM sigma in correspondence of a 55% height reduction is the highest. A strong difference with the previous cases is represented by the clear reduction of the diagonal elastic deformation in correspondence of 55% height reduction. At the same time, the UTS deformation is the same for all the specimens. At this temperature, the horizontal and diagonal specimens are equal, but sometimes inferior to the conventional.
- At room temperature, the diagonal $\sigma_{0.05}$ and $\sigma_{0.2}$ are higher than the conventional. Nevertheless, the horizontal $\sigma_{0.05}$ is consistently the smallest. The highest sigma and elastic deformation in correspondence of a 55% height reduction is shown by the AM horizontal specimens. Finally, the UTS deformation is one again the same for all the specimens. At room temperature the best compromise behavior is shown by the diagonal or horizontal building direction.

The investigation of mechanical properties, by varying the temperature, show as the best compromise is represented by the diagonal (45°) building direction (Table 6.1).

Table 6.1. *Comparison between the AM building direction in the compression results*

Compression test	500°C	250°C	100°C	RT
Best compromise	Diagonal	Diagonal	Diagonal, Horizontal	Diagonal, Horizontal

On average, the compression additive mechanical properties are close to the conventional in any temperature level.

Concerning the compression mean flow curves, for each additive building direction at 500°C, 250°C and 100°C in correspondence of low strain values, is present a clear additive weakness in the stress resistance and a higher stress resistance capability in correspondence of high strains, compared to the conventional. This trend is clear for the horizontal and diagonal building direction, while being less evident at 250°C and 500°C in correspondence of high strains for the vertical building direction. Precisely at high and room temperature, the additive $\sigma_{0.05}$ and $\sigma_{0.2}$ are clearly inferior compared to the conventional, therefore the additive material starts for equal strain to flow for lower stress values: the additive starts to flow before the conventional.

Nevertheless, this facilitated initial additive flow after a 55% height reduction becomes more prevented than the conventional.
Regarding the room temperature for the diagonal building direction the opposite trend can be observed: the additive $\sigma_{0.05}$ and $\sigma_{0.2}$ are superior in the comparison with the conventional. This last result is in agreement with the reflection from Table 6.1.

A different trend, however, is shown by the tensile results. With the tensile load, the additive material starts to flow at higher stresses, which is later, than the conventional. Nevertheless, the additive uniform elongation is really limited compared to the conventional: an additive 20% compared to a conventional 60%. Moreover, focusing on the additive building direction comparison, the horizontal specimens show higher yield strength but less uniform elongation than the vertical specimens. This is also in agreement with the state of art [37].
If the RT additive compression and tensile mean stress strain curves are analysed together, the flow under compression loads starts for higher stress values than the tensile load (compression for horizontal and vertical : $\sigma_{0.2} = 527 \pm 27$ MPa and $\sigma_{0.2} = 522 \pm 2$ MPa; tensile for horizontal and vertical: $R_{p0.2} = 525 \pm 14$ and $R_{p0.2} = 434 \pm 2$ MPa). Nevertheless, the opposite trend appears visible for the conventional, where the material starts to flow at lower stresses than under compression load (compression: $\sigma_{0.2} = 547 \pm 18$ MPa; tensile 2 mm RD0: $R_{p0.2} = 292.8 \pm 1$ MPa, tensile 2 mm RD90: $R_{p0.2} = 329.7 \pm 1$ MPa, tensile 1.5 mm RD0: $R_{p0.2} = 304.2 \pm 2$ MPa, tensile 1.5 mm RD90: $R_{p0.2} = 324.1 \pm 3$ MPa). Therefore, the additive material presents an opposite material behaviour compared to the conventional.
Moreover, while the compression mechanical properties of AM are on average close to the conventional, the tensile mechanical properties of AM continue to show an overly different uniform elongation.

Within this Master Thesis the mechanical properties of additively manufactured specimens of austenitic stainless steel of the alloy 316L are being investigated. In this regard other analyses can be conducted. The next steps, regarding the compression tests, would be to understand which process parameters, analysed in the state of art, allow to have in the additive material with compression loads a higher flow resistance at high strain values.
Future works would focus on developing a flow numerical stress model that accurately describes the flow behaviour, taking into account the microscopic mechanisms during the forming operations of L-PBF pre-forms.
Instead, regarding the tensile tests, the next study should focus on the data analysis from high temperature tensile tests, in order to give a wide overview as it was done for the compression tests.
In order to study resistance, also fatigue life should be analysed. This could be achieved by studying the strain-life curves, plotted through an uniaxial strain-controlled fully-reversed (R = -1) cyclic loading.
In addition, a deep microstructural characterization regarding binding defects, gas pores and voids associated to residual stresses would allow to further optimize the process parameters.
Finally, future research would focus on thermal-mechanical-metallurgical physic for modelling the printing process.

7 Literature

[1] Turinetti, G.:, „Design the Difference: Liberare il potenziale dell'Additive Manufacturing con nuove tecniche di progettazione," *Altair,* 2018.

[2] F. Meiners, J. Ihne, P. Jürgens, S. Hemes, M. Mathes, I. Sizova, M. Bambach, R. Hama-Saleh und A. Weisheit, „New Hybrid Manufactruing Routes Combining Forging and Additive Manufacturing to Efficiently Produce High Perfomance Components from Ti-6Al-4V," *ScienceDirect,* pp. 261-267, 2020.

[3] Z. Tan und J. Jang, „Additive Manufacturing and subsequent forging," *Imperial College London,* 2020.

[4] Khairallah, S. A.; Anderson, A, T,; Rubenchik, A.; King, W. E.:, „Laser powder-bed fusion additive manufacturing: Physics of complex melt flow and formation mechanisms of pores, spatter, and denudation zones," *Acta Materialia,* pp. 39-41, 2016.

[5] King, W. E.; Anderson A. T.; Ferencz, R. M.; Hodge, N. E.; Kamath, C.; Khairallah, S. A.; Rubenchik A. M.:, „Laser powder bed fusion additive manufacturing of metals; physics, computational, and materials challenges," *Applied Physics Reviews,* pp. 2-3, 2015.

[6] Dadbakhsh, S.; Hao, L. and Sewell, N., „Effect of selective laser melting layout on the quality of stainless steel parts," *Rapid Prototyping Journal,* p. 241, 2011.

[7] Huckstepp, A., „Digital Alloys' Guide to Metal Additive Manufacturing - Part 8 Powder Bed Fusion (PBF)," *DigitalAlloys,* 2019.

[8] Kruth, J. P.; Vandenbroucke, B.; Van Vaerenbergh, J.; Mercelis, P.:, „Benchmarking of different SLS/SLM processes as rapid manufacturing techniques," *Int. Conf. Polymers & Moulds Innovations,* pp. 1-5, 2005.

[9] Berger, R.:, „Advancements in metal 3D printing," *Roland Berger Focus,* p. 9, 2018.

[10] Gibson, I.; Rosen, D.; Stucker, B.:, Additive Manufacturing Technologies, 3D Printing, Rapid Prototyping, and Direct Digital Manufacturing, New York: Springer, 2015.

[11] Sher, D.:, „The global additive manufacturing market 2018 is worth $9.3 billion," *3D Printing Media Network,* 14 December 2018.

[12] Yap, C. Y.; Chua, C. K.; Dong, Z. L.; Liu, Z. H.; Zhang, D. Q.; Loh, L. E.; Sing, S. L.:, „Review of selective laser melting: Materials and applications," *Applied Physics Reviews,* 2015.

[13] Uckelmann, I.:, „La "buy-to-fly ratio" Come tagliare i costi con la stampa 3D del metallo," *Materialise manufacturing,* 2017.

[14] Li, R. D.; Liu, J. H.; Shi, Y. S.; Du, M. Z.; Xie, Z.:, „316l Stainless Steel with Gradient Porosity Fabricated by Selective Laser Melting," *Journal of Materials Engineering and Performance,* pp. 666-671, 2010.

[15] BS EN ISO/ASTM 52900:2017:, *Additive manufacturing - General principles - Terminology.*

[16] Osakada, K.; Shiomi, M.:, „Flexible manufacturing of metallic products by selective laser melting of powder," *Science direct,* p. 1, 2006.

[17] Halaye, T.:, „Powder Bed Fusion Market, Demand, Supply and Price Analysis 2019 to 2025," *Industry Reports,* 20 April 2019.

[18] TRUMPF, „Laser metal fusion - befenits, working principles, and applications of the additive technology,“ [Online]. Available: https://www.trumpf.com/en_CA/applications/additive-manufacturing/laser-metal-fusion-lmf/.

[19] Spierings, A. B.; Levy, G., „Comparison of density of stainless steel 316L parts produced with selective laser melting using different powder grades,“ pp. 5-6, 2009.

[20] Sander, J.; Hufenbach, J.; Giebeler, L.; Wendrock, H.; Kuhn, U.; Eckert, U.:, „Microstructure and properties of FeCrMoVC tool steel produced by selective laser melting,“ *Mater. Des. 89,* pp. 335-341, 2015.

[21] Montero-Sistiaga, M. L.; Pourbabak, S.; Van Humbeeck, J.; Schryvers, D.; Vanmeensel, K. , „Microstructure and mechanical properties of Hastelloy X produced by HP-SLM (high power selective laser melting),“ *Material and Design,* 2019.

[22] Meier, H.; Haberland, Ch., „Experimental studies on selective laser melting of metallic parts,“ *InterScience,* 2008.

[23] Paolucci, G. M.:, Appunti di Materiali Metallici, Padova: Libreria Progetto, 1998.

[24] Ferro, P.; Bonollo, F.:, Dispense di Materiali Metallici con esercizi, Libreria Progetto, 2018.

[25] Bevan, M.:, „Mechanical properties and behavior of Additive Manufacturing stainless steel 316L,“ *SBLT, School of Engineering & Information Technology,* 2016.

[26] Tresoldi Metalli, „Acciaio Austenitico Inox 316L, Acier Austénitique inoxydable 316L“.

[27] U. Bertoli, B. MacDonald und J. Schoenung, „Stability of cellular microstructure in Laser Powder Bed Fusion of 316L stainless steel,“ *Materials Science and Engineering,* pp. 106-117, 2019.

[28] Miranda, G.; Faria, S.; Bartolomeu F.; Pinto E.; Madeira, S.; Mateus A.; Carreira, P.; Alves, N.; Silva, F. S.; Carvalho, O.:, „Predictive models for physical and mechanical properties of 316L stainless steel produced by selective laser melting,“ *Materials Science & Engineering A,* pp. 50-55, 2016.

[29] Buchanan, C.; Salmlnen, A.; Gardner, L.:, „Structural performance of additive manufactured metallic material and cross-sections,“ *Journal of Constructional Steel Research,* September 2017.

[30] Kurzynowski, T.; Chlebus, E.; Kuznicka, B.; Reiner, J.:, „Parameters in selective laser melting for processing metallic powders,“ *SPIE LASE,* 2012.

[31] Song, B.; Dong, S.; Zhang, B.; Liao, H.; Coddet, C.:, „Effects of processing parameters on microstructure and mechanical property of selective laser melted Ti6Al4V,“ *Material & Design,* 2012.

[32] Ghiotti, A:, „Workability“.*Design and vitual prototyping of manufacturing process.*

[33] Ham, Gi-Su; Park, Soon-Hong; Lee, Kee-Ahn:, „Room and Elevated Temperature Compressive Deformation Behavior of AISI 316L Alloy Fabricated by Selective Laser Melting Process,“ *Korean Journal of Metals and Materials,* pp. 295-303, 2019.

[34] Liverani, E.:, „Studio e ottimizzazione del processo di fabbricazione additiva (SLM) per applicazioni in ambito biomedicale: produzione di protesi e strutture reticolari,“ *Master thesis, University of Bologna,* 2017.

[35] SLM Solutions Group AG, „3D METALS Discover the variety of Metal Powders," *SLM SOLUTIONS.*

[36] Mower, T. M.; Long, M. J.:, „Mechanical behavior of additive manufactured, powder-bed laser-fused materials," *Materials Science & Engineering A,* pp. 202-212, 2015.

[37] R. Shrestha, J. Simsiriwong, N. Shamsaei und S. B. L. Thompson, „EFFECT OF BUILD ORIENTATION ON THE FATIGUE BEHAVIOR OF STAINLESS STEEL 316L MANUFACTURED VIA A LASER-POWDER BED FUSION PROCESS," Department of Mechanical Enginnering, Auburn University; Department of Industrial and Systems Engineering, Mississippi State University.

[38] Choi, H.; Lee, C.:, „A mathematical model to predict thickness distribution and formability of incremental forming combined with stretch forming," *Robotics and Computer Integrated Manufacturing,* p. 1, 2018.

[39] METAL AM, „DMG MORI announces new metal Additive Manufacturing machine," 13 July 2017. [Online].

[40] DMG MORI, „ADDITIVE MANUFACTURING Reinvent your Metal Production," [Online].

[41] Yadroitsev, I.; Thivillon, L.; Bertrand, P.; Smurov, I.:, „Strategy of manufacturing components with designed internal structure by selective laser melting of metallic powder," *Applied Surface Science,* 2007.

[42] GLEEBLE, „GLEEBLE SYSTEMS," [Online]. Available: https://www.gleeble.com/products/gleeble-systems/gleeble-3500.html.

[43] DSI Gleeble systems , Application note.

[44] Zwick/Roell, „Produktinformation Materialprüfmaschine Z300E - 300 kN / Z400E - 400 kN," [Online].

[45] Casini, Vasta, „Scienza delle Costruzioni," pp. 317 - 340.

[46] Hearn, E. J.; , „An introduction to the Mechanics of Elastic and Plastic Deformation of Solids and Structural Materials," *Mechanics of Materials 2,* pp. 443-508, 1997.

[47] Vilaro, T.; Colin, C.; Bartout, JD.:, „As-fabricated and heat-treated microstructures of the Ti-6Al-4V alloy processed by selective laser melting. Metallurgical and Materials Transactions," *A: Physical Metallurgy and Materials Science,* 2011.

[48] I. Sizova und M. Bambach, „Hot workability and microstructure evolution of pre-forms for forgings by Additive Manufacturing," *Procedia Engineering,* 2017.

[49] C. Pruncu, C. Hopper, P. Hooper, Z. Tan, H. Zhu, J. Lin und J. Jiang, „Study of the Effects of Hot Forging on the Additively Manufactured Stainless Steel Preforms," *Journal of Manufacturing Processes,* pp. 668-676, 2020.

8 Appendix

Compression test: mean engineering stress strain curves of additive specimens

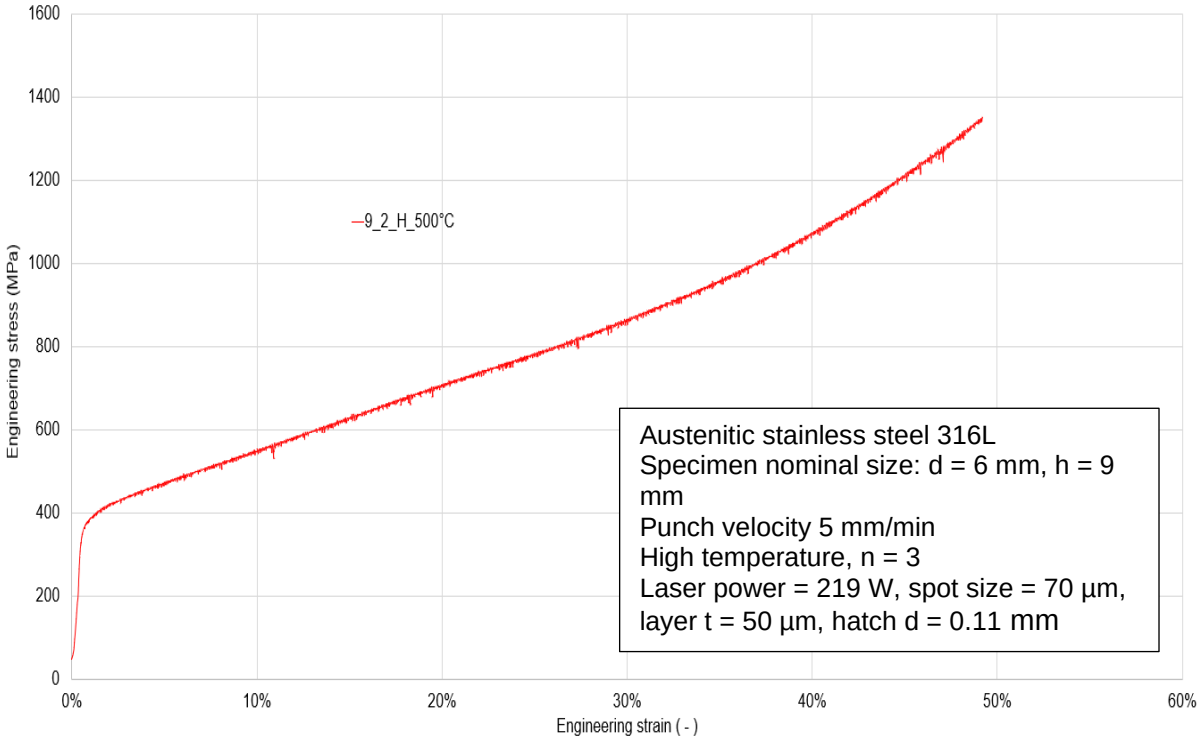

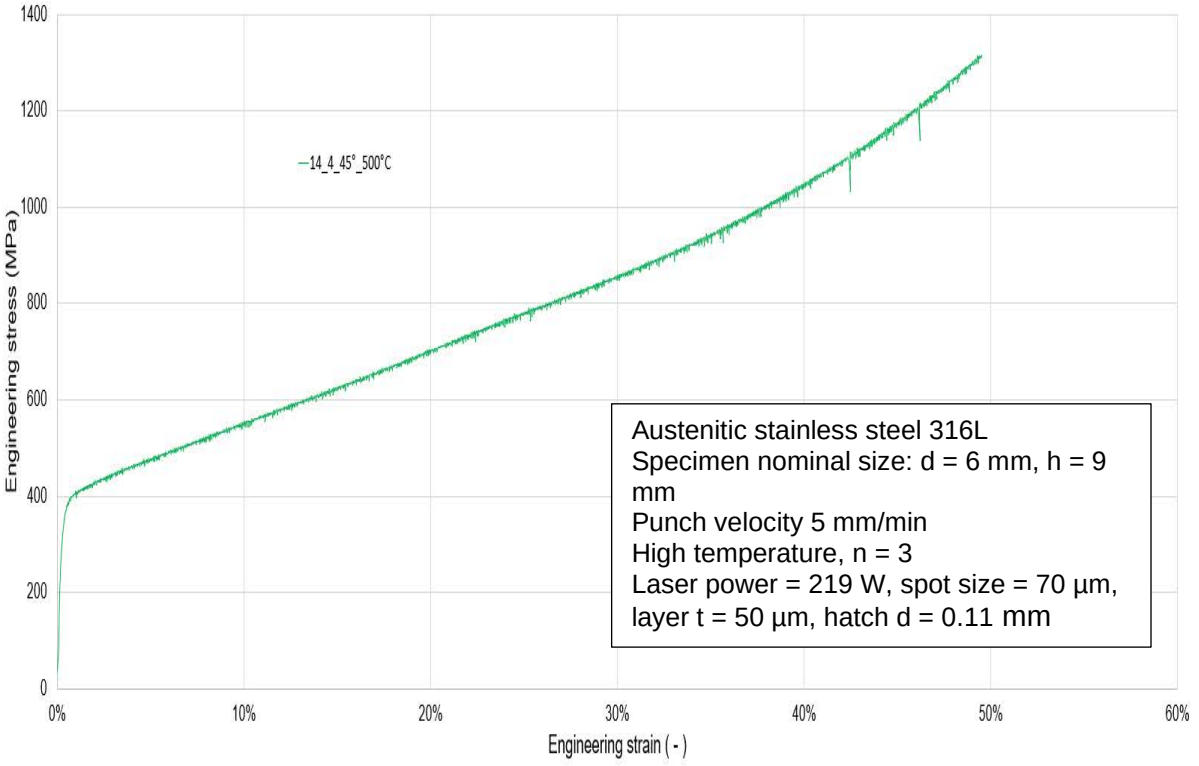

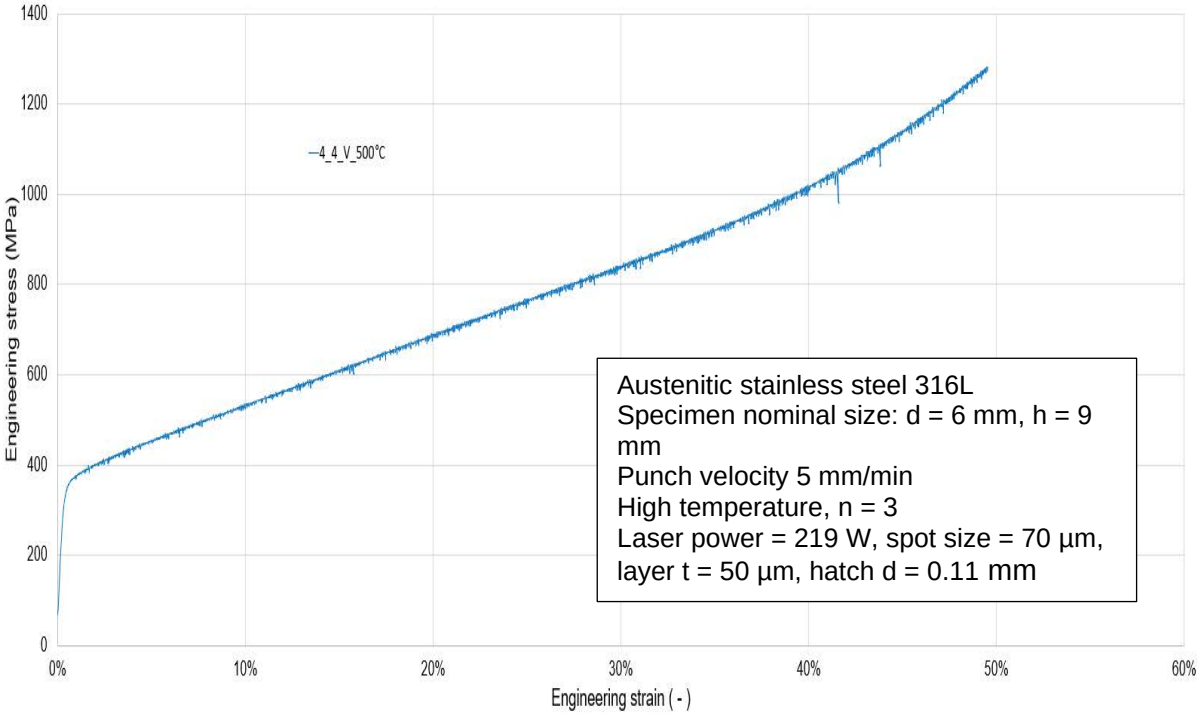
1400
1200
1000
800
600
400
200
0
Engineering stress (MPa)
4_4_V_500°C
0%
10%
20%
30%
40%
50%
60%
Engineering strain (-)
Austenitic stainless steel 316L
Specimen nominal size: d = 6 mm, h = 9 mm
Punch velocity 5 mm/min
High temperature, n = 3
Laser power = 219 W, spot size = 70 µm, layer t = 50 µm, hatch d = 0.11 mm

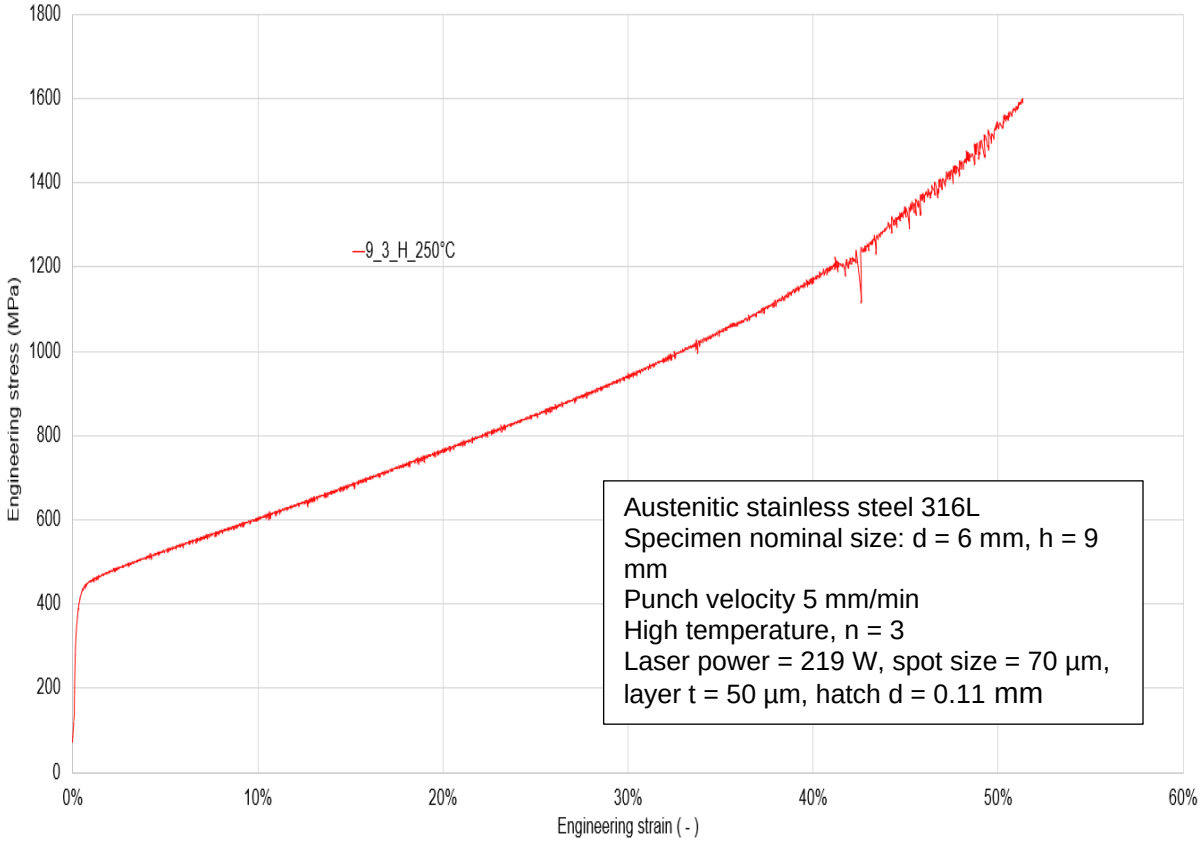
1800
1600
1400
1200
1000
800
600
400
200
0
Engineering stress (MPa)
9_3_H_250°C
0%
10%
20%
30%
40%
50%
60%
Engineering strain (-)
Austenitic stainless steel 316L
Specimen nominal size: d = 6 mm, h = 9 mm
Punch velocity 5 mm/min
High temperature, n = 3
Laser power = 219 W, spot size = 70 µm, layer t = 50 µm, hatch d = 0.11 mm

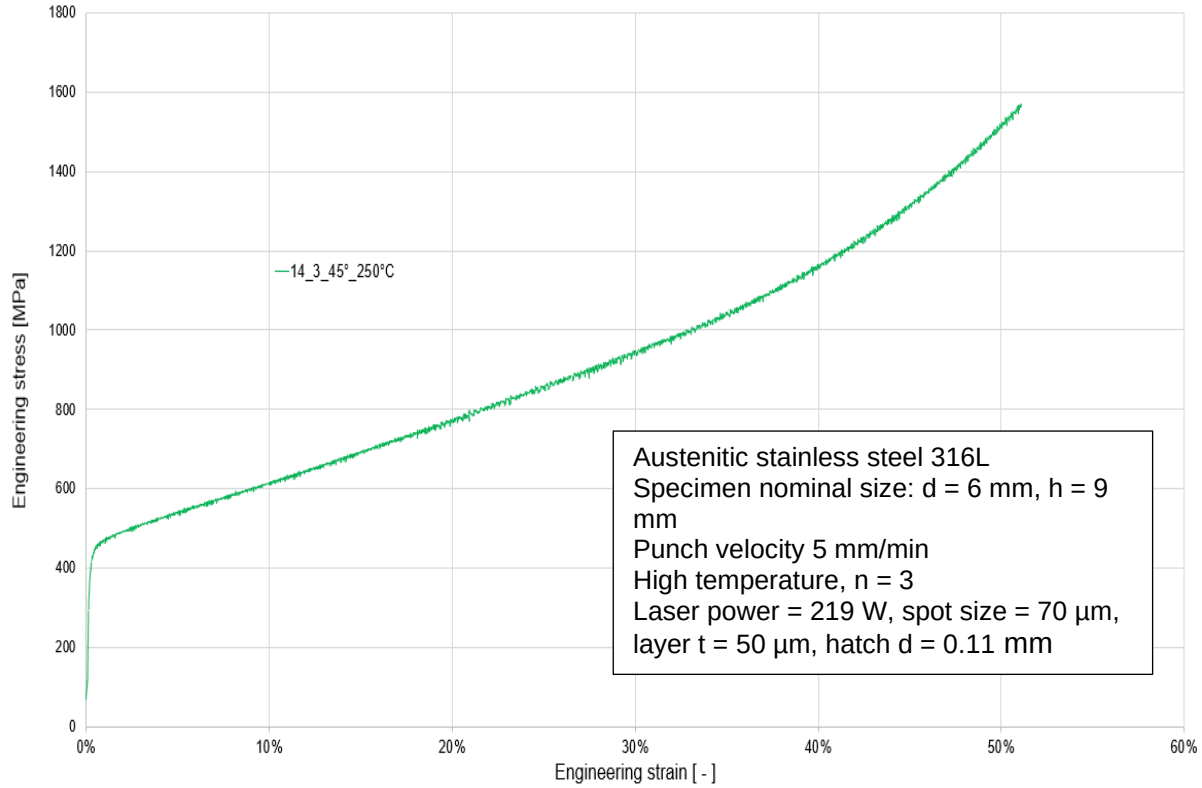
1800
1600
1400
1200
1000
800
600
400
200
0
Engineering stress [MPa]
14_3_45°_250°C
0%
10%
20%
30%
40%
50%
60%
Engineering strain [-]
Austenitic stainless steel 316L
Specimen nominal size: d = 6 mm, h = 9 mm
Punch velocity 5 mm/min
High temperature, n = 3
Laser power = 219 W, spot size = 70 µm, layer t = 50 µm, hatch d = 0.11 mm

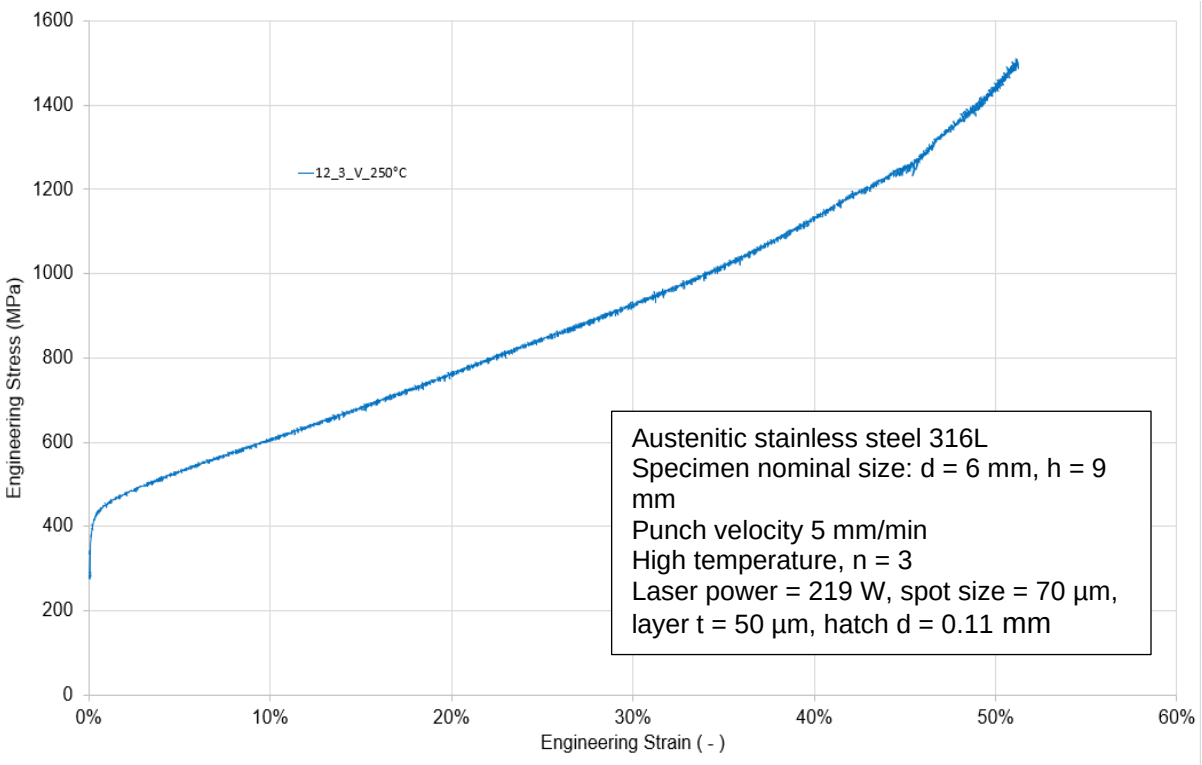
1600
1400
1200
1000
800
600
400
200
0
Engineering Stress (MPa)
12_3_V_250°C
0%
10%
20%
30%
40%
50%
60%
Engineering Strain (-)
Austenitic stainless steel 316L
Specimen nominal size: d = 6 mm, h = 9 mm
Punch velocity 5 mm/min
High temperature, n = 3
Laser power = 219 W, spot size = 70 µm, layer t = 50 µm, hatch d = 0.11 mm

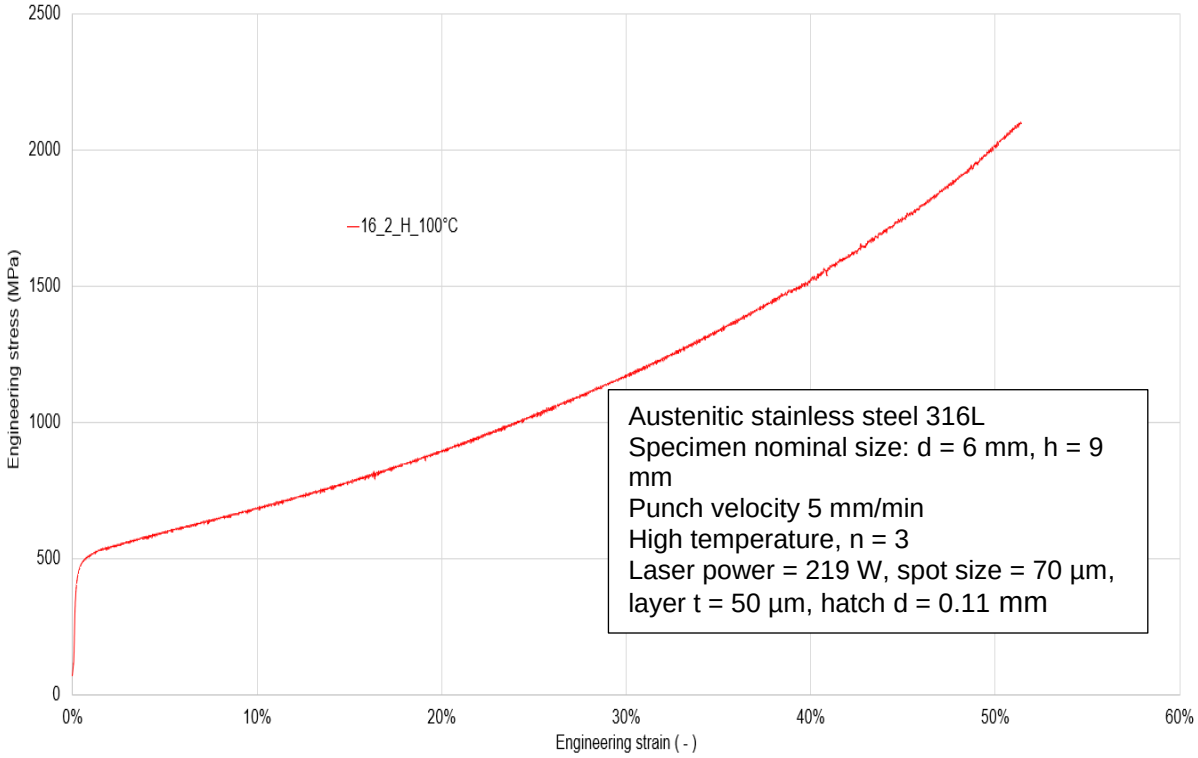
2500
2000
1500
1000
500
0
Engineering stress (MPa)
16_2_H_100°C
0%
10%
20%
30%
40%
50%
60%
Engineering strain (-)
Austenitic stainless steel 316L
Specimen nominal size: d = 6 mm, h = 9 mm
Punch velocity 5 mm/min
High temperature, n = 3
Laser power = 219 W, spot size = 70 µm, layer t = 50 µm, hatch d = 0.11 mm

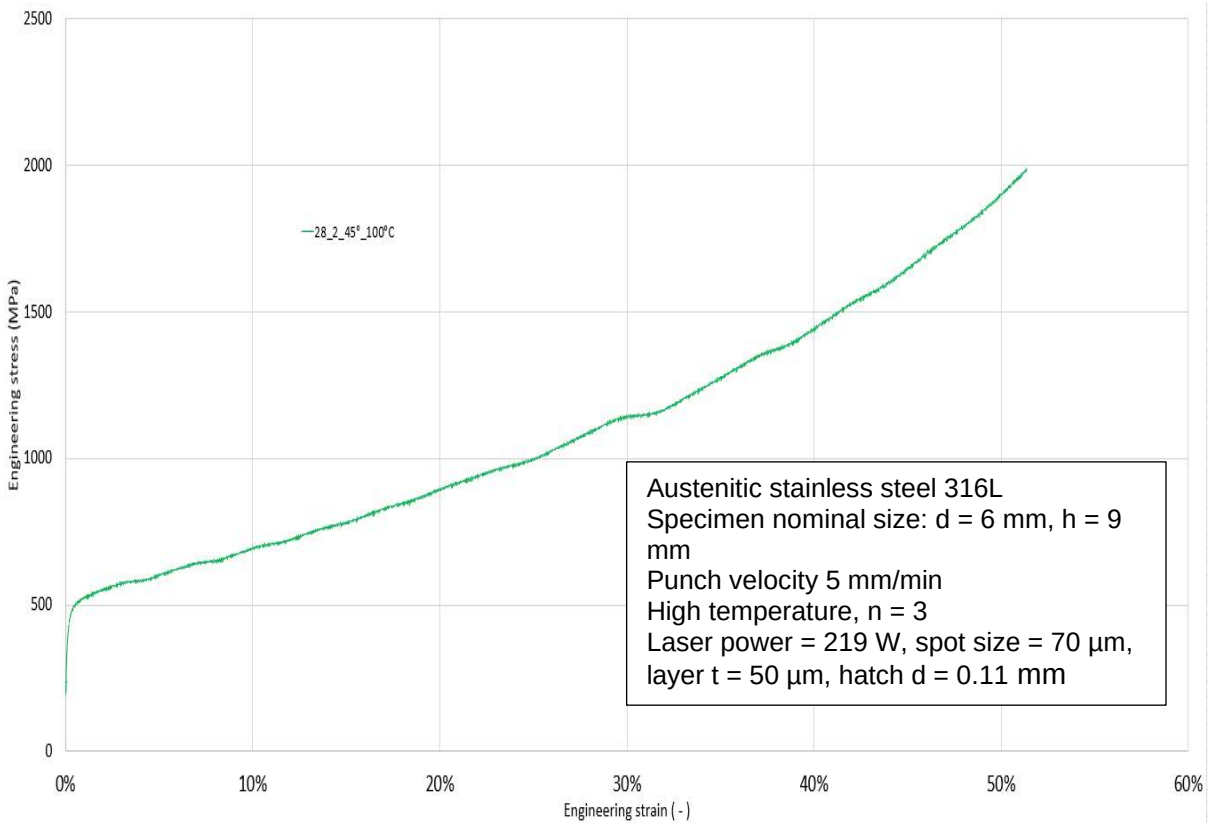
2500
2000
1500
1000
500
0
Engineering stress (MPa)
28_2_45°_100°C
0%
10%
20%
30%
40%
50%
60%
Engineering strain (-)
Austenitic stainless steel 316L
Specimen nominal size: d = 6 mm, h = 9 mm
Punch velocity 5 mm/min
High temperature, n = 3
Laser power = 219 W, spot size = 70 µm, layer t = 50 µm, hatch d = 0.11 mm

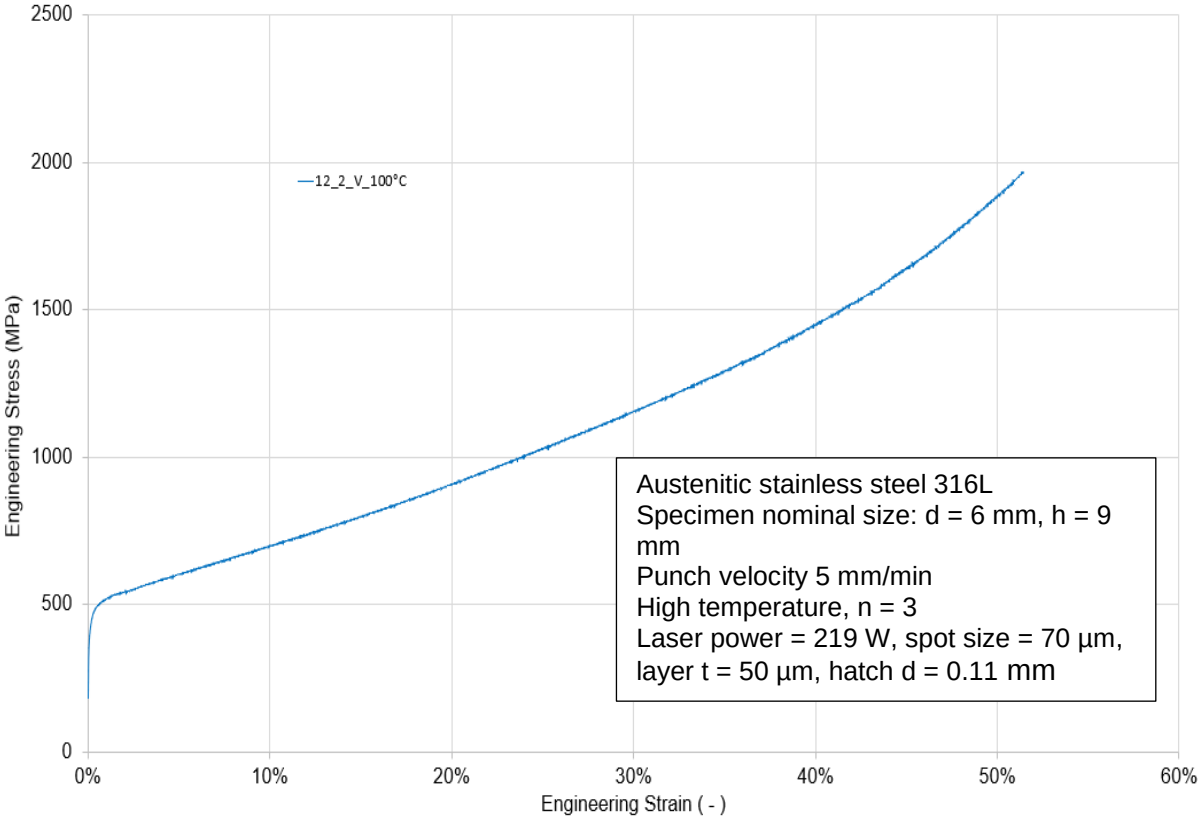
2500
2000
1500
1000
500
0
Engineering Stress (MPa)
12_2_V_100°C
0%
10%
20%
30%
40%
50%
60%
Engineering Strain (-)
Austenitic stainless steel 316L
Specimen nominal size: d = 6 mm, h = 9 mm
Punch velocity 5 mm/min
High temperature, n = 3
Laser power = 219 W, spot size = 70 µm, layer t = 50 µm, hatch d = 0.11 mm

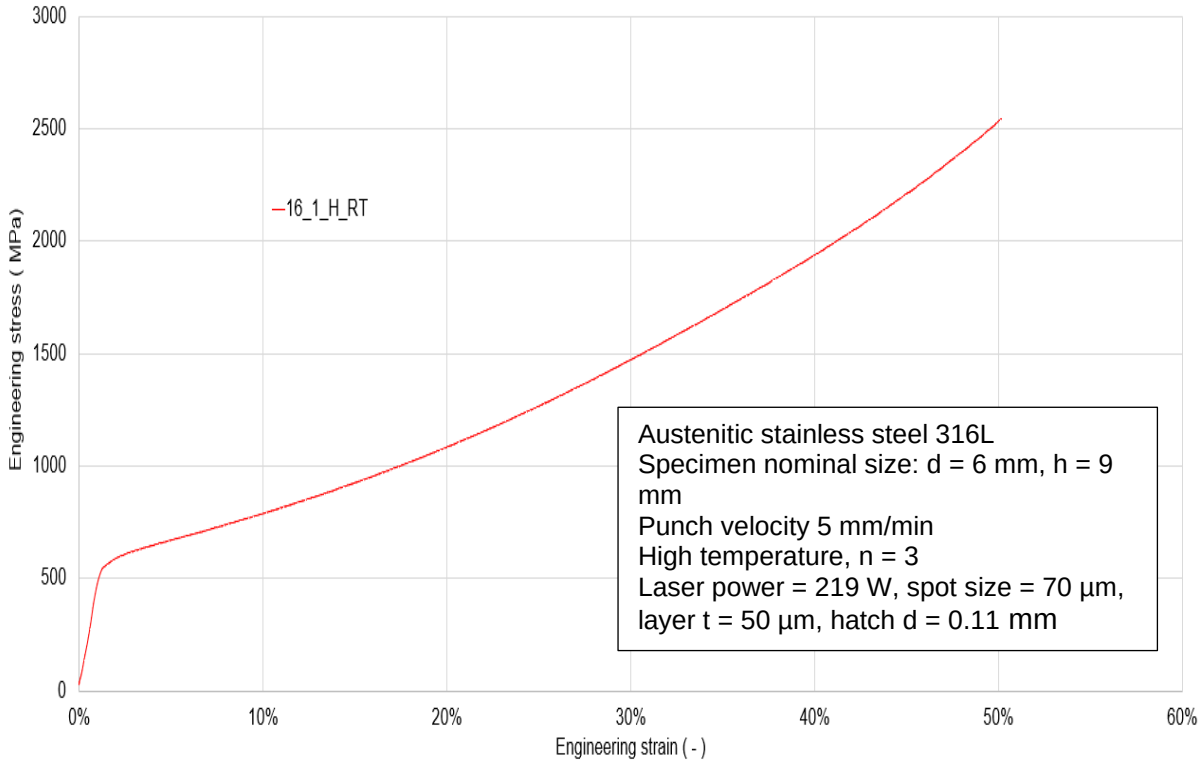
3000
2500
2000
1500
1000
500
0
Engineering stress (MPa)
16_1_H_RT
0%
10%
20%
30%
40%
50%
60%
Engineering strain (-)
Austenitic stainless steel 316L
Specimen nominal size: d = 6 mm, h = 9 mm
Punch velocity 5 mm/min
High temperature, n = 3
Laser power = 219 W, spot size = 70 µm, layer t = 50 µm, hatch d = 0.11 mm

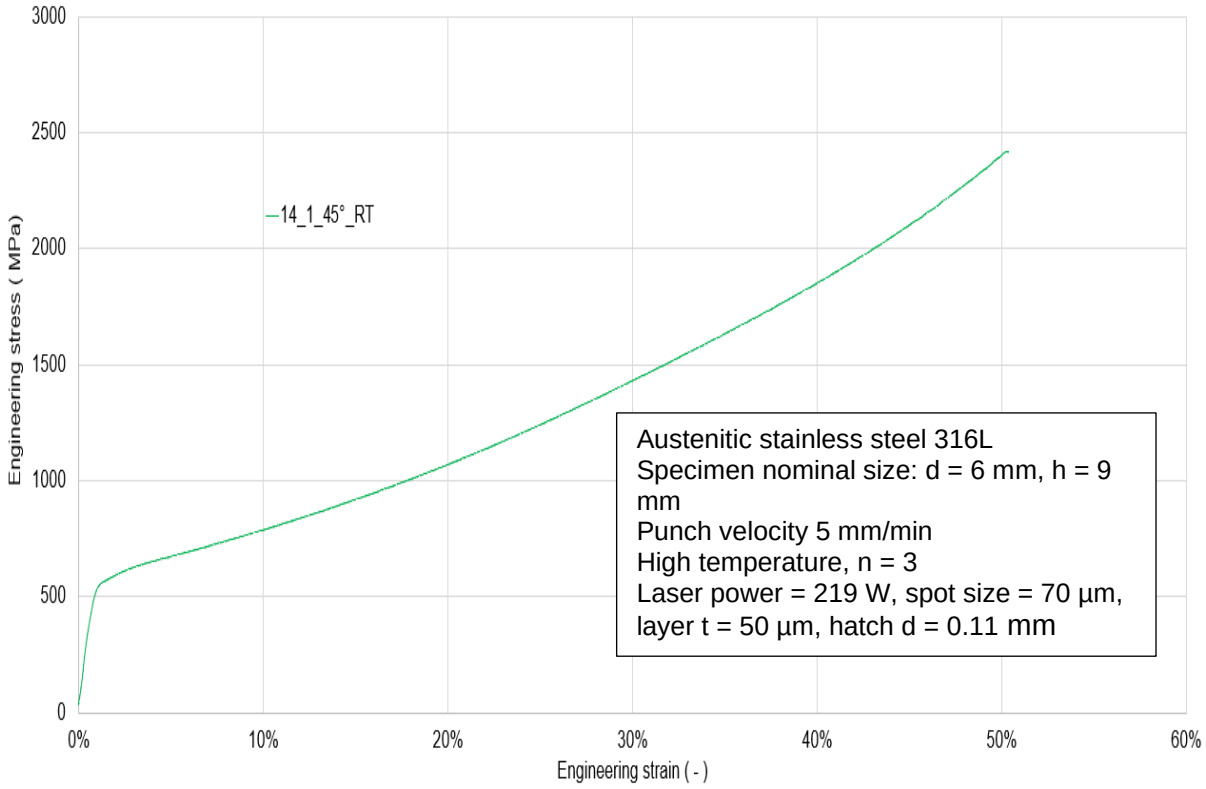
3000
2500
2000
1500
1000
500
0
Engineering stress (MPa)
14_1_45°_RT
0%
10%
20%
30%
40%
50%
60%
Engineering strain (-)
Austenitic stainless steel 316L
Specimen nominal size: d = 6 mm, h = 9 mm
Punch velocity 5 mm/min
High temperature, n = 3
Laser power = 219 W, spot size = 70 µm, layer t = 50 µm, hatch d = 0.11 mm

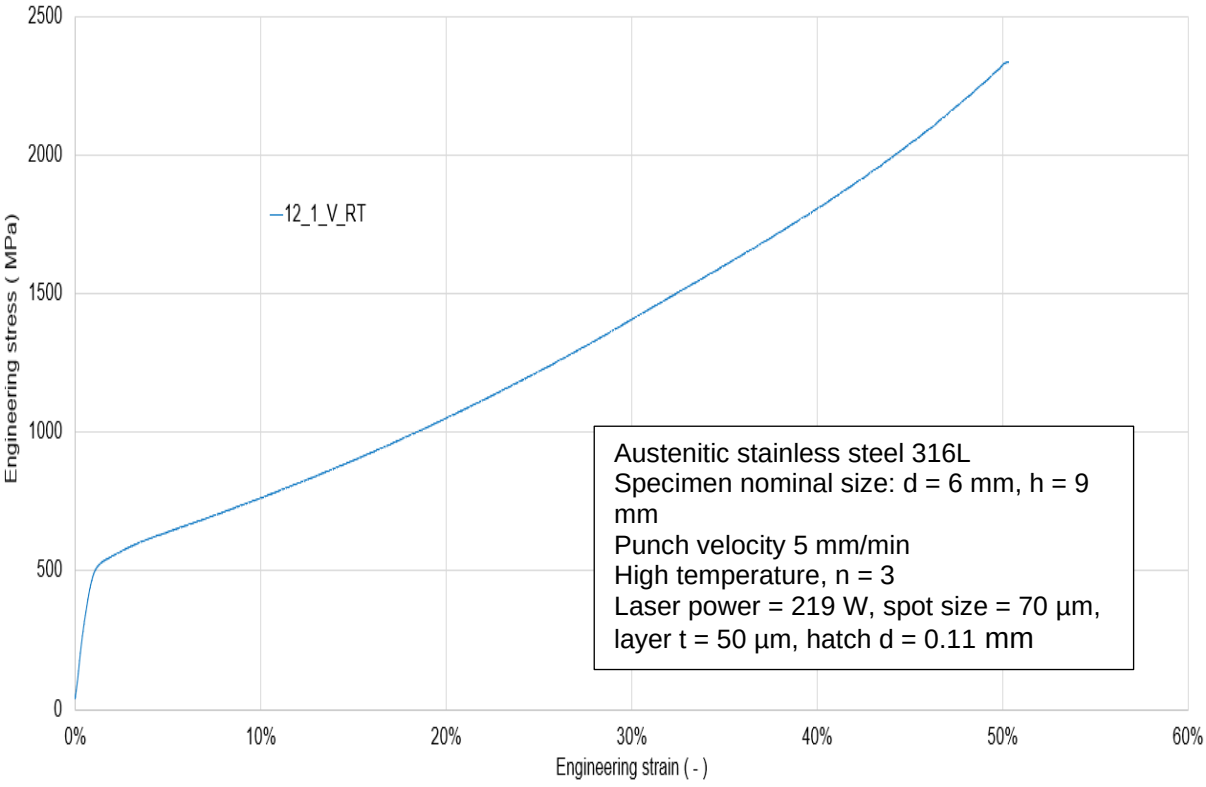
2500
2000
1500
1000
500
0
Engineering stress (MPa)
12_1_V_RT
0%
10%
20%
30%
40%
50%
60%
Engineering strain (-)
Austenitic stainless steel 316L
Specimen nominal size: d = 6 mm, h = 9 mm
Punch velocity 5 mm/min
High temperature, n = 3
Laser power = 219 W, spot size = 70 µm, layer t = 50 µm, hatch d = 0.11 mm

Compression test: mean true stress strain curves of additive specimens

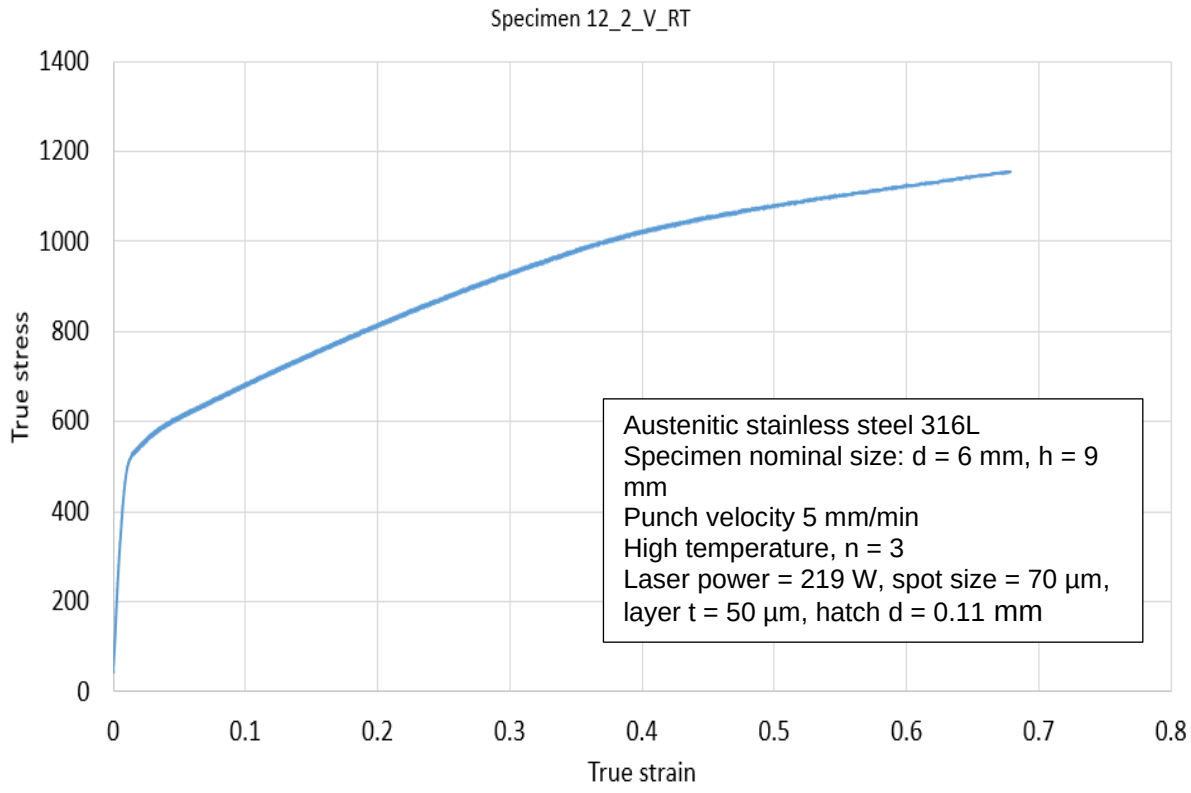

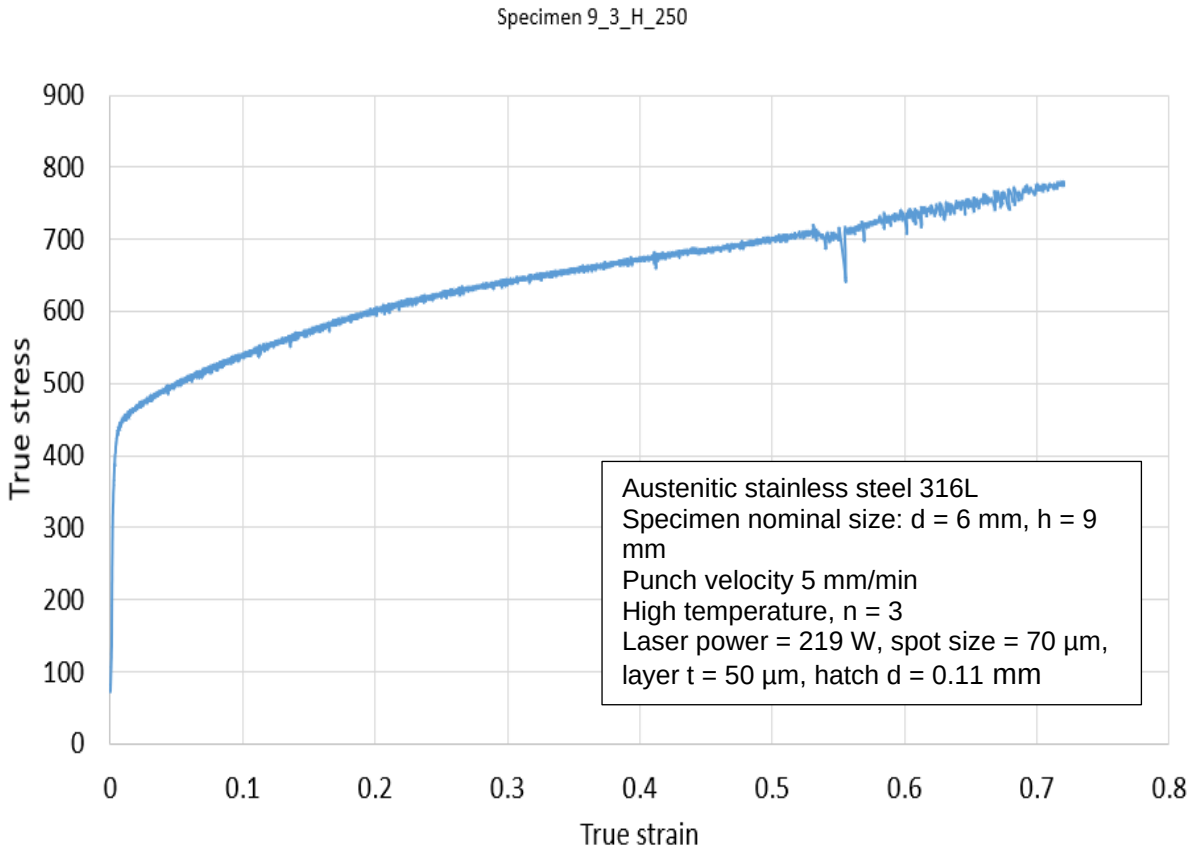

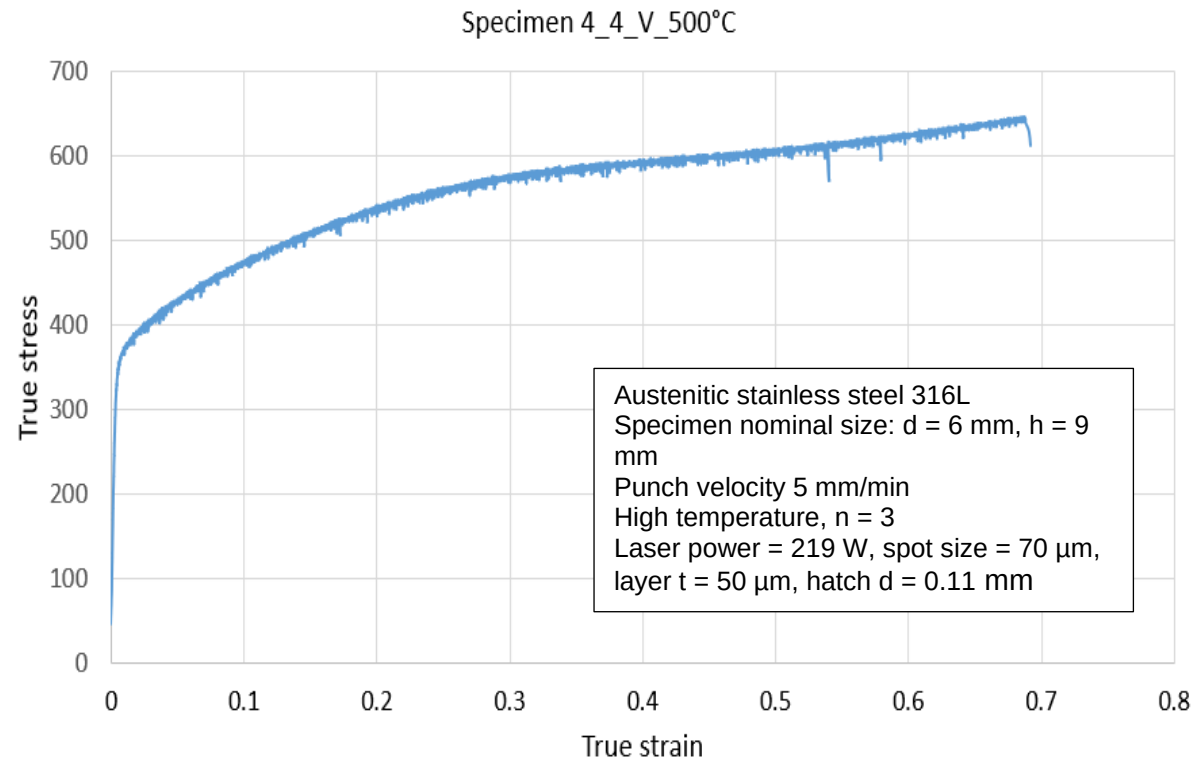

Compression test: mean engineering stress strain curves of conventional specimens

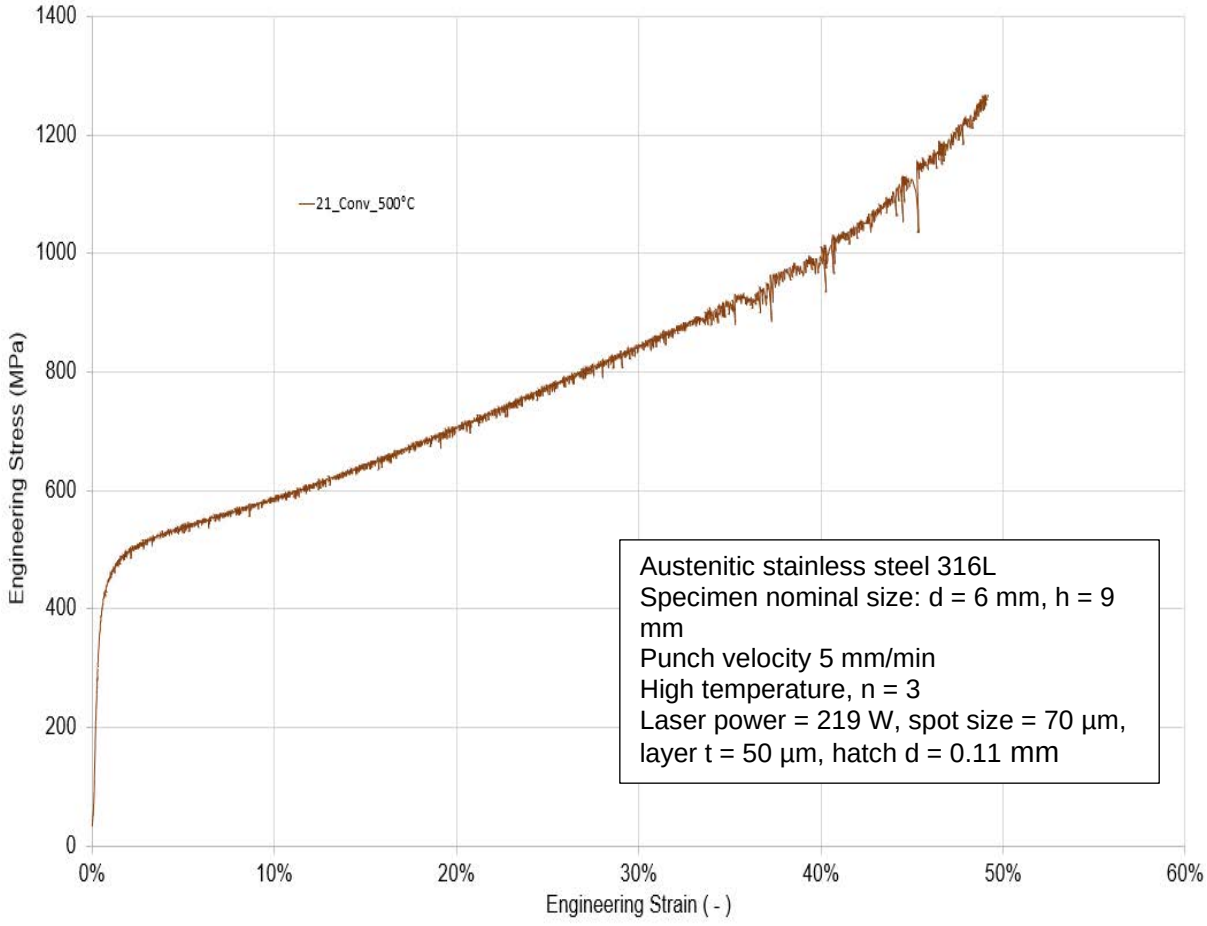

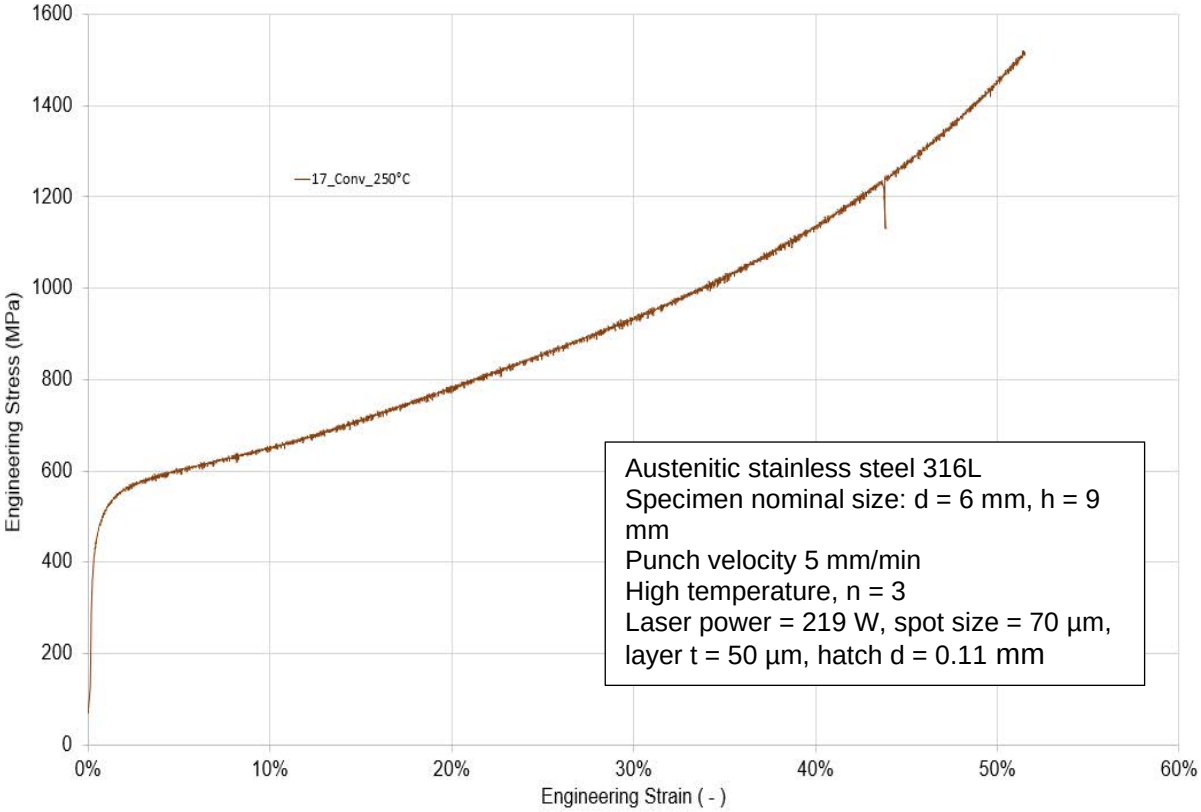
1600
1400
1200
1000
800
600
400
200
0
Engineering Stress (MPa)
17_Conv_250°C
0%
10%
20%
30%
40%
50%
60%
Engineering Strain (-)
Austenitic stainless steel 316L
Specimen nominal size: d = 6 mm, h = 9 mm
Punch velocity 5 mm/min
High temperature, n = 3
Laser power = 219 W, spot size = 70 µm, layer t = 50 µm, hatch d = 0.11 mm

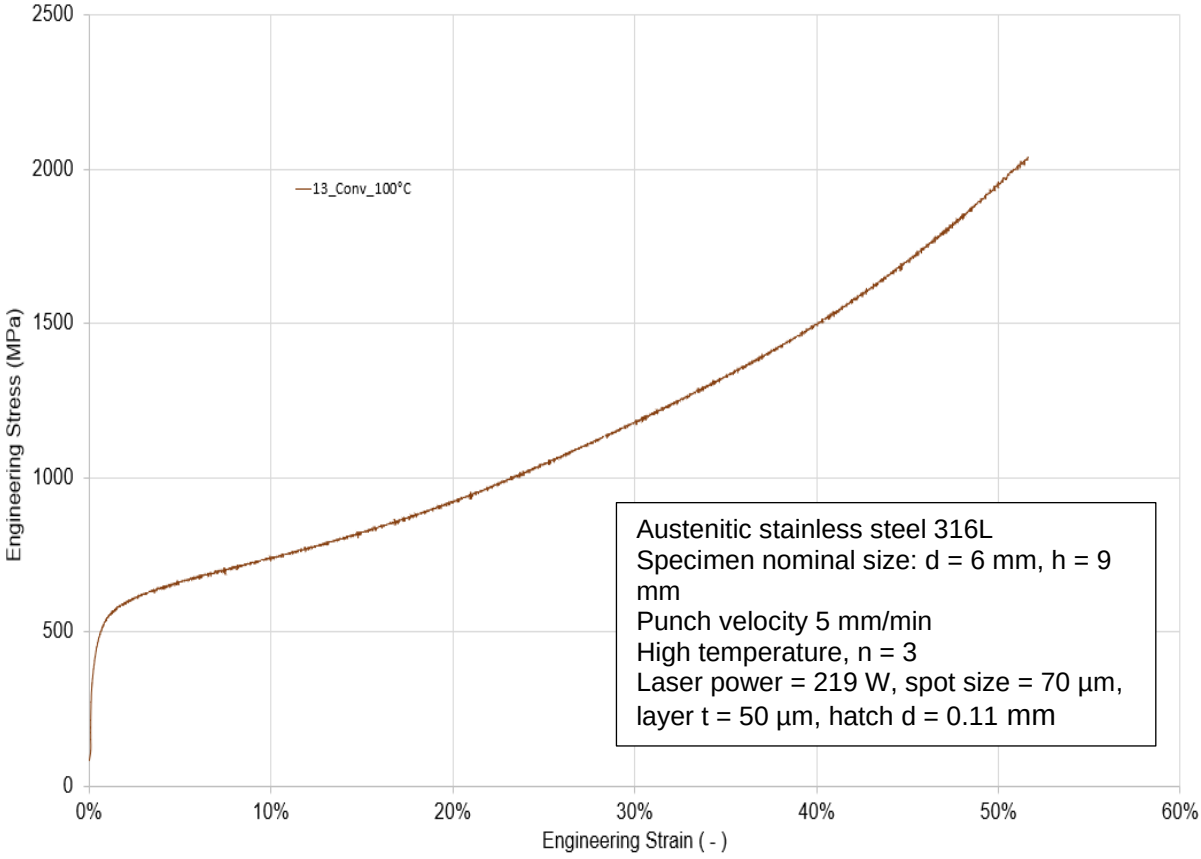
2500
2000
1500
1000
500
0
Engineering Stress (MPa)
13_Conv_100°C
0%
10%
20%
30%
40%
50%
60%
Engineering Strain (-)
Austenitic stainless steel 316L
Specimen nominal size: d = 6 mm, h = 9 mm
Punch velocity 5 mm/min
High temperature, n = 3
Laser power = 219 W, spot size = 70 µm, layer t = 50 µm, hatch d = 0.11 mm

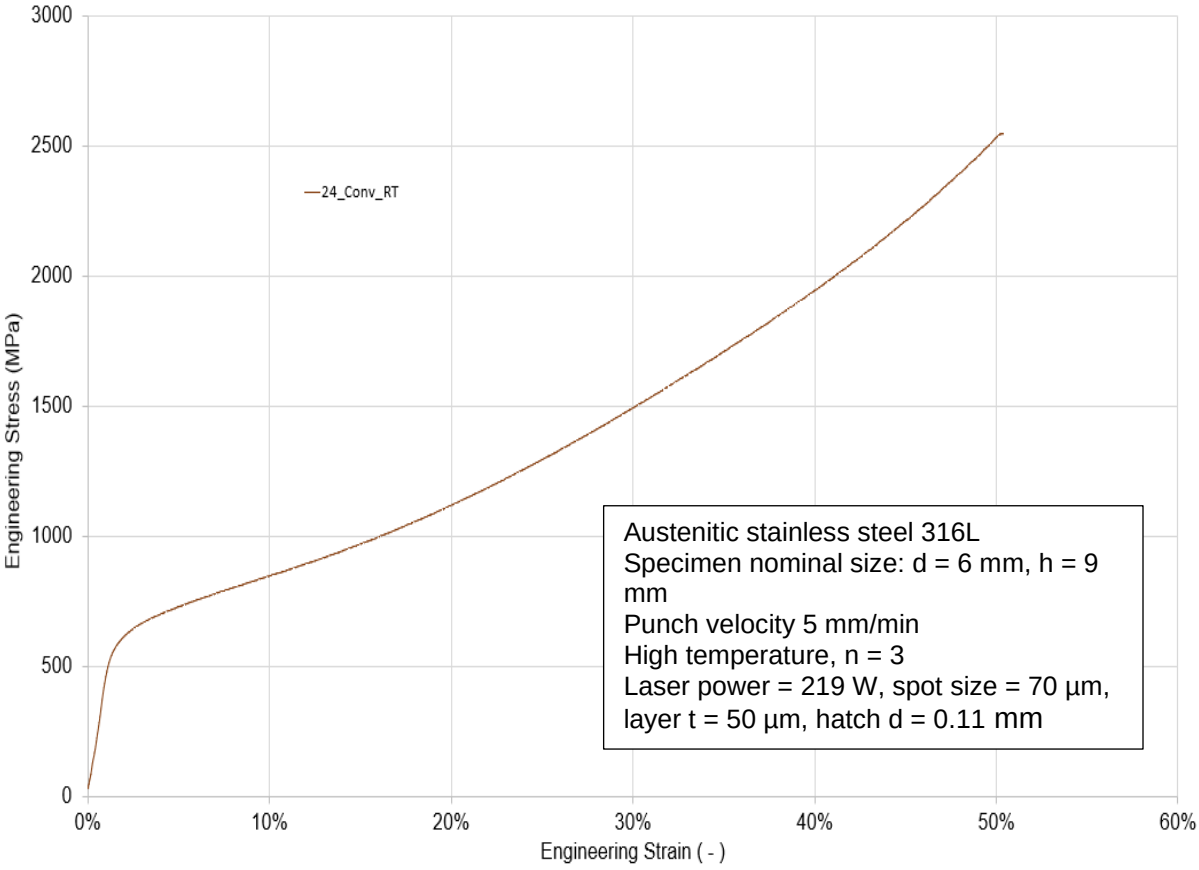
3000
2500
2000
1500
1000
500
0
Engineering Stress (MPa)
24_Conv_RT
0%
10%
20%
30%
40%
50%
60%
Engineering Strain (-)
Austenitic stainless steel 316L
Specimen nominal size: d = 6 mm, h = 9 mm
Punch velocity 5 mm/min
High temperature, n = 3
Laser power = 219 W, spot size = 70 µm, layer t = 50 µm, hatch d = 0.11 mm

Tensile tests

Additive values together mean conventional values of specimens

	Rp0.2	Rm	A
	MPa	MPa	%
AM_V_UL_1	433.6	578.0	21.2
AM_V_UR_9	436.6	579.8	23.0
AM_V_M_14	430.5	576.4	21.9
AM_V_LL_19	433.9	581.7	21.7
AM_V_LR_25	435.2	573.6	17.3
AM_H_U_4	515.9	643.1	17.3
AM_H_ML_10	505.2	633.0	18.6
AM_H_MR_16	529.8	653.6	20.6
AM_H_L_24	537.6	645.4	17.0
AM_Average	473.2	607.2	19.8
±	44.6	33.1	2.2
Average 2 mm_RD0	292.8	609.3	55.9
±	1.0	0.7	0.2
Average 2 mm_RD90	329.7	624.5	62.6
±	0.7	0.7	0.3
Average 1.5 mm_RD0	304.2	627.9	56.7
±	2.4	3.9	0.3
Average 1.5 mm_RD90	324.1	619.9	60.9
±	3.3	5.9	0.3

Tensile test: conventional mechanical properties

	Yield Stress	Tensile strength	Uniform elongation
	Rp0.2	Rm	Ag
	MPa	MPa	%
2 mm_RD0_15	293.5	609.8	55.7
2 mm_RD0_19	292.1	610.2	56.1
2 mm_RD0_18	293.3	609.0	55.9
2 mm_RD0_14	291.4	608.6	55.9
2 mm_RD0_16	293.7	608.9	55.7
Average 2 mm_RD0	292.8	609.3	55.9
±	1.0	0.7	0.2
2 mm_RD90_1	329.1	624.8	62.7
2 mm_RD90_2	330.3	625.2	62.2
2 mm_RD90_3	328.7	623.7	62.8
2 mm_RD90_4	330.3	625.0	63.0
2 mm_RD90_5	329.9	623.9	62.6
Average 2 mm_RD90	329.7	624.5	62.6
±	0.7	0.7	0.3
1,5 mm_RD0_1	303.2	621.7	56.9
1,5 mm_RD0_2	303.0	630.7	57.1
1,5 mm_RD0_3	305.9	627.3	56.5
1,5 mm_RD0_4	301.7	628.3	56.7
1,5 mm_RD0_5	307.5	631.5	56.4
Average 1.5 mm_RD0	304.2	627.9	56.7
±	2.4	3.9	0.3
1,5 mm_RD90_1	323.1	618.6	61.0
1,5 mm_RD90_2	327.1	625.9	61.0
1,5 mm_RD90_3	323.7	618.4	61.2
1,5 mm_RD90_4	319.3	611.3	60.6
1,5 mm_RD90_5	327.1	625.1	60.5
Average 1.5 mm_RD90	324.1	619.9	60.9
±	3.3	5.9	0.3

Tensile test: engineering stress strain curves of additive specimens

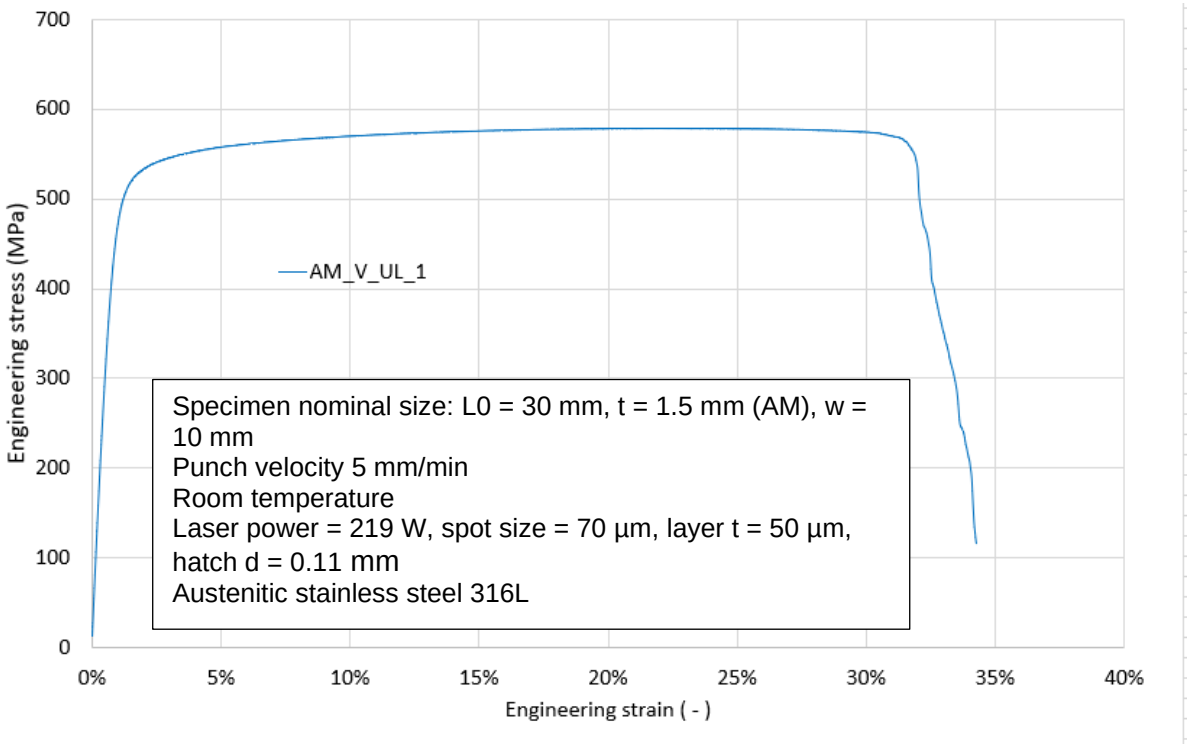

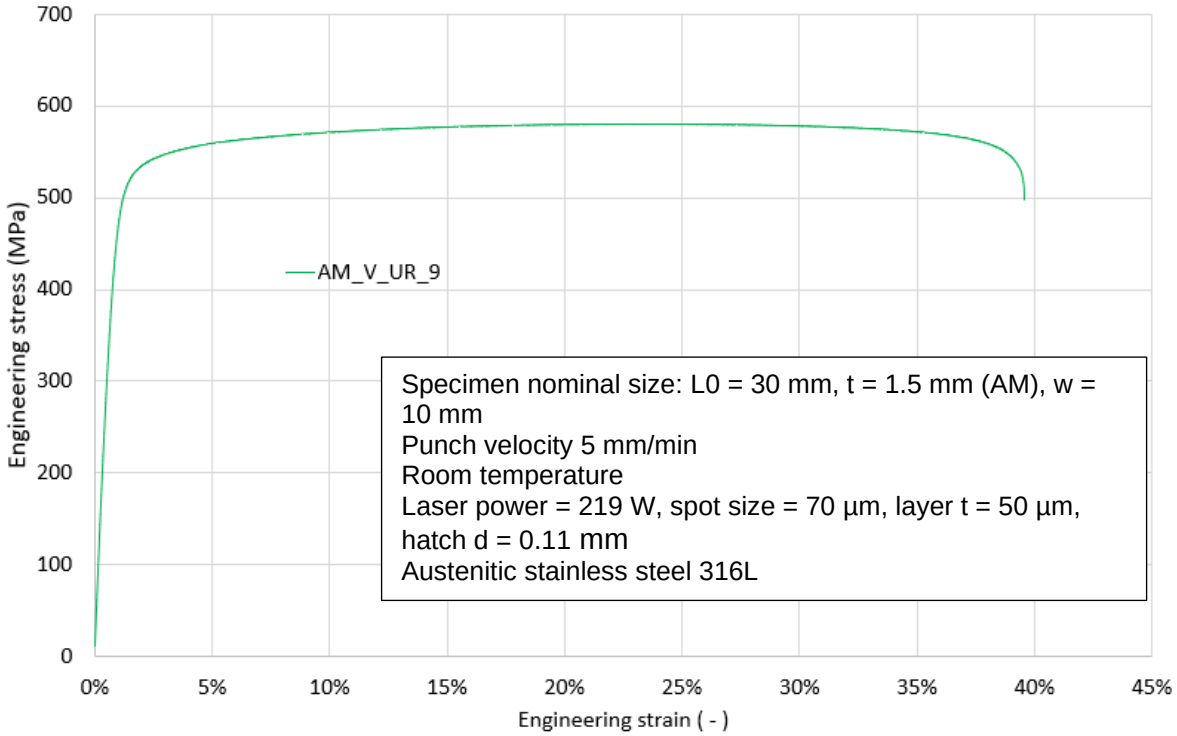

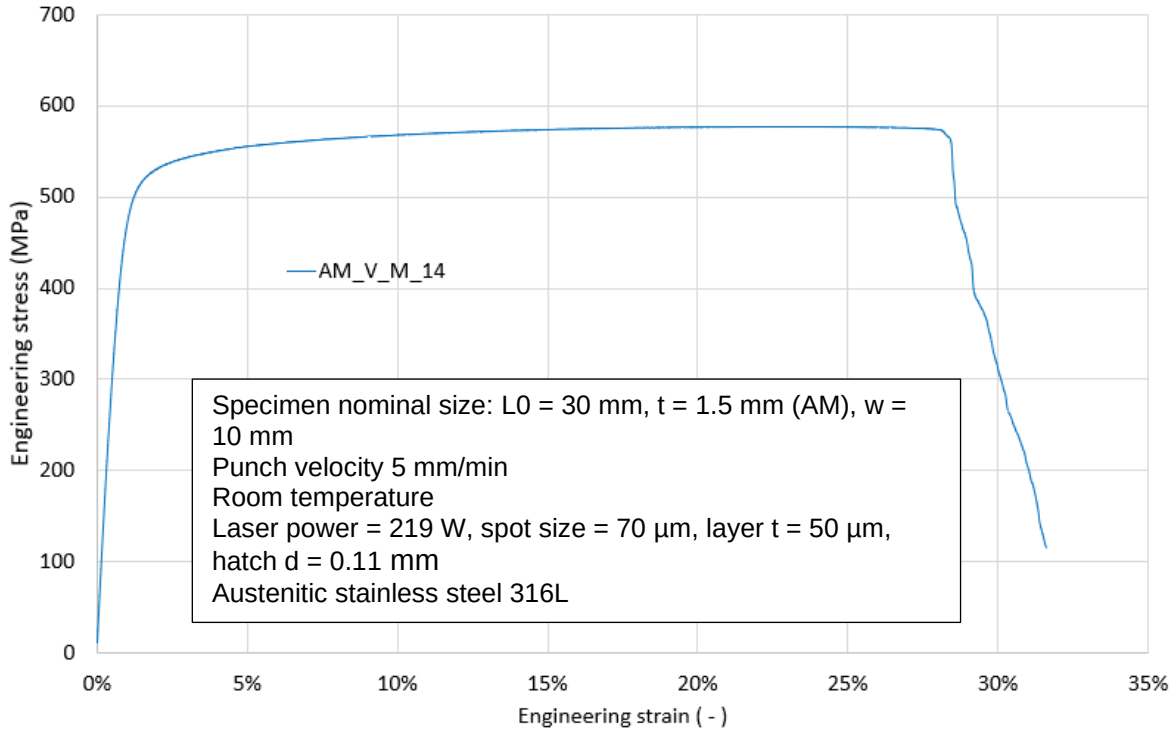
700
600
500
400
300
200
100
0
Engineering stress (MPa)
AM_V_M_14
Specimen nominal size: L0 = 30 mm, t = 1.5 mm (AM), w = 10 mm
Punch velocity 5 mm/min
Room temperature
Laser power = 219 W, spot size = 70 µm, layer t = 50 µm, hatch d = 0.11 mm
Austenitic stainless steel 316L
0%
5%
10%
15%
20%
25%
30%
35%
Engineering strain (-)

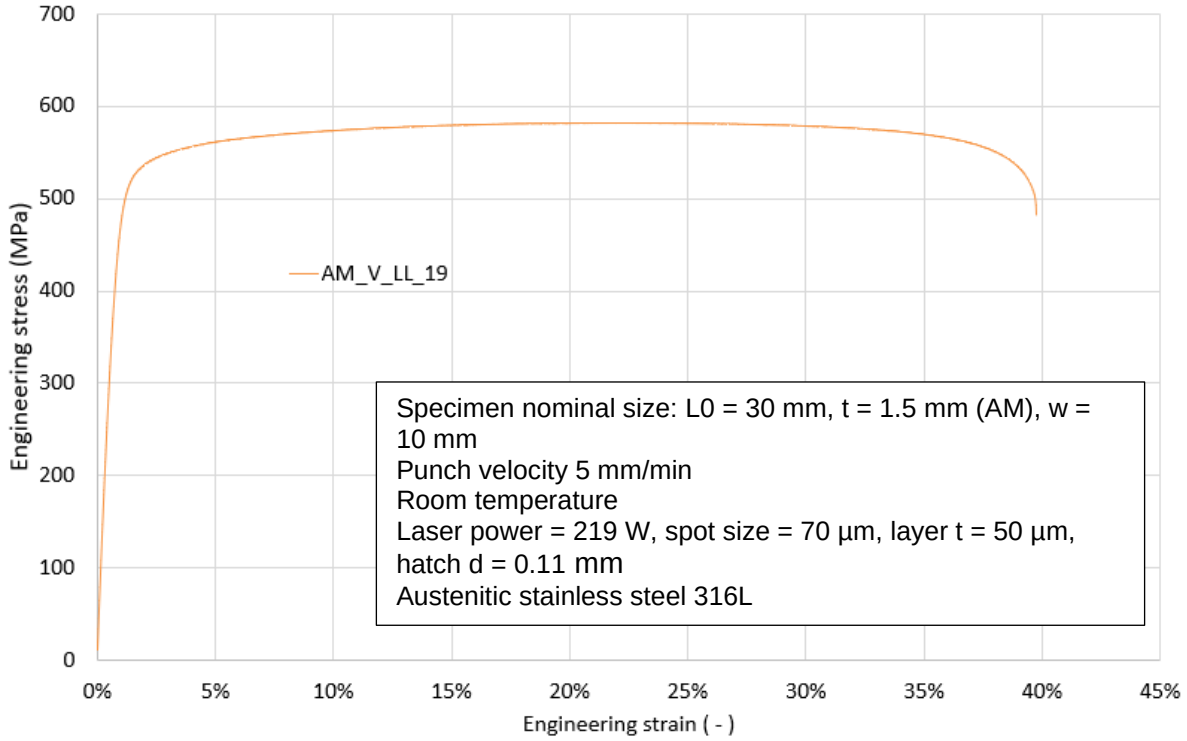
700
600
500
400
300
200
100
0
Engineering stress (MPa)
AM_V_LL_19
Specimen nominal size: L0 = 30 mm, t = 1.5 mm (AM), w = 10 mm
Punch velocity 5 mm/min
Room temperature
Laser power = 219 W, spot size = 70 µm, layer t = 50 µm, hatch d = 0.11 mm
Austenitic stainless steel 316L
0%
5%
10%
15%
20%
25%
30%
35%
40%
45%
Engineering strain (-)

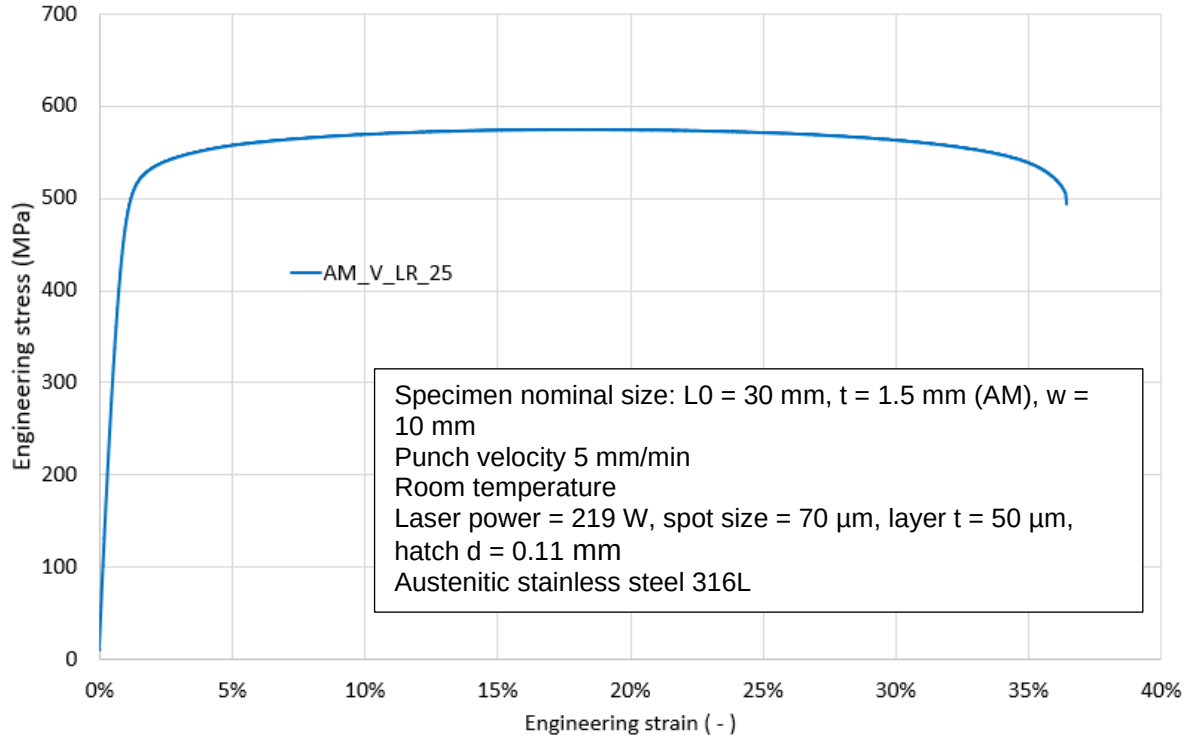
700
600
500
400
300
200
100
0
Engineering stress (MPa)
AM_V_LR_25
Specimen nominal size: L0 = 30 mm, t = 1.5 mm (AM), w = 10 mm
Punch velocity 5 mm/min
Room temperature
Laser power = 219 W, spot size = 70 µm, layer t = 50 µm, hatch d = 0.11 mm
Austenitic stainless steel 316L
0%
5%
10%
15%
20%
25%
30%
35%
40%
Engineering strain (-)

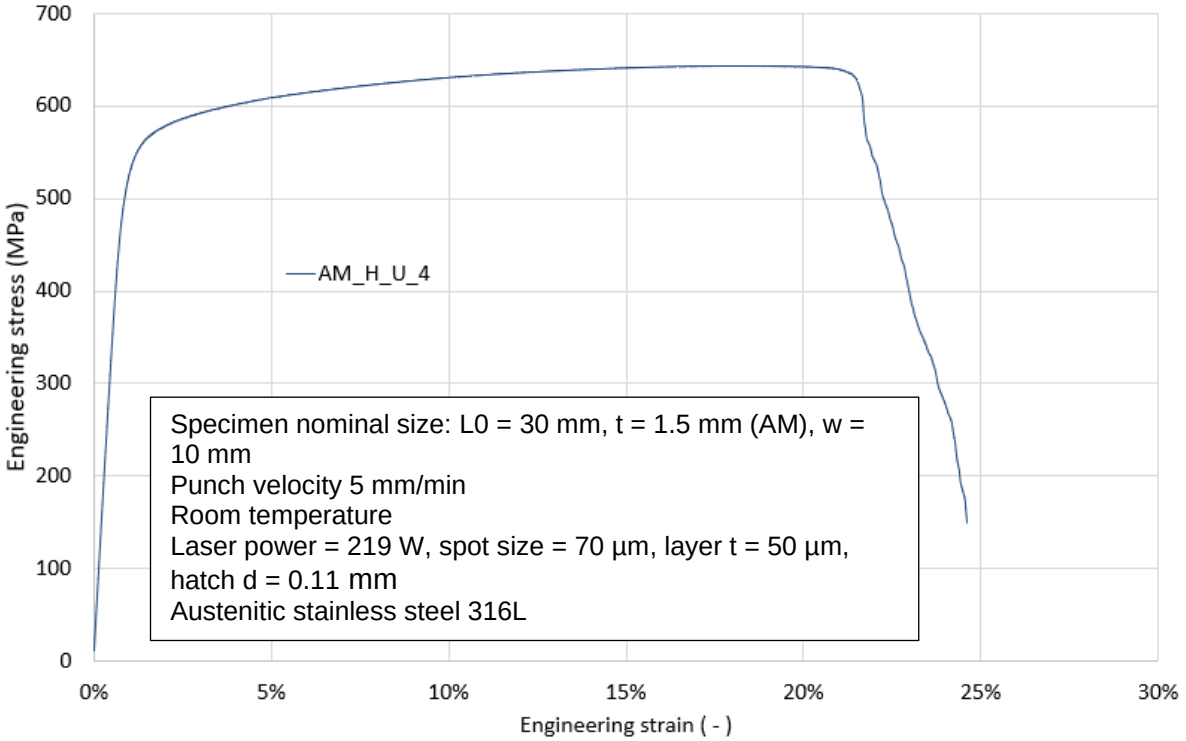
700
600
500
400
300
200
100
0
Engineering stress (MPa)
AM_H_U_4
Specimen nominal size: L0 = 30 mm, t = 1.5 mm (AM), w = 10 mm
Punch velocity 5 mm/min
Room temperature
Laser power = 219 W, spot size = 70 µm, layer t = 50 µm, hatch d = 0.11 mm
Austenitic stainless steel 316L
0%
5%
10%
15%
20%
25%
30%
Engineering strain (-)

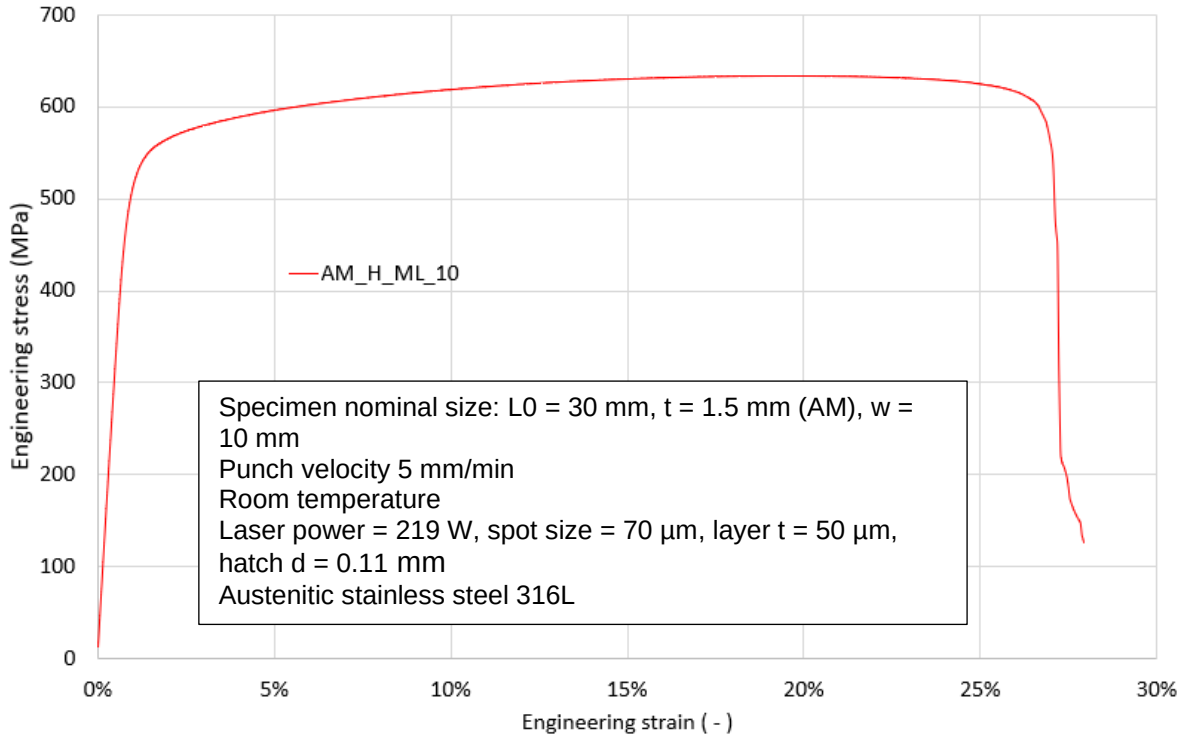
700
600
500
400
300
200
100
0
Engineering stress (MPa)
AM_H_ML_10
Specimen nominal size: L0 = 30 mm, t = 1.5 mm (AM), w = 10 mm
Punch velocity 5 mm/min
Room temperature
Laser power = 219 W, spot size = 70 µm, layer t = 50 µm, hatch d = 0.11 mm
Austenitic stainless steel 316L
0%
5%
10%
15%
20%
25%
30%
Engineering strain (-)

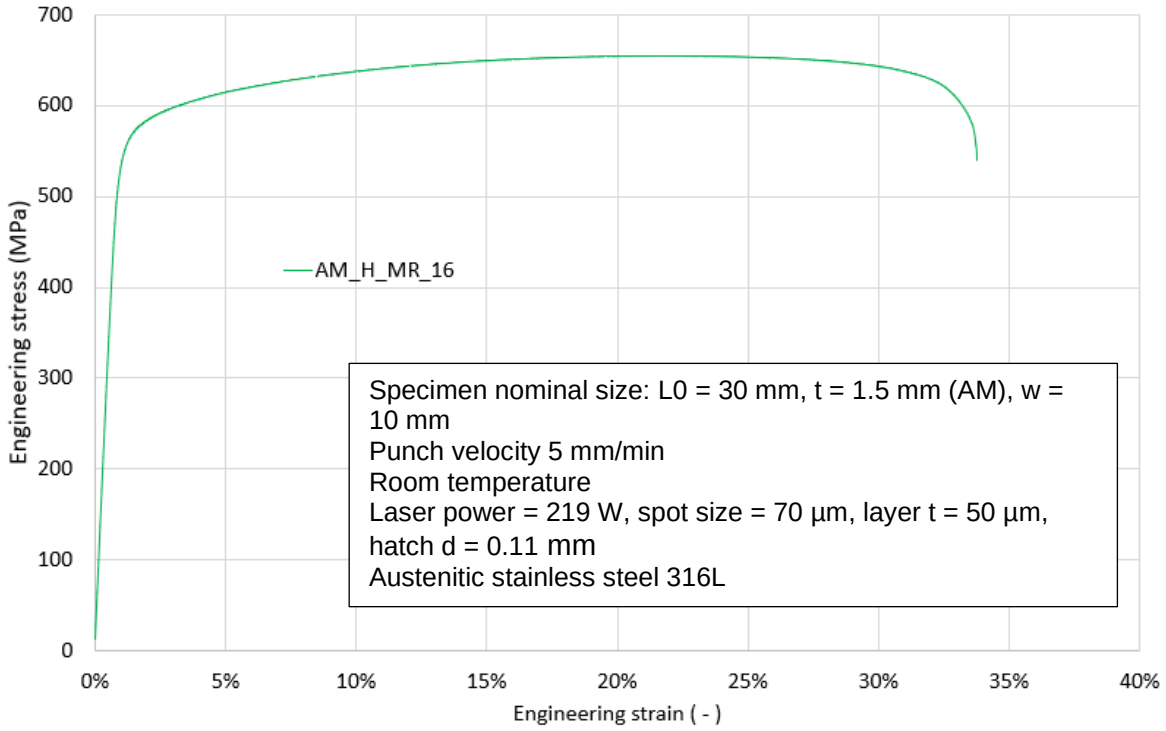
700
600
500
400
300
200
100
0
Engineering stress (MPa)
AM_H_MR_16
Specimen nominal size: L0 = 30 mm, t = 1.5 mm (AM), w = 10 mm
Punch velocity 5 mm/min
Room temperature
Laser power = 219 W, spot size = 70 µm, layer t = 50 µm, hatch d = 0.11 mm
Austenitic stainless steel 316L
0%
5%
10%
15%
20%
25%
30%
35%
40%
Engineering strain (-)

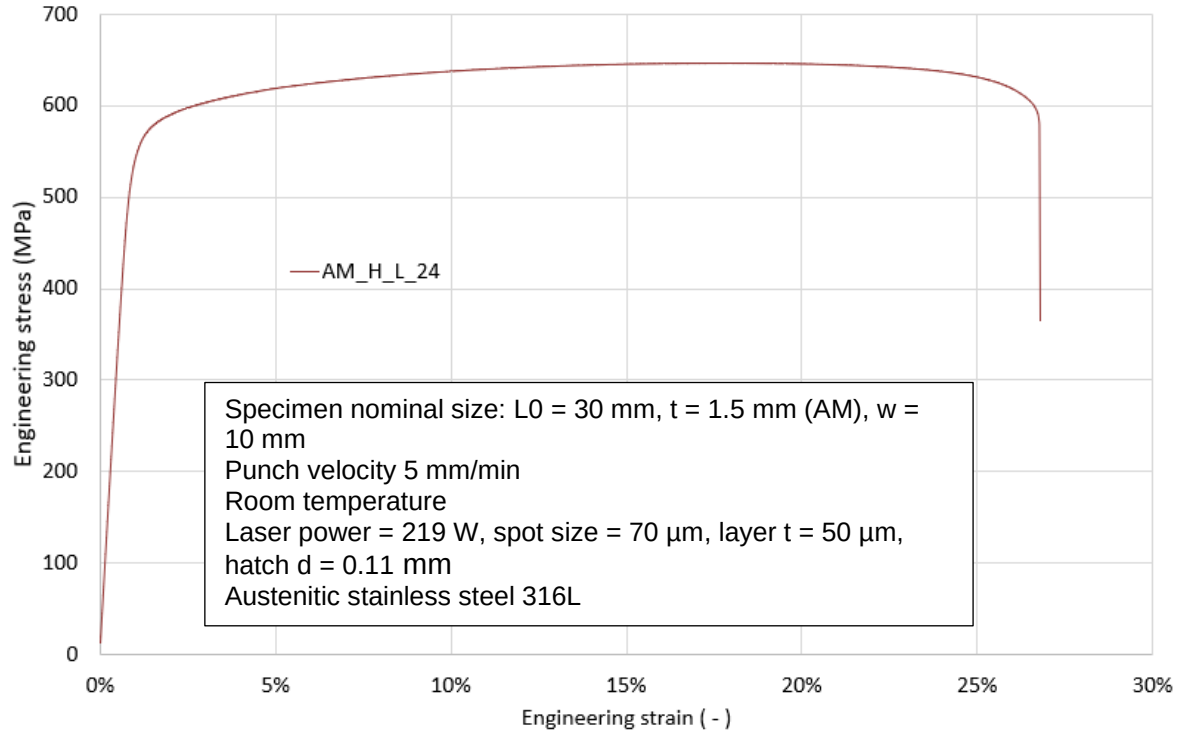

Tensile test: mean engineering stress strain curves of conventional specimens

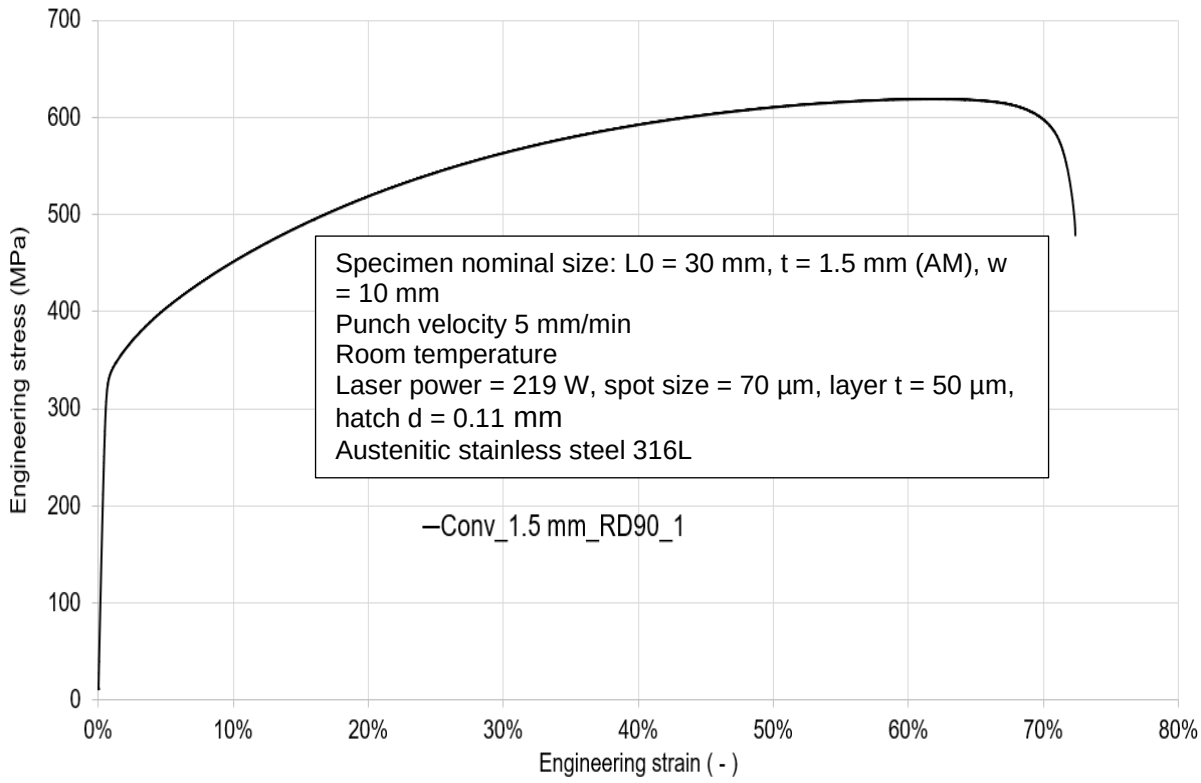

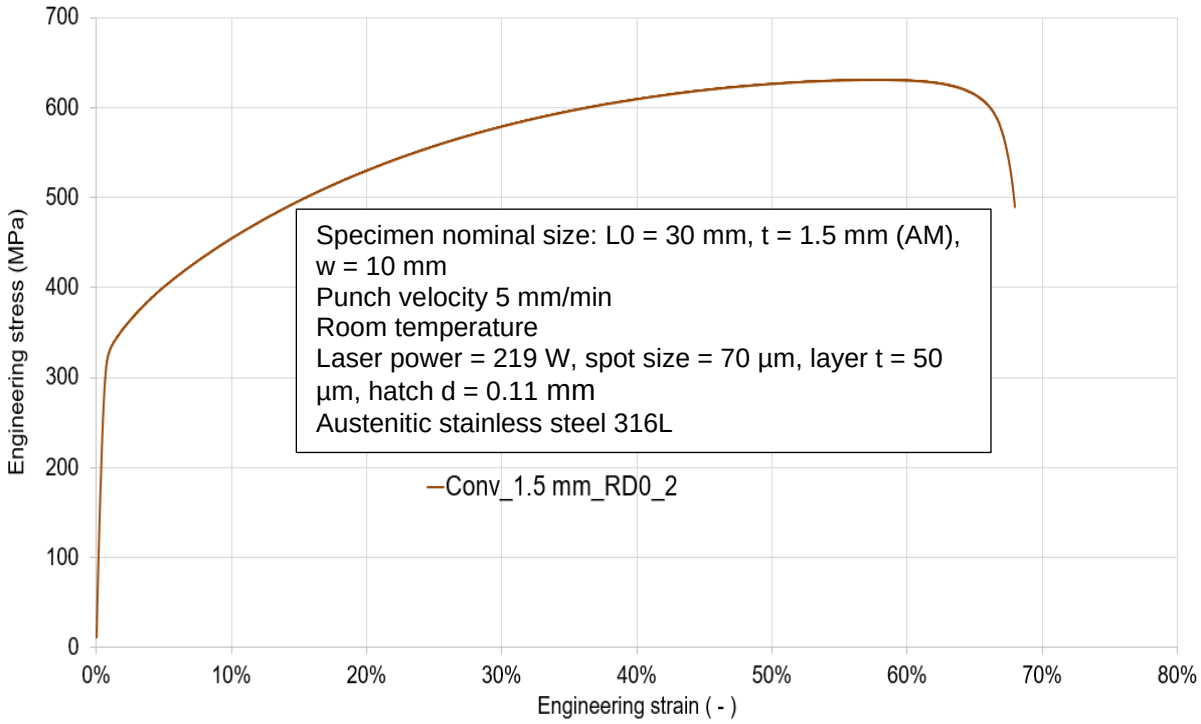
Specimen nominal size: L0 = 30 mm, t = 1.5 mm (AM), w = 10 mm
Punch velocity 5 mm/min
Room temperature
Laser power = 219 W, spot size = 70 µm, layer t = 50 µm, hatch d = 0.11 mm
Austenitic stainless steel 316L
Conv_1.5 mm_RD0_2
Engineering stress (MPa)
Engineering strain (-)
0
100
200
300
400
500
600
700
0%
10%
20%
30%
40%
50%
60%
70%
80%

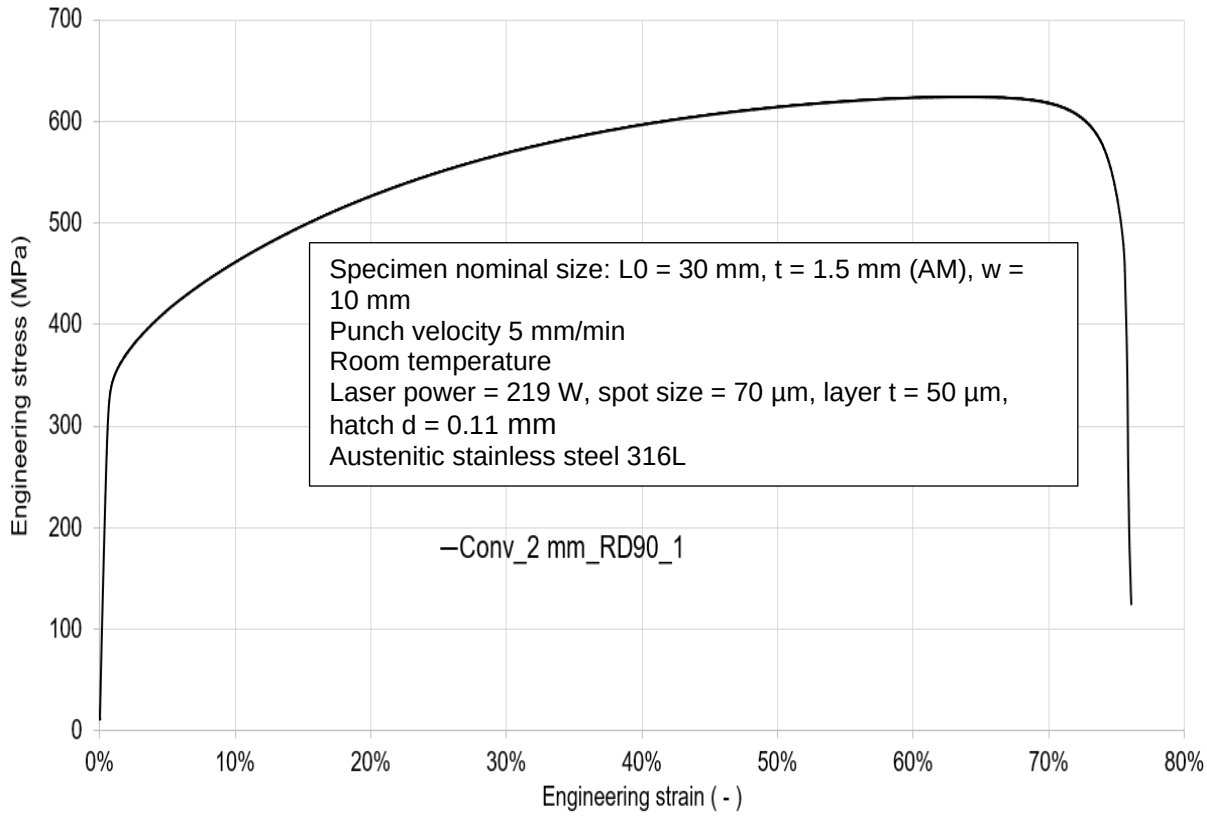
Specimen nominal size: L0 = 30 mm, t = 1.5 mm (AM), w = 10 mm
Punch velocity 5 mm/min
Room temperature
Laser power = 219 W, spot size = 70 µm, layer t = 50 µm, hatch d = 0.11 mm
Austenitic stainless steel 316L
Conv_2 mm_RD90_1
Engineering stress (MPa)
Engineering strain (-)
0
100
200
300
400
500
600
700
0%
10%
20%
30%
40%
50%
60%
70%
80%

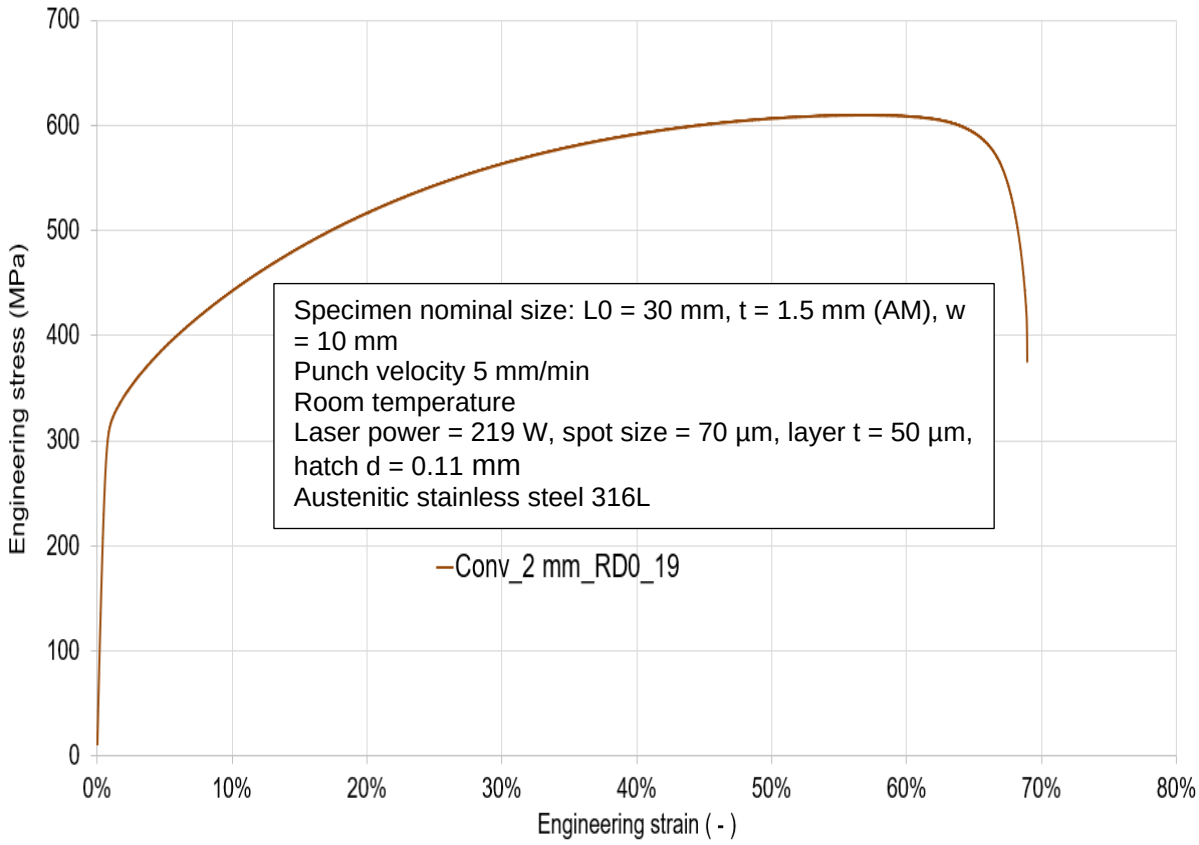

Tensile test: true stress strain curves of additive specimens

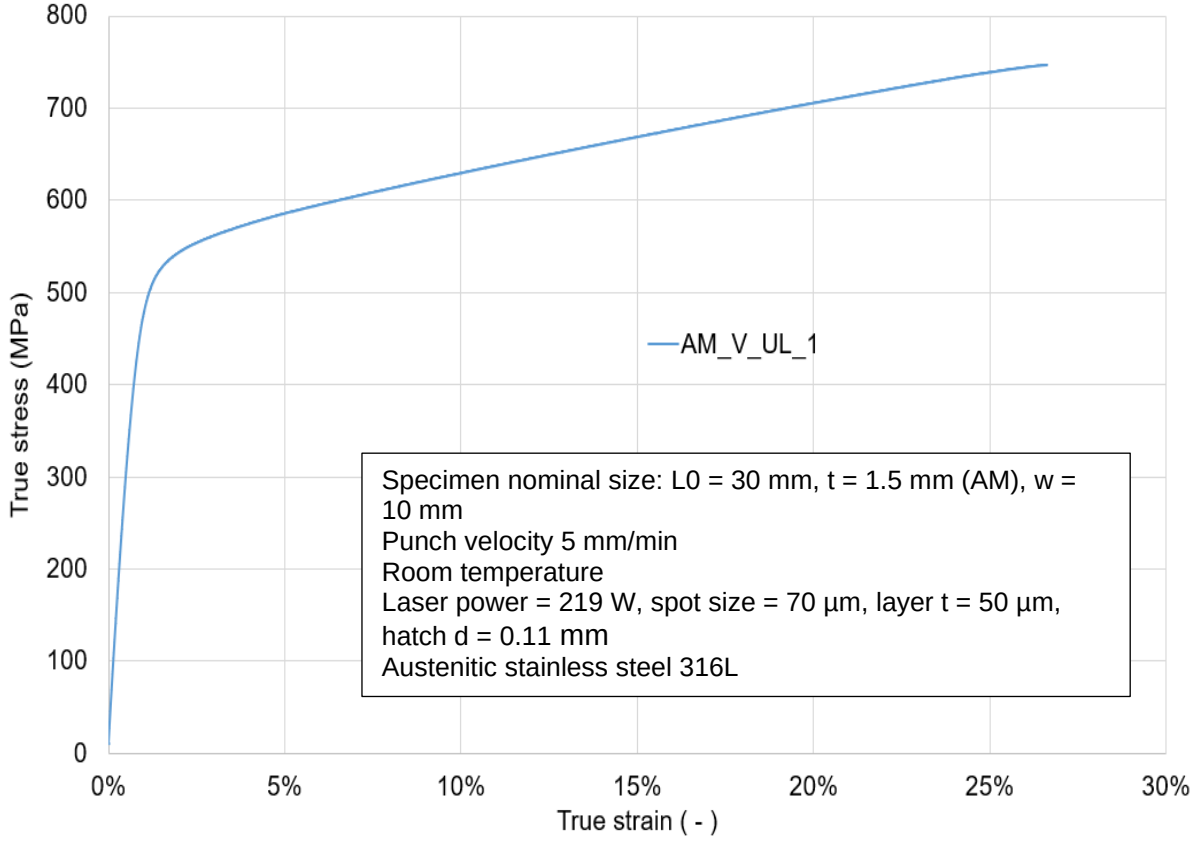

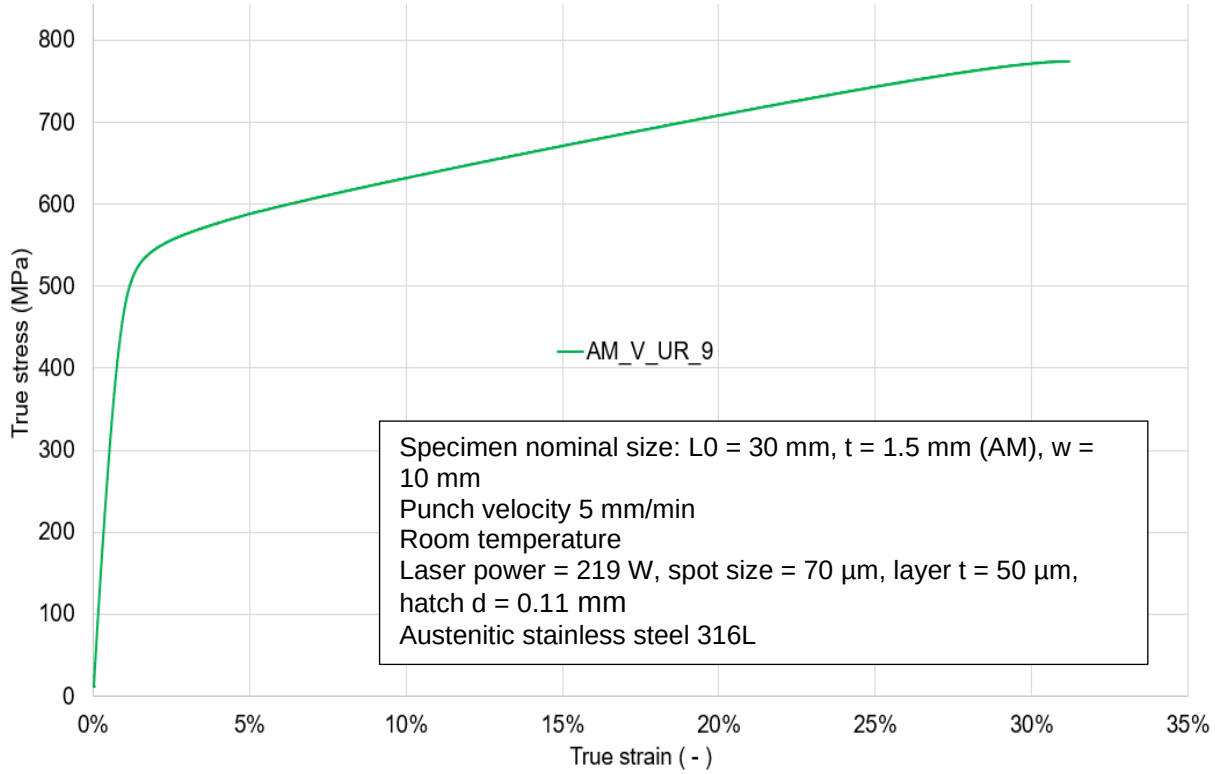
800
700
600
500
400
300
200
100
0
True stress (MPa)
AM_V_UR_9
Specimen nominal size: L0 = 30 mm, t = 1.5 mm (AM), w = 10 mm
Punch velocity 5 mm/min
Room temperature
Laser power = 219 W, spot size = 70 µm, layer t = 50 µm, hatch d = 0.11 mm
Austenitic stainless steel 316L
0%
5%
10%
15%
20%
25%
30%
35%
True strain (-)

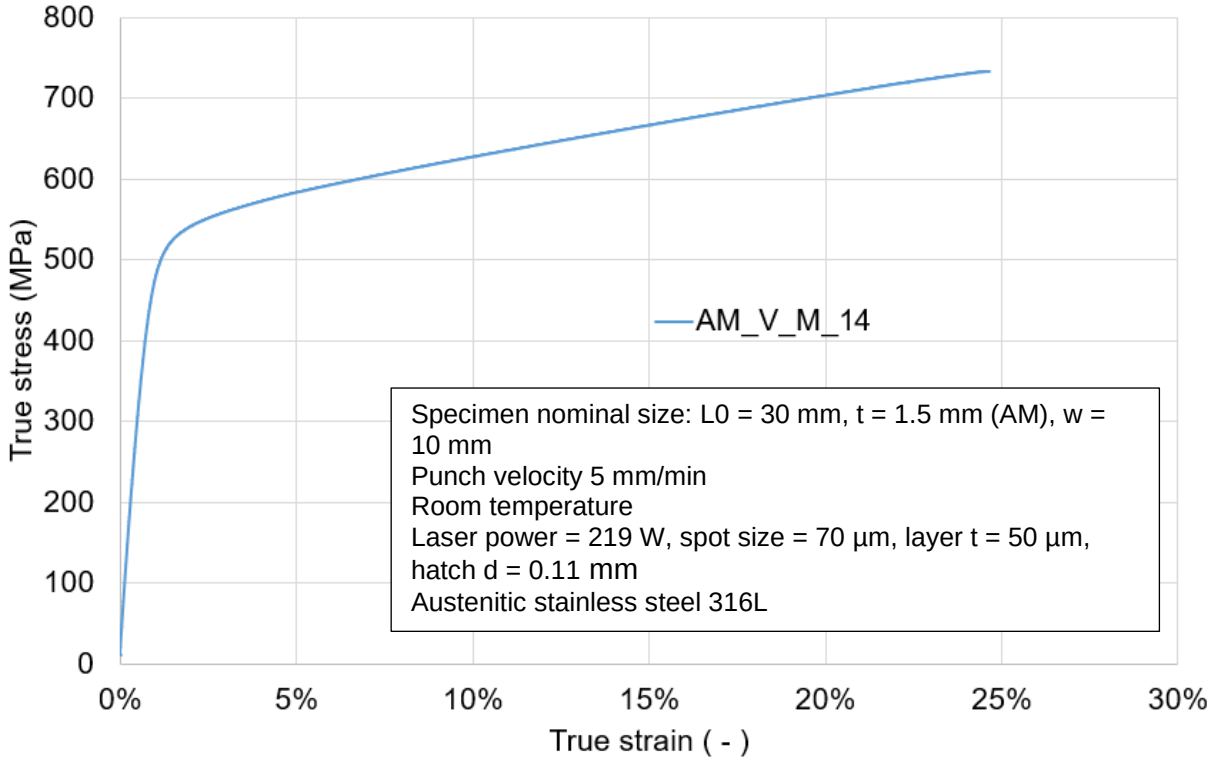
800
700
600
500
400
300
200
100
0
True stress (MPa)
AM_V_M_14
Specimen nominal size: L0 = 30 mm, t = 1.5 mm (AM), w = 10 mm
Punch velocity 5 mm/min
Room temperature
Laser power = 219 W, spot size = 70 µm, layer t = 50 µm, hatch d = 0.11 mm
Austenitic stainless steel 316L
0%
5%
10%
15%
20%
25%
30%
True strain (-)

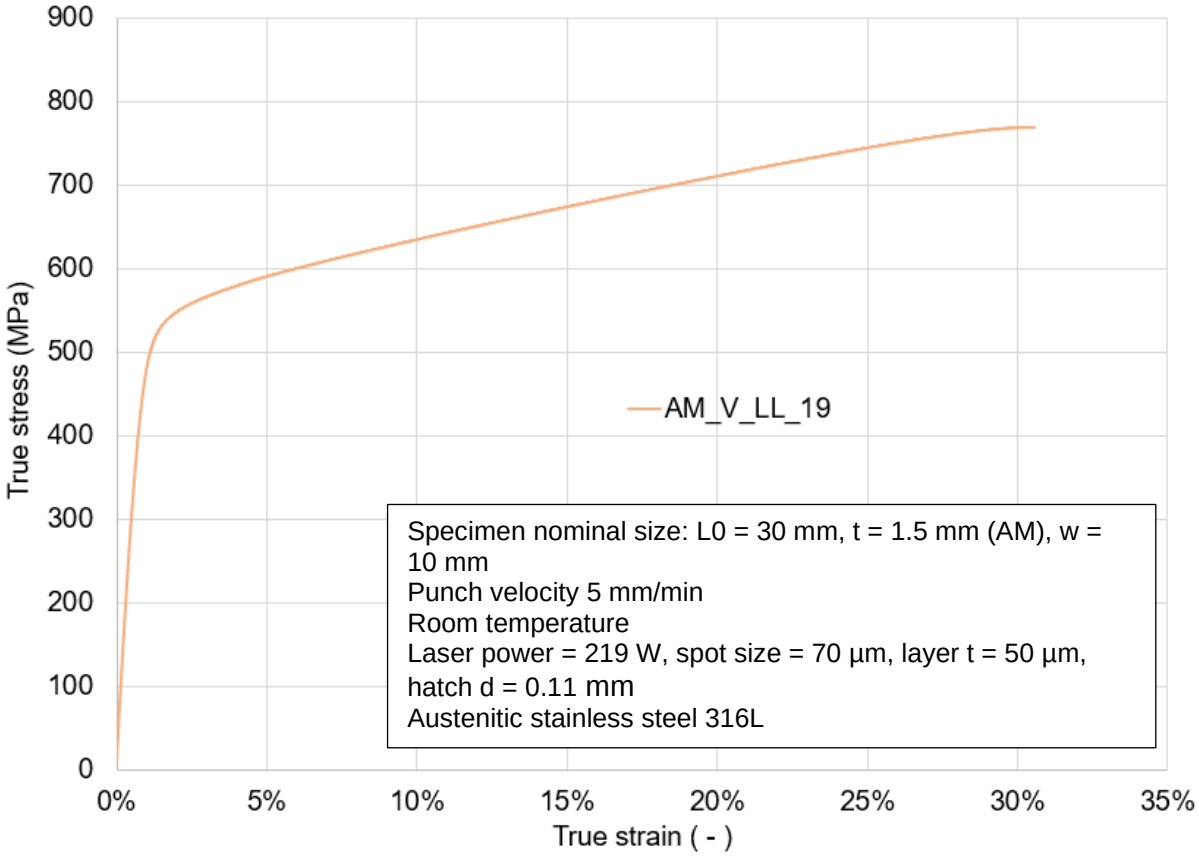
900
800
700
600
500
400
300
200
100
0
True stress (MPa)
0%
5%
10%
15%
20%
25%
30%
35%
True strain (-)
AM_V_LL_19
Specimen nominal size: L0 = 30 mm, t = 1.5 mm (AM), w = 10 mm
Punch velocity 5 mm/min
Room temperature
Laser power = 219 W, spot size = 70 µm, layer t = 50 µm, hatch d = 0.11 mm
Austenitic stainless steel 316L

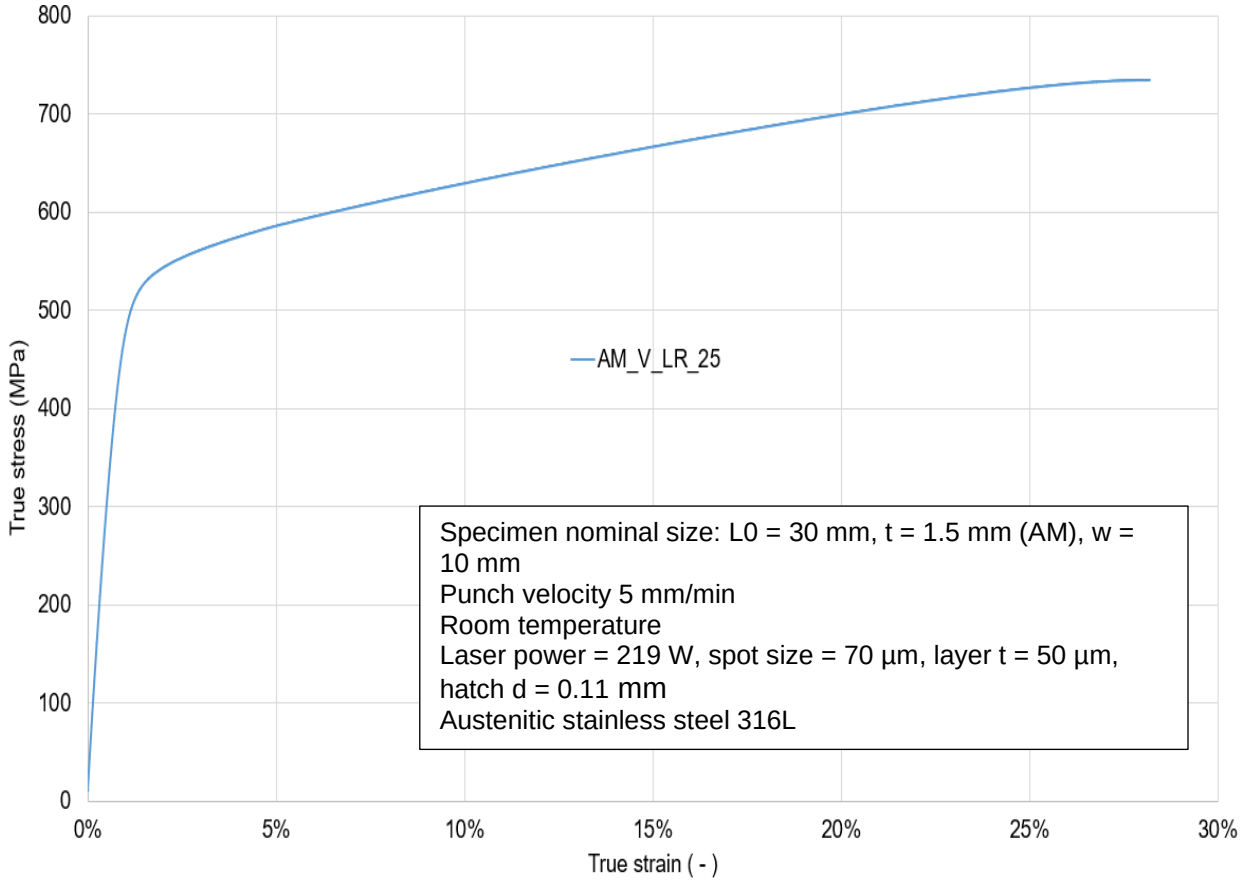
800
700
600
500
400
300
200
100
0
True stress (MPa)
0%
5%
10%
15%
20%
25%
30%
True strain (-)
AM_V_LR_25
Specimen nominal size: L0 = 30 mm, t = 1.5 mm (AM), w = 10 mm
Punch velocity 5 mm/min
Room temperature
Laser power = 219 W, spot size = 70 µm, layer t = 50 µm, hatch d = 0.11 mm
Austenitic stainless steel 316L

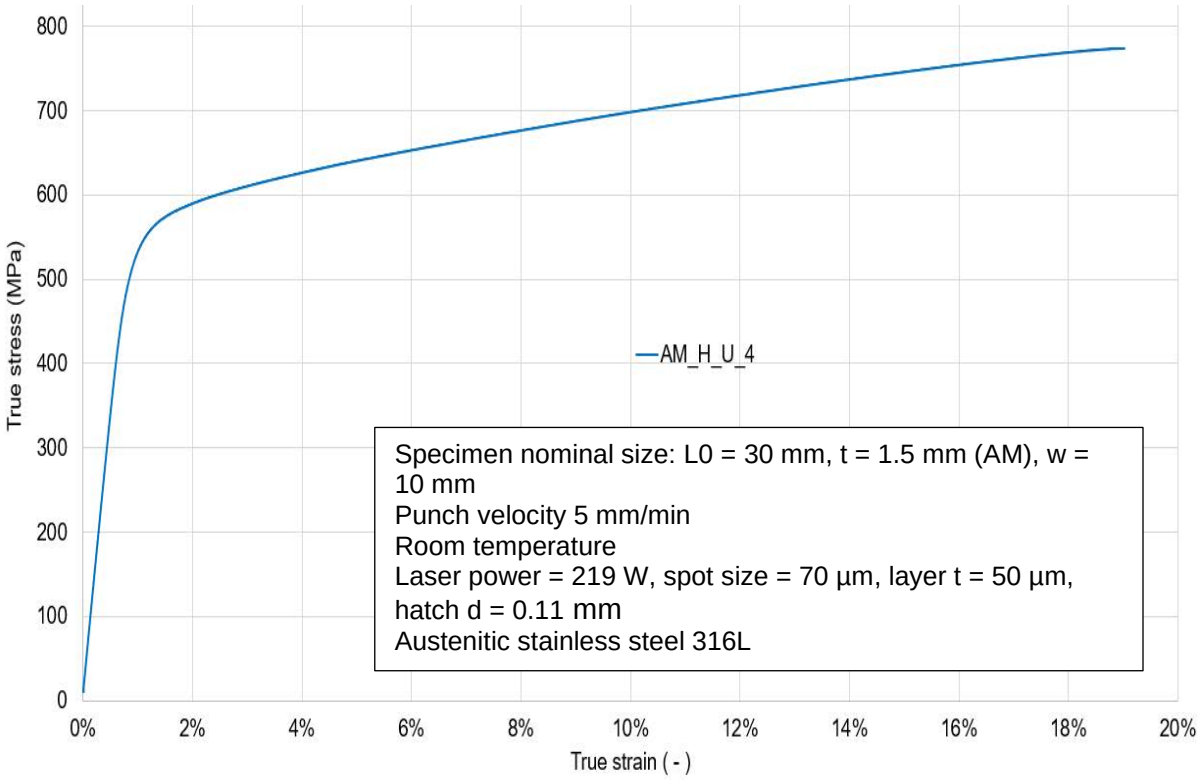
800
700
600
500
400
300
200
100
0
True stress (MPa)
AM_H_U_4
Specimen nominal size: L0 = 30 mm, t = 1.5 mm (AM), w = 10 mm
Punch velocity 5 mm/min
Room temperature
Laser power = 219 W, spot size = 70 µm, layer t = 50 µm, hatch d = 0.11 mm
Austenitic stainless steel 316L
0%
2%
4%
6%
8%
10%
12%
14%
16%
18%
20%
True strain (-)

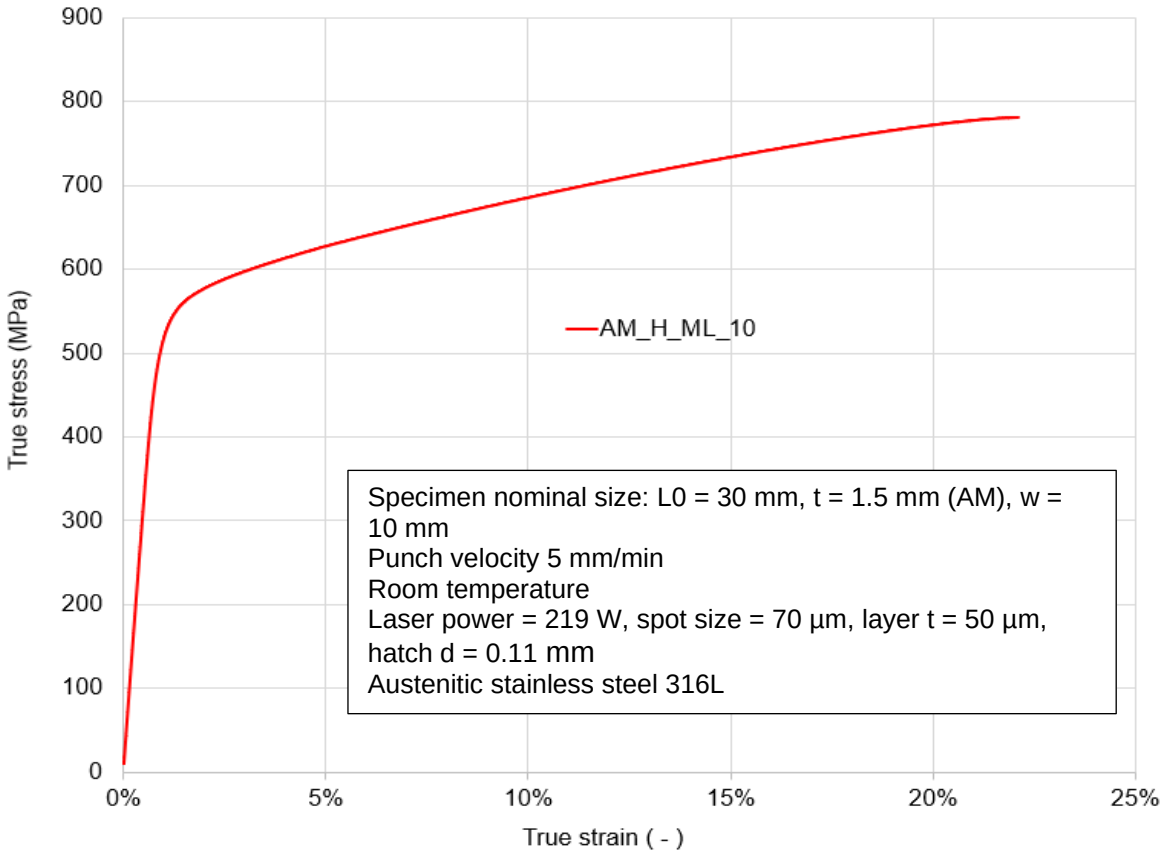
900
800
700
600
500
400
300
200
100
0
True stress (MPa)
AM_H_ML_10
Specimen nominal size: L0 = 30 mm, t = 1.5 mm (AM), w = 10 mm
Punch velocity 5 mm/min
Room temperature
Laser power = 219 W, spot size = 70 µm, layer t = 50 µm, hatch d = 0.11 mm
Austenitic stainless steel 316L
0%
5%
10%
15%
20%
25%
True strain (-)

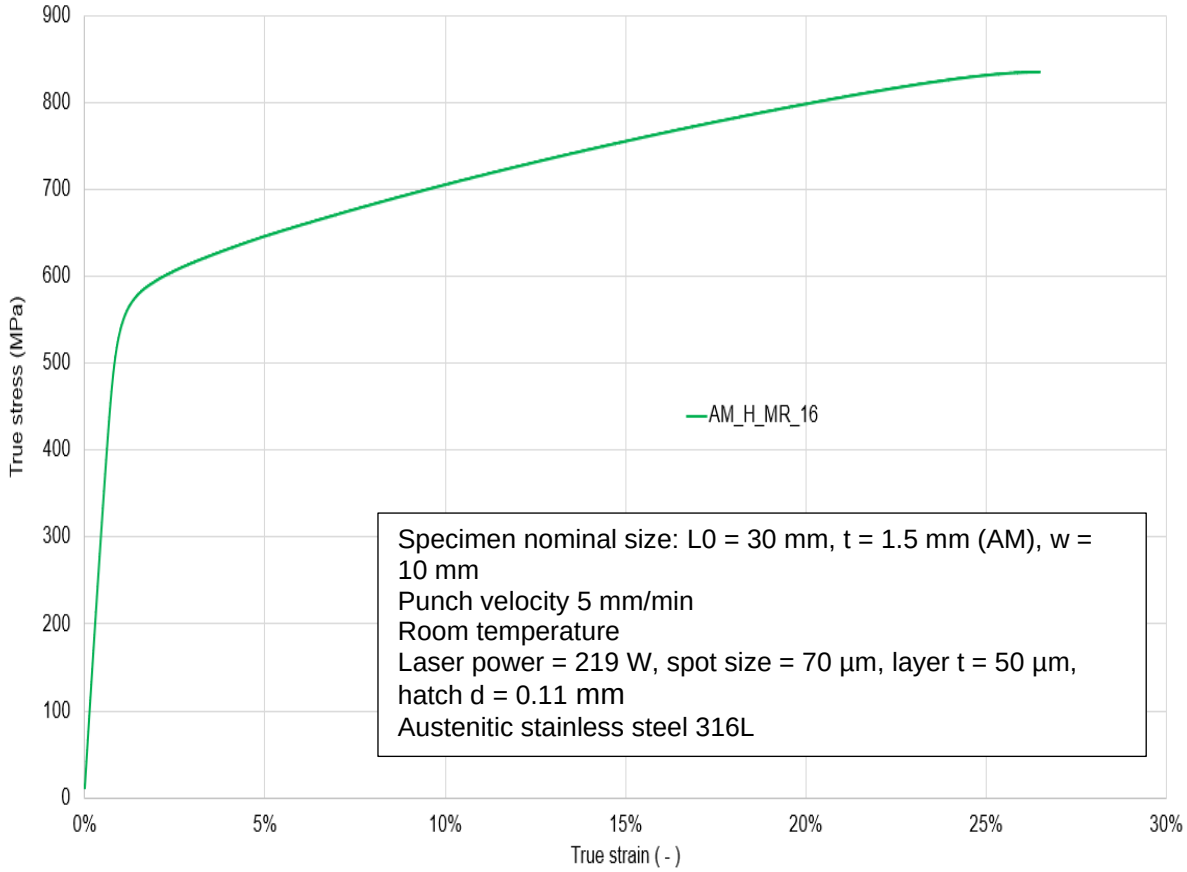
900
800
700
600
500
400
300
200
100
0
True stress (MPa)
0%
5%
10%
15%
20%
25%
30%
True strain (-)
AM_H_MR_16
Specimen nominal size: L0 = 30 mm, t = 1.5 mm (AM), w = 10 mm
Punch velocity 5 mm/min
Room temperature
Laser power = 219 W, spot size = 70 µm, layer t = 50 µm, hatch d = 0.11 mm
Austenitic stainless steel 316L

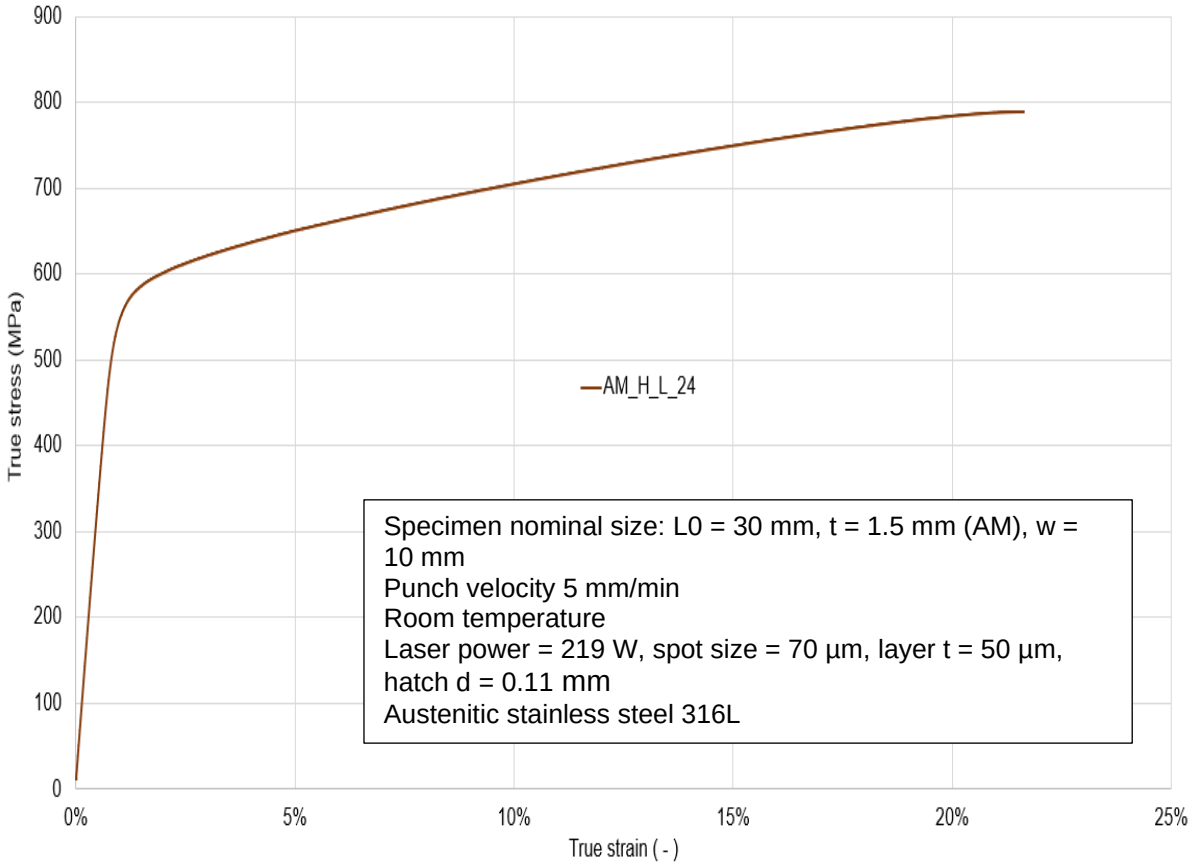
900
800
700
600
500
400
300
200
100
0
True stress (MPa)
0%
5%
10%
15%
20%
25%
True strain (-)
AM_H_L_24
Specimen nominal size: L0 = 30 mm, t = 1.5 mm (AM), w = 10 mm
Punch velocity 5 mm/min
Room temperature
Laser power = 219 W, spot size = 70 µm, layer t = 50 µm, hatch d = 0.11 mm
Austenitic stainless steel 316L